SDSU-RSI-A1-04

EVALUATION OF HCMM DATA FOR ASSESSING SOIL MOISTURE AND WATER TABLE DEPTH

FINAL REPORT
For
GODDARD SPACE FLIGHT CENTER
Contract NAS 5-24206
GREENBELT, MARYLAND
20771

August 1981

RSI REMOTE SENSING INSTITUTE
SOUTH DAKOTA STATE UNIVERSITY
BROOKINGS, SOUTH DAKOTA, U.S.A.
57007

TECHNICAL REPORT STANDARD TITLE PAGE

1. Report No.	2. Government Accession No.	3. Recipient's Catalog No.

4. Title and Subtitle	5. Report Date
Evaluation of HCMM Data For Assessing Soil Moisture and Water Table Depth.	March 1981
	6. Performing Organization Code SDSU-RSI-81-04
7. Author(s) D.G. Moore, J.L. Heilman, J.A. Tunheim, F.C. Westin, W.E. Heilman, G.A. Beutler, S.D. Ness	8. Performing Organization Report No.
9. Performing Organization Name and Address Remote Sensing Institute South Dakota State University Brookings, South Dakota 57007	10. Work Unit No.
	11. Contract or Grant No. NAS5-24206
	13. Type of Report and Period Covered Final Report June 1977-March 1981
12. Sponsoring Agency Name and Address NASA Goddard Space Flight Center Greenbelt, Maryland 20771	14. Sponsoring Agency Code
15. Supplementary Notes	

16. Abstract HCMM data were analyzed for assessing soil moisture and water table depth variation in eastern South Dakota. Soil moisture in the 0-4 cm layer could be estimated with 1-mm soil temperatures throughout the growing season of a rainfed barley crop (% cover ranging from 30% to 90%) with an r^2=0.81. Empirical equations were developed to reduce the effect of canopy cover when radiometrically estimating the 1-mm soil temperature, r^2=0.88. The corrective equations were applied to an aircraft simulation of HCMM data for a diversity of crop types and land cover conditions to estimate the 0-4 cm soil moisture. The average difference between observed and measured soil moisture was 1.6% of field capacity. HCMM data were used to estimate the soil moisture for four dates with an r^2=0.55 after correction for crop conditions. Location of shallow alluvial aquifers could be accomplished with HCMM predawn data. After correction of HCMM day data for vegetation differences, equations were developed for predicting water table depths within the aquifer (r=0.8). The largest correlation coefficient was derived during September during the period of maximum annual downward temperature gradient. Thermal infrared data were useful for assessing differences in soil texture, slope aspect, elevations, and apparent vegetation vigor. The soil surveyor can operationally use the information. A finite-difference computer model simulating soil moisture and soil temperature showed that soils with different moisture profiles differed in surface temperatures in a well-defined functional manner. The functional form of temperature differences between two sites was changed less by variations in canopy cover than the form of the diurnal temperature changes at a single site. A significant surface thermal anomaly is associated with shallow water tables.

17. Key Words Suggested by Author	18. Distribution Statement
Groundwater, soil moisture, HCMM, heat sink, thermography, emissivity, remote sensing, longwave radiation, radiometry, radiance, energy balance, thermal inertia, water table depth, finite difference model, soil temperature	

19. Security Classif. (of this report)	20. Security Classif. (of this page)	21. No. of Pages	22. Price
Unclassified	Unclassified		

TABLE OF CONTENTS

TABLE OF CONTENTS

LIST OF FIGURES

Chapter I: Executive Summary

LIST OF FIGURES

CHAPTER I: EXECUTIVE SUMMARY

Section 1: Need for Study

Various investigations and model calculations yield evidence that thermal infrared remote sensors are useful in assessing water-related surface and near-surface land conditions. Soil moisture is highly dynamic having extreme spatial and temporal variability. This characteristic makes ground point-sampling observation programs expensive and relatively ineffective for the sequential and synoptic, yet detailed, information required in management programs. Remote sensing systems have the capability to provide these data characteristics if the information content of the data can be quantitatively used to assess moisture related ground variables.

The agriculturalist has an interest in soil moisture which is available to the growing plants. This varies with season and crop but ranges from surface moisture to profile soil moisture at depths of a meter or more. Conversely, the hydrologist may have an interest only in the surface few centimeters of the land surface. Of special interest in South Dakota is the depth to the zone of saturation. Where this depth is within a few centimeters to approximately one meter, the soils may have a limited rooting depth and may tend to develop soil salinity caused by upward mobility of the water table moisture with subsequent evaporation and deposition of salts. The contamination of water table water associated with leaching of the soil horizons has a higher potential if the water table is near the land surface.

The depth to the saturated zone provides an indication of the water budget of surficial aquifers. Where discharge through evapotranspiration of phreatrophytes or of irrigated crops and the domestic consumption of water in combination with other loss factors exceeds recharge, water tables will lower. The importance of understanding aquifer water budgets is acknowledged since tedious ground observation programs are already in place in eastern South Dakota. A remote sensing program could potentially aid these programs for appropriate placement of sounding wells or inferring contours among the point observations for final mapping.

For many areas in South Dakota and other regions, monitoring the depth to the saturated zone, where it occurs in the top 2-3 meters of the land surface, would provide a valuable input into water and land management. Remote sensing approaches to a monitoring program would use surface or near-surface measurements (i.e. thermal or microwave) to infer certain water-related properties. Therefore, changes in the energy budget of the surface which result from a variety of factors must be evaluated and understood before thermal-infrared remote sensing data can provide the desired information. The shading effects of the crop canopy, water use by evapotranspiration, incomplete canopy cover, temperature indicators associated with variations of thermal diffusivity, slope, etc., are all candidate topics which must be addressed and understood to fully utilize the data derived from thermography.

The objectives pursued under this investigation were to:

(1) Develop a finite-difference simulation model for specific application to HCMM data which simulates and predicts the thermal regime associated with occurrence of shallow groundwater.

(2) Evaluate HCMM data for locating regions of shallow groundwater and estimating the depth to the water table.

Section 2: Report Format

Detailed results are presented as various chapters. Each chapter includes published or submitted papers which identify results relevant to the dual objectives. An additional topic beyond the original objectives was investigated which was to determine the uses of HCMM or similar data in soil geography studies.

The specific background, procedures, and discussion are presented within each chapter. A generalized summary of the investigation results is presented in the following section. Since potential applications of HCMM-type data have many questions to be resolved, any number of valid experimental topics could be addressed. Many were pursued under this program using ground or aircraft observations since it was questionable during the investigation if appropriate HCMM data would be received in a timely manner to use the data for analysis. Therefore, results and publications were fragmented and are presented in entirety in this report since procedures, test sites, etc. were not consistent for all investigations.

Section 3: Summary of Significant Results

Section 3.1. - Introduction

Landforms associated with areas of shallow groundwater in glaciated eastern South Dakota can be recognized using standard image interpretation techniques of multidate Landsat data. Therefore, this investigation was

to determine, once these regions were identified and mapped, if synoptic thermal data from HCMM could be used to assess the depth to the water table. Since the thermal signal measured by HCMM is a function of emitted radiation from the atmosphere and from the land surface, both must be considered when relating HCMM data to land or water features. The approach to reduce atmospheric variation used spatial differences within dates for analysis. No further attempts were utilized to reduce the influence of the atmosphere on the thermal signal even though the authors realize this as a significant problem in quantitative remote sensing using thermography. Therefore, most equations and statistical relationships presented in this report require that some form of quantitative field data are required to implement any of the algorithms.

Since the composite "surface" radiance is that which is sensed from the remote sensor, evaluations of the effects of vegetation cover and soil moisture were investigated. Sections 1-5 of Chapter II detail each specific study. In general, the topics included the use of thermal data for assessing actual soil temperatures under conditions of incomplete and complete canopy covers and the assessment of near-surface soil moisture. Chapter III follows with the relationship of ground, aircraft, and HCMM data to the depth-to-water tables. Since the program had considerable delays in dissemination of HCMM data, another objective was pursued to evaluate HCMM for use in operational soil surveys. Chapter IV clearly illustrates and demonstrates examples where HCMM or similar data could provide input to the field soil surveyor. The final Chapter V defines a model and its results for developing a theoretical base to

understand thermal infrared potentialities in water resources monitoring.

Section 3.2 - Qualitative Monitoring of Wet Versus Dry Surfaces

In its simplest form, daytime thermography should provide a qualitative mapping tool to locate regions which have a water saturated surface versus a surface where the soil moisture is at less than saturation. The effects of higher thermal inertia and increased partitioning of incoming energy into latent heat (increased evapotranspiration) result in cooler surface temperatures. Chapter II, Section 1 (II-1) and Figures 1-3 illustrate the phenomena. The predawn image in Figure 1 demonstrates that the area of a cool anomaly presented in Figure 2 was probably both a function of differences in evapotranspiration and of thermal inertia. The warmer apparent temperatures predawn results from a thermal inertia change of increased moisture when compared to surrounding regions. The cooler apparent temperatures of the saturated area during daytime hours results from both thermal inertia variations and increased evapotranspiration.

Section 3.3 - Thermography of Incomplete Canopy Cover

The remotely measured land surface emission includes radiation emitted from both soil and vegetated surfaces. If the intended application requires either soil or vegetation temperatures independently, a method to separate and calibrate the contribution of each emitting component must be developed. For the water table monitoring objective, the need is to measure soil surface temperature. If the application is to monitor transpiration of plants as an indicator of moisture or other

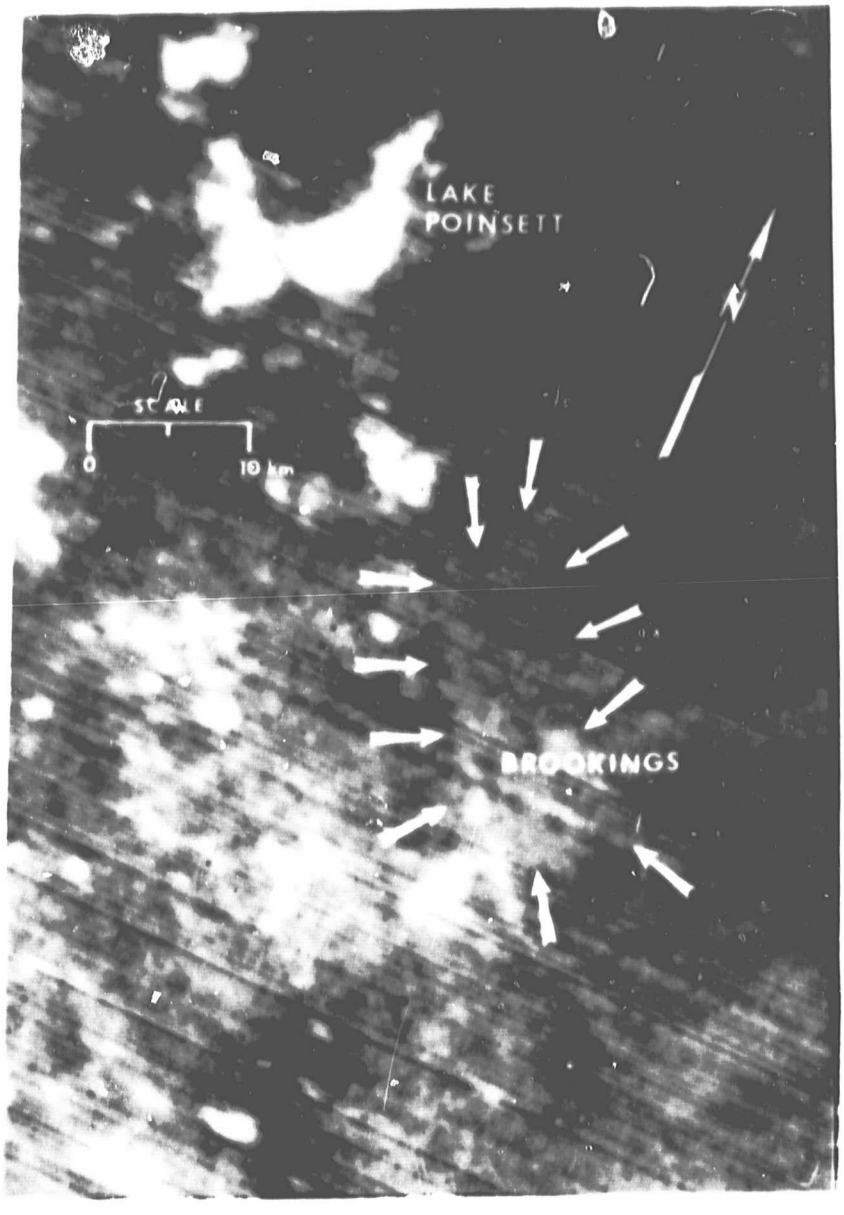

Figure 1. Photographic enlargement of a May 14, 1978 night thermal infrared image (scene I.D. A-A0018-08420) showing a high soil moisture area (arrows) in southeastern South Dakota. Thermal inertia is apparently causing a warmer signature during the predawn cooling portion of the diurnal cycle. Dark is cool.

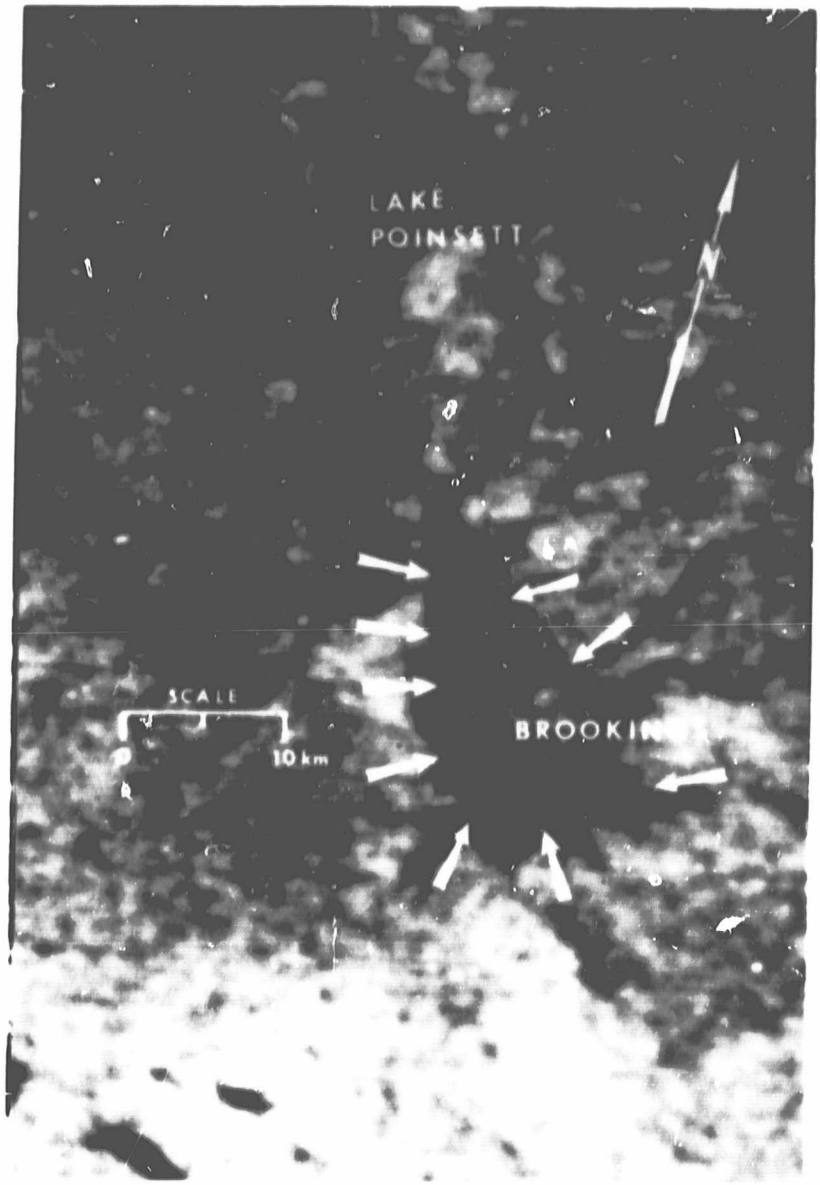

Figure 2. Photographic enlargement of a May 15, 1978 day thermal infrared image (scene I.D. A-A0029-19575) showing a high soil moisture area (arrows) in southeastern South Dakota. The area is approximately that of Figures 1 and 3. Increased evapotranspiration and increased thermal inertia are probably responsible for the cooler apparent temperatures of the wetter area. Dark is cool.

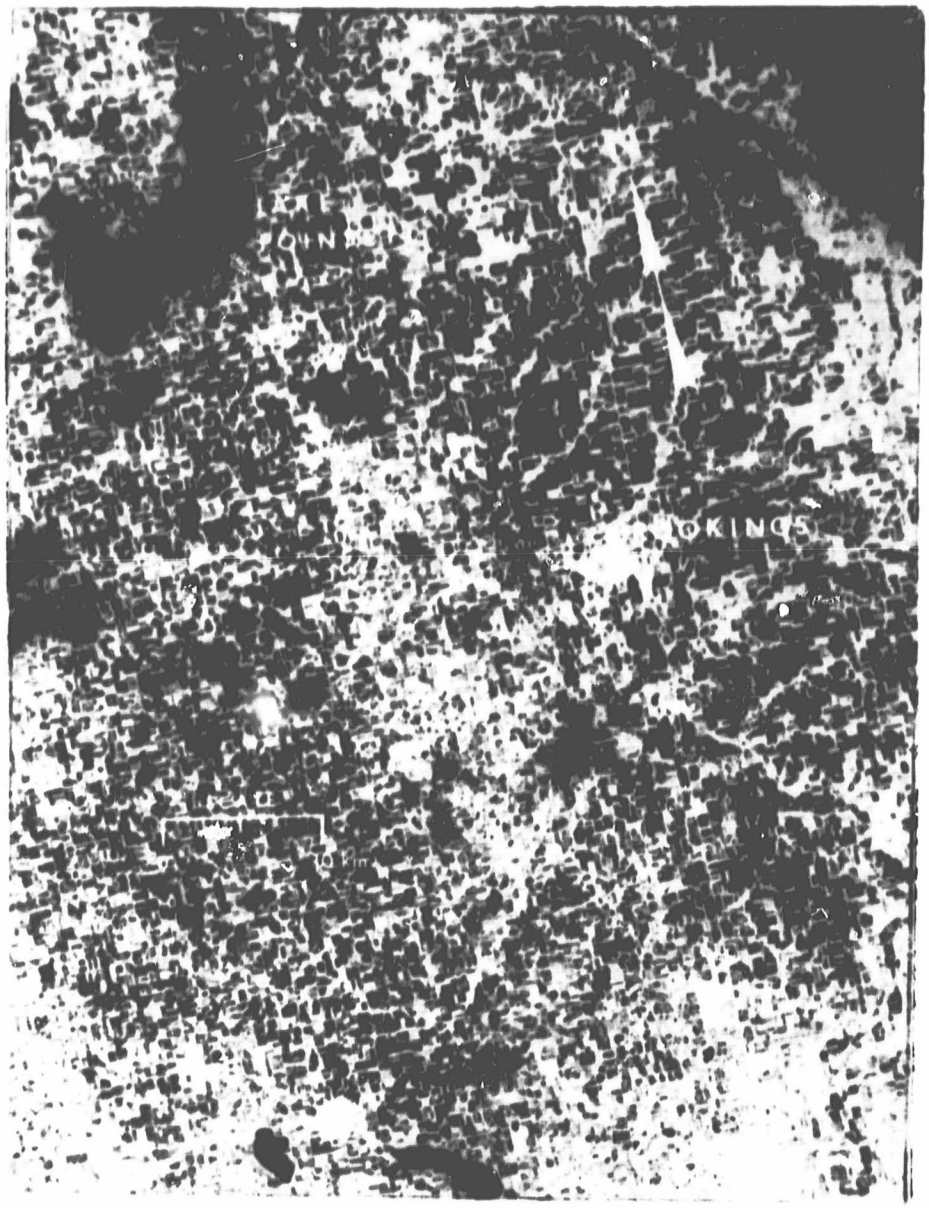

Figure 3. Photographic enlargement of a May 13, 1978 Landsat MSS7 image (scene I.D. E-21207-16083) of the same approximate area as Figures 1 and 2. The area in question does not have standing surface water but has either bare or vegetated fields as the emitting surface.

stress, the vegetation component must be estimated. Section 2 in Chapter II presents an algorithm to extract canopy temperature from radiometric measurements at incomplete cover.

A ground-based study was conducted on a developing barley canopy in which canopy temperatures were measured with an infrared radiometer at 30^{o} from horizontal. Contact soil temperatures at a 1-mm depth were measured using thermocouples. Composite radiometric temperatures which included radiance contributions both from the soil and from the barley vegetation were measured with a radiation thermometer at 2-m above the canopy. This measurement simulates that of vertical remote sensors. Emissivity and sky irradiance corrections were applied to the data. The measurements were acquired at approximately 1330 LST (HCMM overpass time) throughout the barley growing season. The canopy covers seasonably varied from 30% to 90% (≈LAI 0.3 to 3.2).

The radiometric temperatures of the composite radiating surface, including both soil and crop canopy, were 0.5 to 11.5 C higher than canopy temperatures alone. Surface soil temperatures were 1.5 to 20.0 C higher than canopy temperatures. Correlation between measured canopy temperatures and composite temperatures was not statistically significant.

The difference between composite and canopy temperatures was highly correlated with percent canopy cover (r^2 = 0.52). Therefore, an approximation equation was applied which separated the radiance contributions of the bare soil and the canopy. The equation incorporated terms for canopy and soil emissivities, percent crop cover, longwave sky irradiance,

and composite temperatures. Applying the correction resulted in a r^2 = 0.88 for relating predicted versus observed values for estimating the temperature of the canopy. Differences between predicted and observed values ranged from -1.84 to 2.5 C for the data acquired throughout the barley growing season.

The significance of the procedure was, even at low canopy covers estimates of canopy or soil temperatures can be successfully measured using remote sensors. Figure 4 summarizes the data for the barley study. Remote sensing estimates of percent cover and composite temperatures are available with existing technology. When emissivity corrections were not applied, prediction accuracy varied with percent cover. The largest errors occurred at low canopy cover. Canopy emissivity was measured as 0.98 and was assumed constant throughout the growing season. Soil emissivity varied with water content. Measured values ranged between 0.95 and 0.97. Wider ranges of soil emissivities can be experienced since the value is soil specific. If emissivities were assumed to be one for the calculations in this field experiment, predicted canopy temperatures would range from 6.4 C lower to 1.7 higher than actual observed values. Where measured emissivities were used in the equation but the longwave sky irradiance was ignored, differences between predicted and observed canopy temperatures ranged from 0.8 to 10.7 C.

The significance of the study was that canopy temperatures at incomplete covers can be estimated using a nadir-viewing radiometer if appropriate considerations are given to soil background radiance,

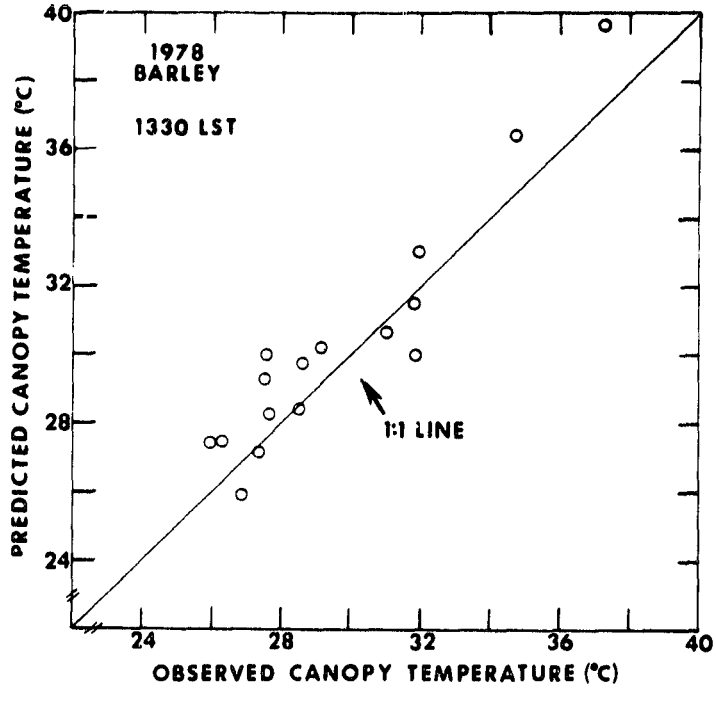

Figure 4. Comparison of predicted and observed canopy temperatures where the predicted temperatures utilized terms of canopy and soil emissivities, percent crop cover, longwave sky irradiance, and composite radiometric temperatures (or remotely sensed temperatures).

emissivities, and sky irradiance. Techniques are available for measuring or estimating some of the inputs required for the canopy model. Various models which have been developed for simulating bare surface soil temperatures can feasibly be extended to soil surfaces including crop canopies.

Section 3.4 - Diurnal Surface Temperature Change as a Measure of Near-Surface Soil Moisture

The basic assumption in using thermography to estimate near-surface soil moisture is that surface temperatures or their changes in time are related to the thermal properties of soils in a predictable fashion when other components of the energy budget are not accounted for or can be accounted by use of auxiliary data which are easily available. The paper presented in Chapter II, Section 3 describes in detail the experimental framework to determine if ΔT of the surface relates to near-surface moisture and if this relationship is maintained with the variability introduced throughout a barley growing season having variations in canopy cover. The same rainfed barley field as described in the previous section was instrumented and measured on 22 dates over a 45-day period.

Volumetric soil water content of the 0-4 cm layer was the variable to be predicted by thermography. The field data were collected throughout a barley growing season where percent cover ranged from 30% to 90% and leaf area index from 0.3 to 3.2. Diurnal changes in 1-mm soil temperatures between 1330 and 0230 LST (ΔT_s) were used in an exponential equation to predict soil moisture content of the 0-4 cm soil layer. An $r^2 = 0.81$ was derived for the equation which incorporated data from the

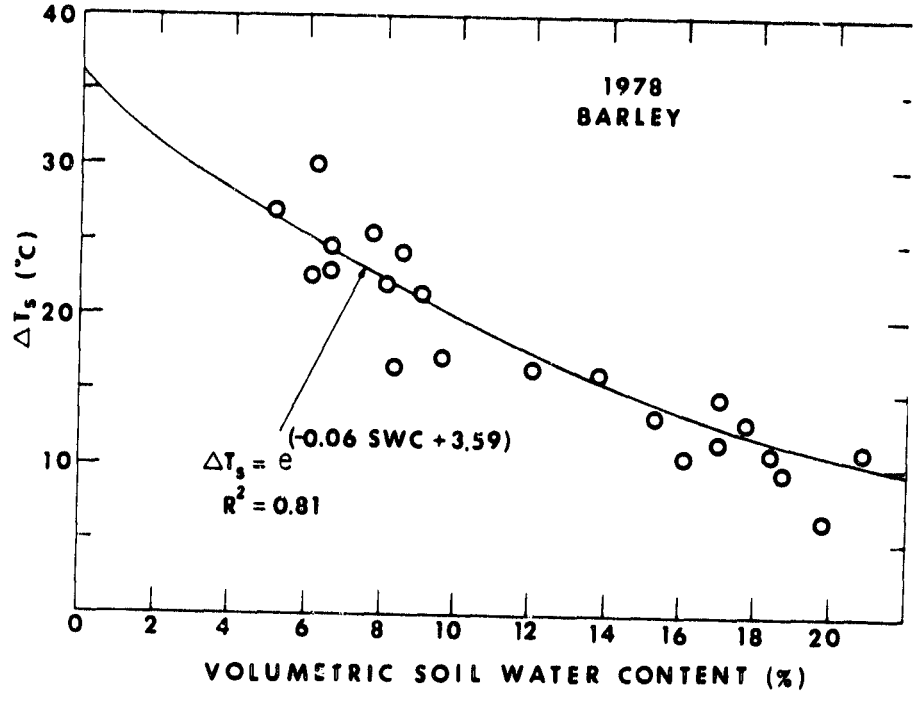

Figure 5. Relationship of the difference (ΔT_S) between soil surface temperatures measured at 1330 and 0230 LST and the average 24 hr volumetric soil water content in the 0 to 4 cm layer of the profile.

total season. The resulting equation and plot is illustrated in Figure 5. Attempts to normalize among dates using air temperatures provided no significant improvement to the results.

The quantitative relationship is significant in illustrating that if an estimate of actual daily surface temperature difference is available, it is statistically highly significant in direct relation to near-surface moisture. The diversity in canopy cover, air temperature and humidity, and other energy budget terms did not mask the relationship.

Section 3.5 - Surface Soil Temperature and Moisture Estimates Using Radiometry.

The same barley canopy and experimental data were evaluated to determine if radiometric temperatures of "composite" land surfaces (including both canopy and bare soil) could be used to quantitatively relate to the 0-4 cm soil moisture. The actual 0230 LST composite temperatures ranged from 1.1 - 2.2 C higher than canopy temperatures (excluding soil background). This predawn background soil irradiance was typically higher than the canopy temperature. The surface soil temperatures were higher by 1.1 - 5.4 C than canopy temperatures. This trend remains during the 1330 LST measurements. The composite radiometric temperatures were 0.5 - 17.0 C higher and surface soil temperatures 1.5 - 20.0 C higher than temperatures of the vegetation in the canopy. Therefore, changing canopy cover affects the ability to estimate the actual soil surface temperature which is the temperature that is related to near-surface moisture.

Regression equations were developed using the seasonal data of the barley canopy to relate composite (or remotely sensed temperatures) to the actual soil surface temperatures. For the 0230 LST measurement time, the resulting equation included modifying the thermography measurement with National Weather Service daily minimum air temperature. For the 1330 LST measurement, the equation included a term modifying the thermography with an exponential term of fraction of vegetation cover. The two equations had $R^2 = 0.78$ and $r^2 = 0.86$, respectively. Figure 6 illustrates the corrected data after application of the canopy cover correction equations.

The equations were derived empirically and should be questioned and evaluated over a larger set of environmental variables than were included in this original data set. However, the need for some type of correction of the thermal radiance measure is required to relate to actual soil surface conditions where partial or incomplete cover by a crop canopy is present.

The equations presented in this study illustrate that easily derived field properties such as air temperature or percent canopy cover may provide the necessary information. The equations developed were limited in geographic extent but did encompass data throughout a complete growing cycle of one crop.

Section 3.6 - Aerial Thermography as an Estimate of Near-surface Soil Moisture Under a Variety of Land Covers.

The correction equations developed from the barley study were applied to an aircraft study of a larger region in eastern South Dakota which included a diversity of canopy covers (50%-95% cover including

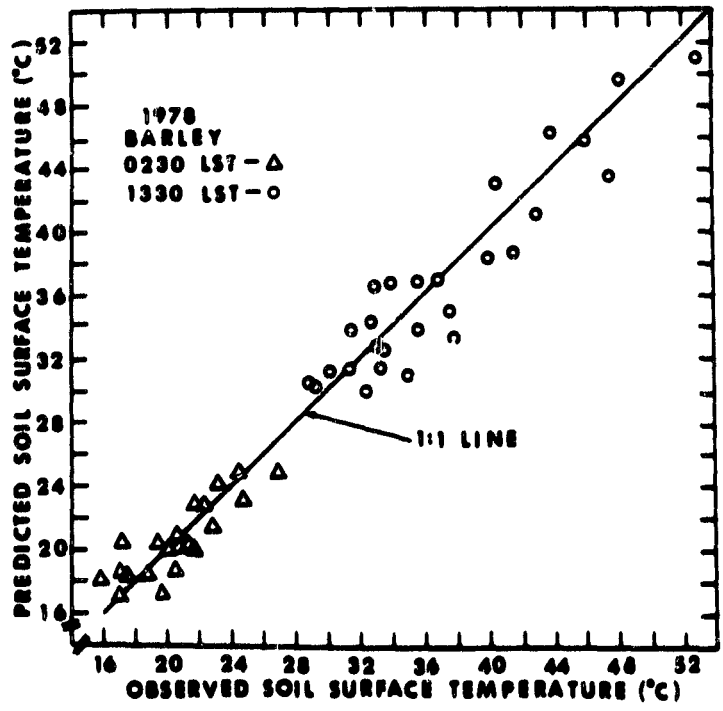

Figure 6. Comparison of predicted and observed values of surface soil temperature at 0230 LST and 1330 LST.

corn, soybeans, millet, and pasture) and differences in soil textures and other soil properties (Chapter II, Section 3). The day/night aircraft thermal data were collected on only one date. Soil moisture was estimated as percent of field capacity to reduce variations associated with soils. The average difference between measured and predicted values was 1.6% of field capacity. Figure 7 provides a plot of the measured versus predicted soil water contents.

The significance of the study was that the correction equations were applicable to a wide range of crop cover conditions. This range is normally prevalent when applying the techniques over large agricultural areas where soil moisture monitoring programs might be established.

Section 3.7 - HCMM Thermography as an Estimate of Near-surface Moisture Under a Variety of Land Covers

Satellite applications have the advantage of covering large regions in a short time period. When the theme to be estimated is confused with other scene variables, the complexity caused by heterogeneity of the terrain normally increases as larger areas are observed. The same correction procedures were tested using data as thermography covering multiple dates over a sizable area in eastern South Dakota having a complex agricultural landscape.

HCMM data were treated with correction equations similar to those discussed in the previous paragraph (Chapter II, Section 5). Soil moisture data from the 0-4 cm soil layer were acquired from 23 fields having a variety of crop covers for four dates ranging from June through early September. The HCMM radiometric temperatures without

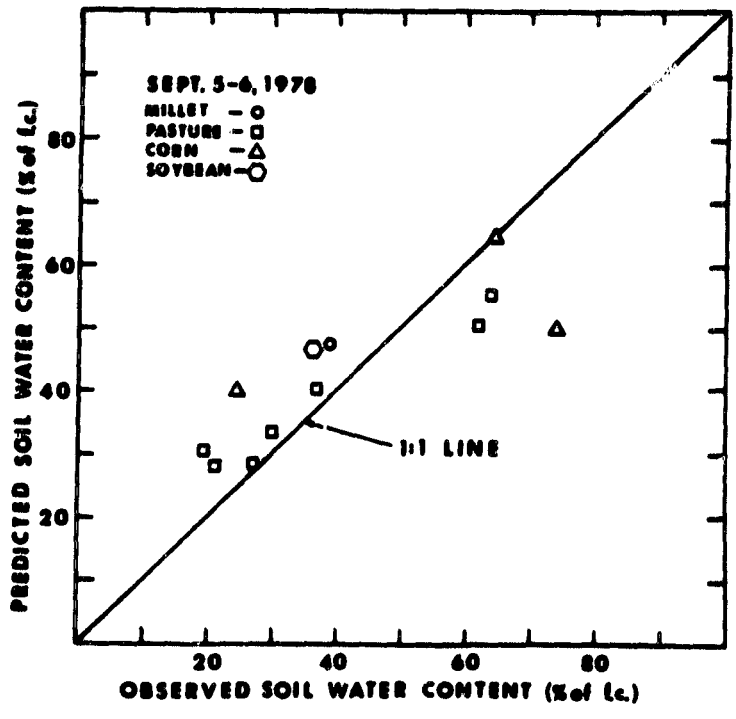

Figure 7. Comparison of predicted and observed values of 24 h average soil water content in the 0 to 4 cm layer of the soil profile. Aircraft thermal scanner data were used in prediction after applying correction equations for canopy variations.

correction for land cover did not significantly relate to soil moisture. However, when actual surface soil temperatures were empirically estimated from HCMM radiometric temperatures using land cover corrections, a highly significant correlation ($r = 0.74$) was obtained between the estimated soil temperatures and 0-4 cm soil moisture content. Figure 8 illustrates the derived relationship.

Section 3.8 - Depth to Water Table

If the water table or zone of saturation is at a greater depth than the diurnal damping depth, the amplitude of the diurnal temperature curve is not affected but a shift in the curve up or down in absolute magnitude will be noticed where the depth to saturation is within the depth of annual temperature variations. Many investigations, as reported in Chapter III, Sections 1 and 2, have demonstrated that 50-cm deep soil temperatures will vary with depth to water table. The saturated zone acts as a heat sink or source which delays warming in the summer and retards cooling in the winter.

The Big Sioux River Basin in eastern South Dakota is a surficial shallow water table aquifer of glacial origin. The land use is predominantly agriculture including small grains, pasture, hayland, and row crops. A considerable difference in the thermography can be expected as associated with land cover. Contact temperature measurements at a 50-cm depth were acquired to determine if a significant relationship between the soil profile temperatures and depth to water table was retained even under varying land cover (Figure 9). Similar to

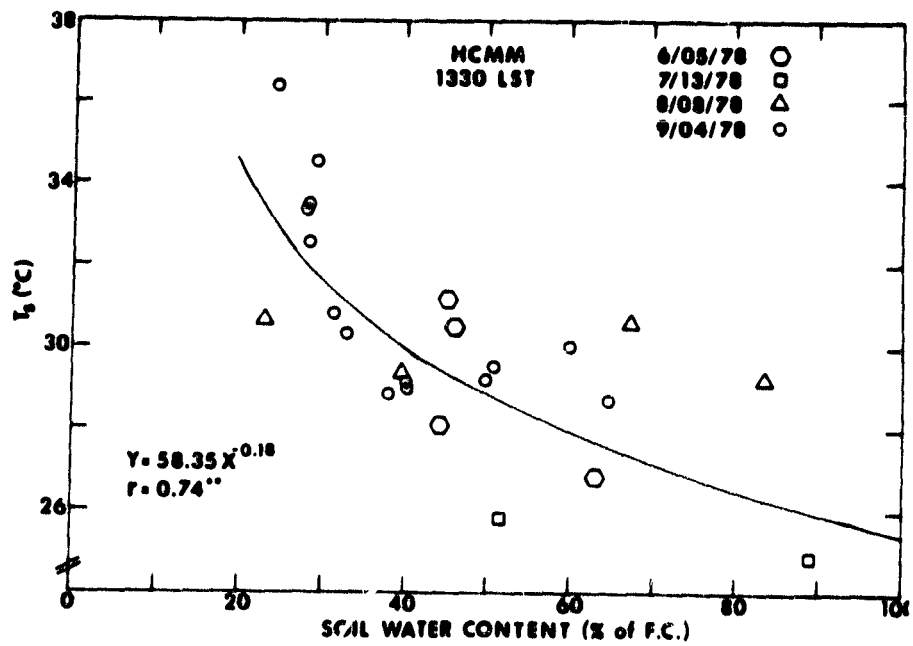

Figure 8. Relationship between predicted soil surface temperatures (T_s) and soil water content in the 0-4 cm layers of the soil profile. Field soil water contents are an average of three measurements.

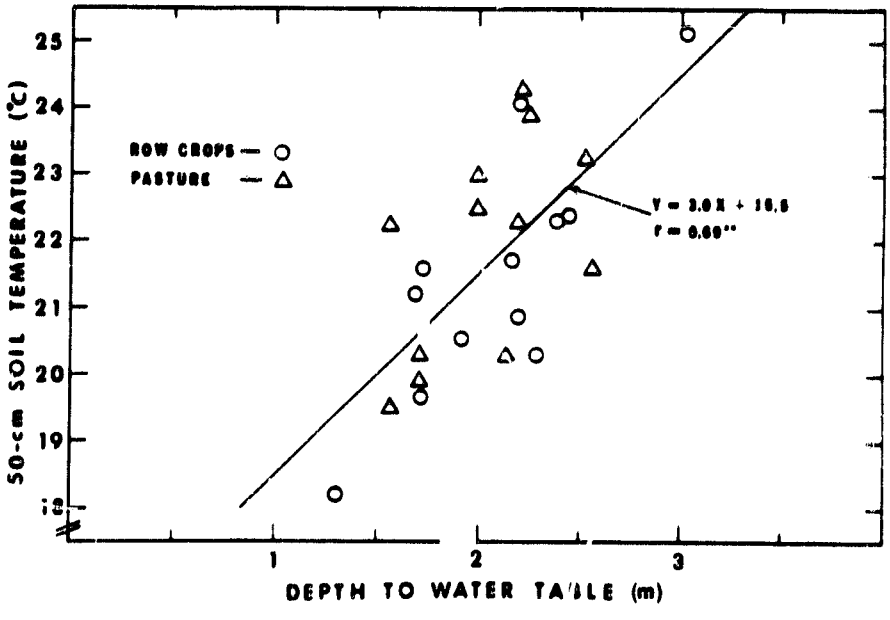

Figure 9. Relationship of 50-cm soil temperatures to depth to groundwater for row crops and pasture. Temperatures were measured in the Big Sioux River Basin during daylight hours on September 5-7, 1978.

observations reported in the literature, a significant relationship between measured 50-cm soil temperatures and depth to water table was observed for water tables in the Big Sioux Basin of eastern South Dakota. Three meters was the depth limitation of a significant correlation. These correlations were observed during early September near the annual maximum downward temperature gradient. The saturated soil materials act as a heat sink as the annual temperature mark progresses into the summer in the northern latitude of South Dakota. This creates cooler land surfaces over the water saturated zone. However, both soil moisture and vegetation cover may obscure any surface expression of this temperaature anomaly.

The range of 50-cm temperatures was about 5 C for the data acquired under this investigation. The 50-cm temperature anomaly predicted by modeling and field observations has previously been shown in the literature to be 1-2 C as associated with water tables. However, data points in this study were in soil profiles having a variety of crop cover conditions on the surface which also affected the 50-cm temperatures. High soil moisture and shallow groundwater tend to affect surface temperatures in the same direction - the surface remains cooler during the day (in periods of maximum downward temperature gradients - August or September) - but in opposite directions at night. At night, the high soil moisture areas should remain warmer when considering thermal inertia, and the shallow groundwater areas should remain cooler.

Previous investigations have shown that aircraft radiometric temperatures were related to water table properties. Predawn HCMM

imagery was effectively used with cooler anomalies delineating the alluvial basin when the water tables were shallow in Figure 10. Landform recognition from Landsat or aircraft image data was also used to locate these potential areas. During the day, the HCMM thermal data did not reveal the locations of the basin as illustrated in Figure 11.

The landforms (alluvium and terraces) where high water tables are commonly located were delineated using a combination of Landsat and HCMM predawn data. Since the depth to the water table had significant correlations to the 50-cm temperatures, HCMM data were evaluated to determine if the radiometric surface temperatures were correlated with water table depths. Uncorrected HCMM data were evaluated for estimating water table depths within the basin for four dates from June through early September. No significant relationship was found. The data were corrected using the empirical vegetation transformation developed under the previous soil moisture studies to reduce the effect of the crop canopies when estimating surface temperatures. Each date was analyzed separately. The correlations improved from 0.59 to 0.8 as the season progressed from June 5 through September 4. The September 4 date is plotted in Figure 12 which relates corrected HCMM data to water table depth.

This parallels model predictions. The maximum anomaly should occur in the season of greatest downward temperature gradient. Since both soil moisture and water table depth can affect surface soil temperature, a multiple regression analysis was conducted to determine the proportion of the HCMM radiometric temperature which could be accounted for with these two variables. The resulting $R^2 = 0.87$ was for the September 4

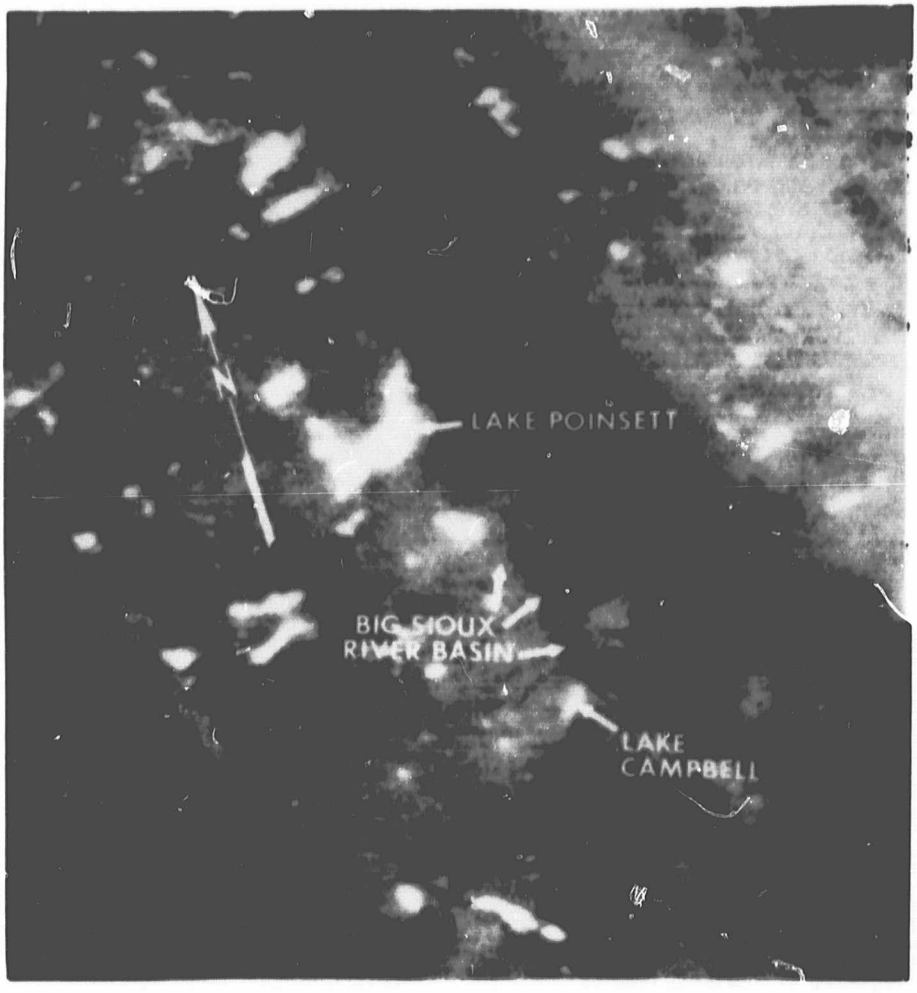

Figure 10. Photographic enlargement of an August 29, 1978 night HCMM thermal infrared image (scene ID A-A-125-08340) showing the Big Sioux Basin. Note that the Basin appears cooler than the surrounding areas, due primarily to the heat sink produced by shallow groundwater within the Basin. (Approximate scale 1:1,000,000; dark is cool)

Figure 11. A September 4, 1978 photographic enlargement of a HCMM day thermal infrared image (scene ID A-A0131-19420) of the same area shown in Figure 10. Note that the Big Sioux River Basin is not visible because of emittance variation associated with land use (Approximate scale 1:1,000,000; dark is cool).

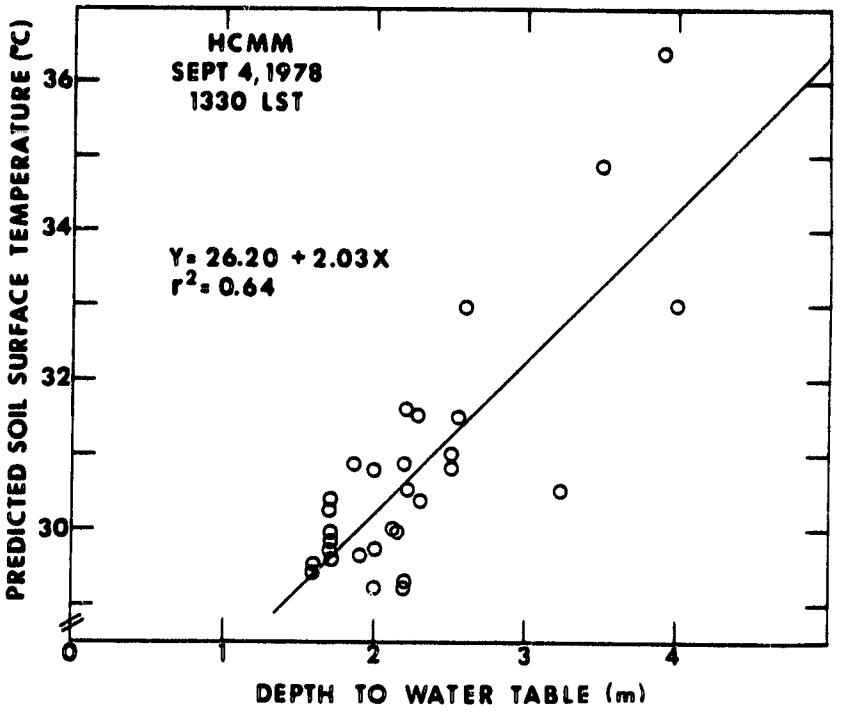

Figure 12. Relationship between predicted soil surface temperature and water table depth on September 4, 1978.

date. This compared to $r^2 = 0.64$ when relating only water table to HCMM thermography. Please note that depth to the water often influences soil moisture.

Data such as HCMM can be beneficial in guiding well drilling programs for monitoring and mapping water table depths where the water tables range from 0 to 3 m. Land cover masks the thermal anomaly associated with water tables but the effect can be reduced by using predawn data or by accounting for land cover in the prediction equation. Since the thermography signal is a function of many variables including the heat sink (or source), land cover, and soil moisture, results of the investigation revealed that if the latter two are introduced into equations to assess depth to water table, improved correlations can be derived.

Section 3.9 - Soil Geography

Soil moisture, vegetation cover, elevation, slope aspect, soil texture, and many additional variables affect land surface temperatures. Many of these variables are useful to the soil surveyor who is classifying soils and estimating land capabilities. Image interpretation of HCMM thermal data of South Dakota was conducted to determine its use for the soil surveyor. Results were that elevated areas, soil textural differences, and slope aspect were apparent in the imagery. Warmer radiometric predawn temperatures of north-facing slopes were evident. The data provide a pictoral illustration of how soil moisture and vegetation variations are associated with aspect of slope. North-facing slope aspect reduces solar insolation to the surface resulting in less

evapotranspiration and higher soil moisture. HCMM or similar data can provide this information by estimating the net effect of slope aspect as it relates to vegetation growth and production (Chapter IV). Similar observations were made for elevation differences between areas where parent materials and soils appear similar but noted differences in soil productivity are present. Figures 13, 14 and 15 illustrate the principles.

Section 3.10 - Model Development

Since the surface temperatures as measured radiometrically by remote sensors can vary with many factors, a finite-difference simulation model was developed to isolate variables and estimate their magnitude of effect. The concept was to measure profile temperatures, insolation, etc. at one site and correlate the differences in variables which are present at a second site and are causing the differences in radiometric temperature. Using this spatial differencing approach also reduces the effects of atmospheric disturbances. The model (Chapter V) showed that the 50-cm soil temperature difference associated with water table depth differences between two sites was apparent as temperature differences at the surface. These surface differences were nearly constant in magnitude throughout the diurnal cycle. However, the difference was destroyed during predawn in areas having dense canopy covers. Therefore, remote measurements can be day or night, whenever the actual soil surface temperature related best to the radiometric temperature as measured with remote sensors if dense crop cover is not present. Soils with different moisture profiles differed in surface temperature variations during the diurnal cycle. This functional form of differences was changed less by variations in

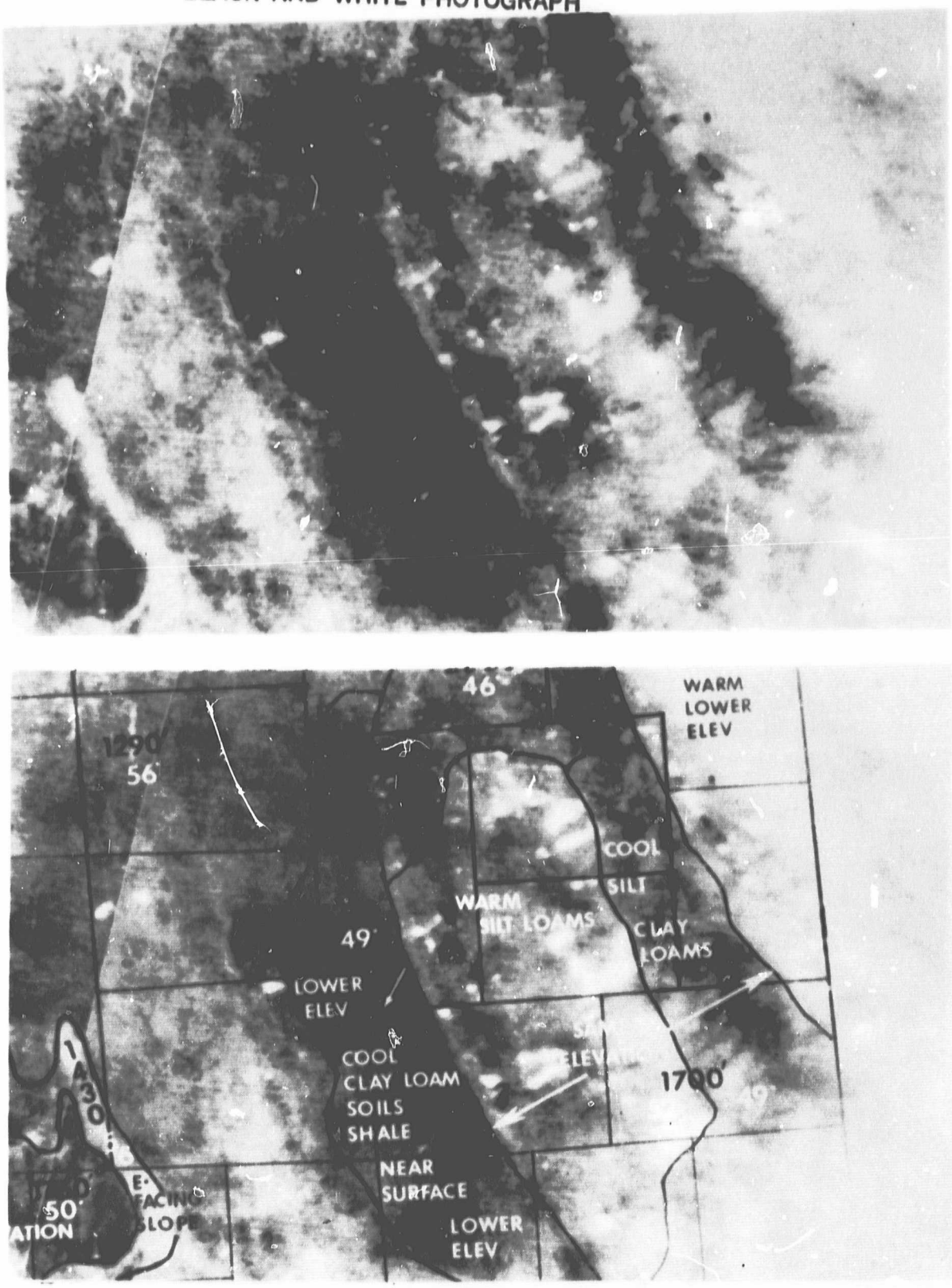

Figure 13. Predawn thermal infrared (HCMM) image for an area in east-central South Dakota (dark is cool).

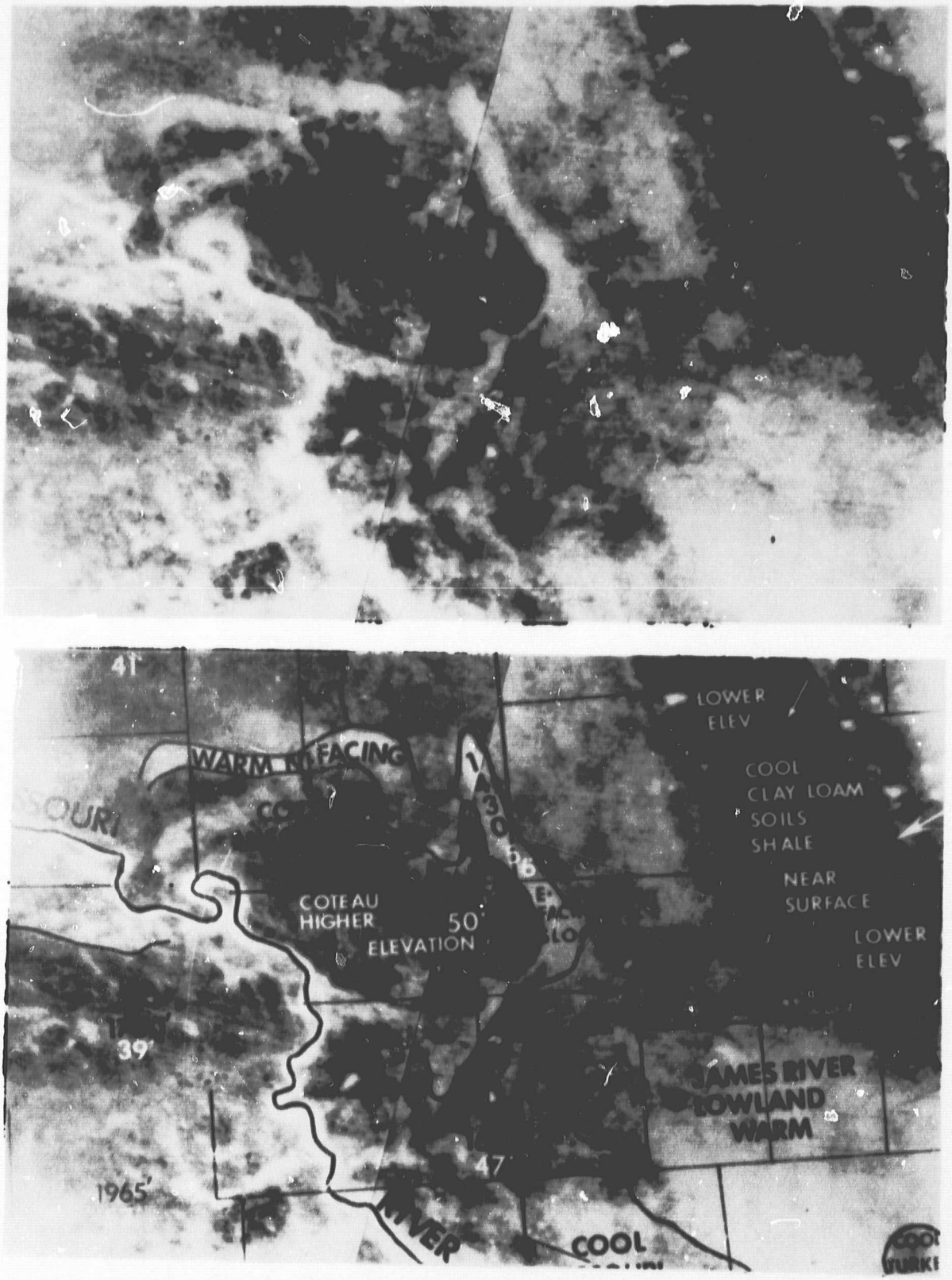

Figure 14. Enlarged area from Figure 13.

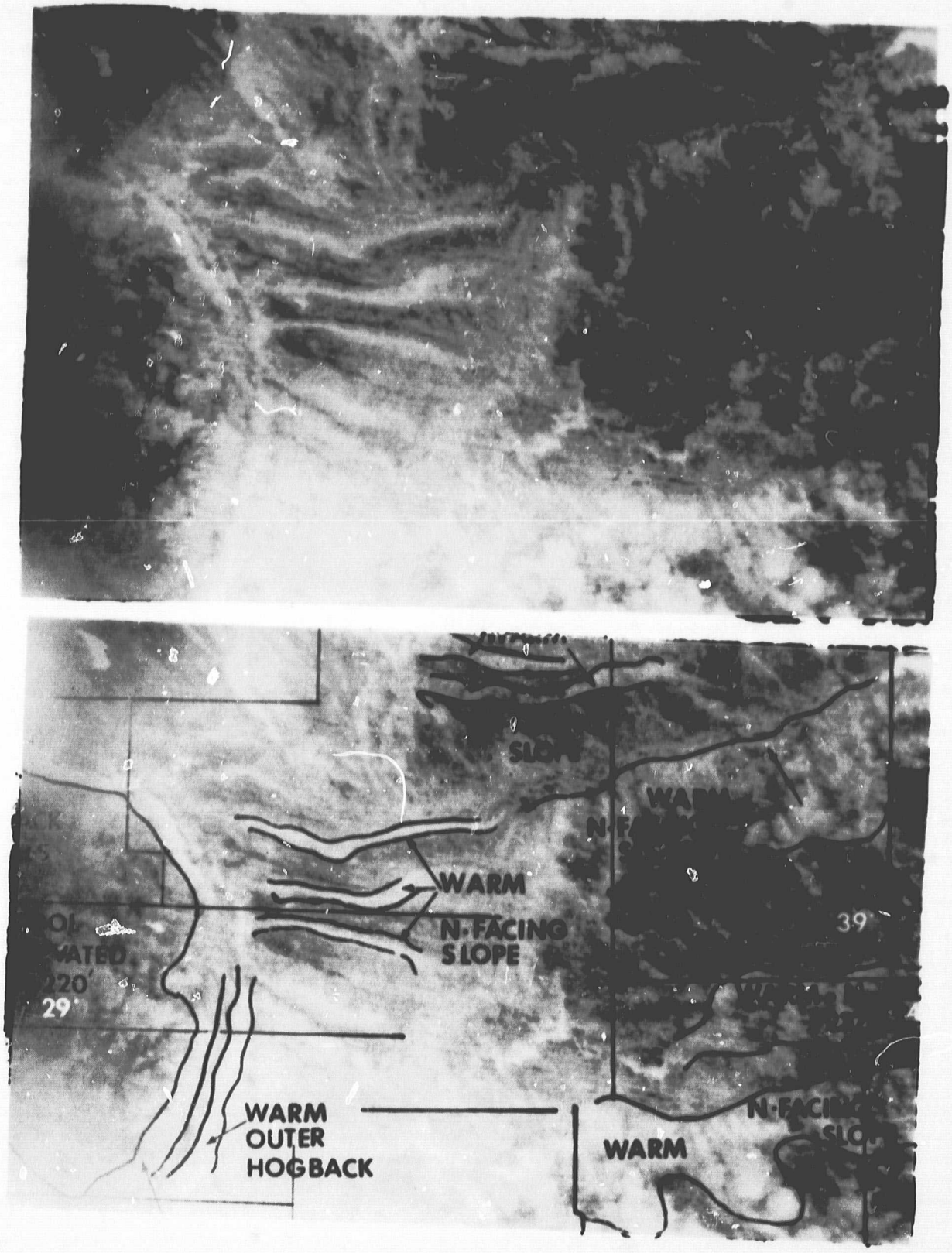

Figure 15. Predawn HCMM thermal infrared image of an area including the Black Hills of South Dakota (dark is cool).

canopy cover than was the functional form of the individual sites. Multiple pass satellite data should be acquired during daylight hours according to the model predictions for assessing temperature differences related to soil moisture. Model calculations using day minus night temperatures were not useful for assessing water table depths since the thermal inertial change was not within the diurnal damping depth. Either day or night data could be used for this relationship. If dense canopy cover was present, the timing of data collection was limited to day periods.

CHAPTER II: SOIL MOISTURE

Section 1: HCMM Detection of High Soil Moisture Areas. Heilman, J.L., and D. G. Moore. Remote Sensing of Environment II: 73-76.

Section 2. Remote Sensing of Canopy Temperature at Incomplete Cover. Heilman, J.L., W.E. Heilman, and D.G. Moore. Agronomy Journal 73: 403-406.

Section 3. Thermography for Estimating Near-Surface Soil Moisture Under Developing Crop Canopies. Heilman, J.L., and D.G. Moore. 1980. Journal of Applied Meteorology 19(3):324-328.

Section 4. Soil Moisture Applications of the Heat Capacity Mapping Mission. Heilman, J.L., and D.G. Moore. In Satellite Hydrology, ed. Deutsch, M., D.R. Wiesnet, and A. Rango. Proc. of Fith Annual William T. Pecora Memorial Symposium on Remote Sensing, Am. Water Resources Association, Minneapolis, Minn. (pp.371-377).

Section 5. Evaluating Near-Surface Soil Moisture Using Heat Capacity Mapping Mission (HCMM) Data. Heilman, J.L., and D.G. Moore. (Submitted to Remote Sensing of Environment).

HCMM DETECTION OF HIGH SOIL MOISTURE AREAS[1/]

J. L. Heilman and D. G. Moore

Remote Sensing Institute

South Dakota State University

Brookings, South Dakota 57007

[1/] Contribution No. SDSU-R[illegible] 79-10 from the Remote Sensing Institute, South Dakota State Uni[illegible]sity. Support was provided by NASA Contract No. NAS5-24206 and the State of South Dakota.

BACKGROUND

Thermal infrared detection and quantification of near-surface soil water content are based on relationships between surface soil temperature and soil moisture. Diurnal variations of surface soil temperature are related to soil thermal properties and meteorological factors such as solar radiation, air temperature, relative humidity, wind, etc. The meteorological factors represent the driving force for diurnal soil temperature variations. Thermal inertia (Jm^{-2} $sec^{-\frac{1}{2}}$ K^{-1}), defined as $(\lambda C)^{\frac{1}{2}}$ where $\lambda(Wm^{-1}$ $K^{-1})$ is thermal conductivity and $C(Jm^{-3}$ $K^{-1})$ is volumetric heat capacity, represents a soil's resistance to the driving force. Since λ and C increase with an increase of soil moisture, the resulting range of surface soil temperature will decrease.

When the soil surface is wet, evaporation is a major factor controlling surface heat loss. As the surface layer dries and the soil water supply cannot meet the evaporative demand, soil temperature is largely influenced by thermal inertia. Thus, the diurnal range of surface soil temperature can be an indication of soil water content. Idso et al. (1975) found a significant relationship between the diurnal range of surface soil temperature (bare soil) and surface soil water content, and reported that the relationship was a function of soil type. Pratt and Ellyett (1979) presented a method for estimating soil thermal properties for changes in composition, porosity, and moisture content. Although temperature versus water content relationships are complicated by vegetation, Heilman et al. (1978) demonstrated the

potential for estimating near-surface soil moisture from remote temperature measurements of crop canopies at incomplete cover.

One objective of NASA's Heat Capacity Mapping Mission (HCMM) is to evaluate the feasibility of using HCMM data to assess soil moisture effects by observing temperatures near the maximum and minimum of the diurnal temperature cycle. The satellite, which carries a two-channel radiometer (0.5 to 1.1 and 10.5 to 12.5 μm), collects data at 1:30 p.m. and 2:30 a.m. local time at mid latitudes with a repeat cycle of 5 or 16 days depending on latitude. Spatial resolutions are 0.5 x 0.5 km at nadir for the visible channel and 0.6 x 0.6 km at nadir for the thermal infrared channel. An example of HCMM detection of a region of high soil moisture is presented in the following discussion.

DISCUSSION

In early April 1978 heavy runoff from snowmelt and ice blockage caused significant flooding of alluvial areas in a portion of the Big Sioux River Basin in southeastern South Dakota (Figure 1). By mid-May, flood waters had receded, but an area of high soil moisture (at or near field capacity) remained. Soil moisture in the surrounding terrace soils was generally less than in the flood plain.

The high moisture area appeared warmer than surrounding areas on May 14 HCMM night thermal imagery (Figure 2) and cooler than surrounding areas on May 15 HCMM day thermal imagery (Figure 3). The temperature differences between alluvial and surrounding areas were probably the result of thermal inertia and evaporation differences associated with soil moisture differences. The high moisture area was not visible on Landsat imagery (Figure 4).

ORIGINAL PAGE
BLACK AND WHITE PHOTOGRAPH

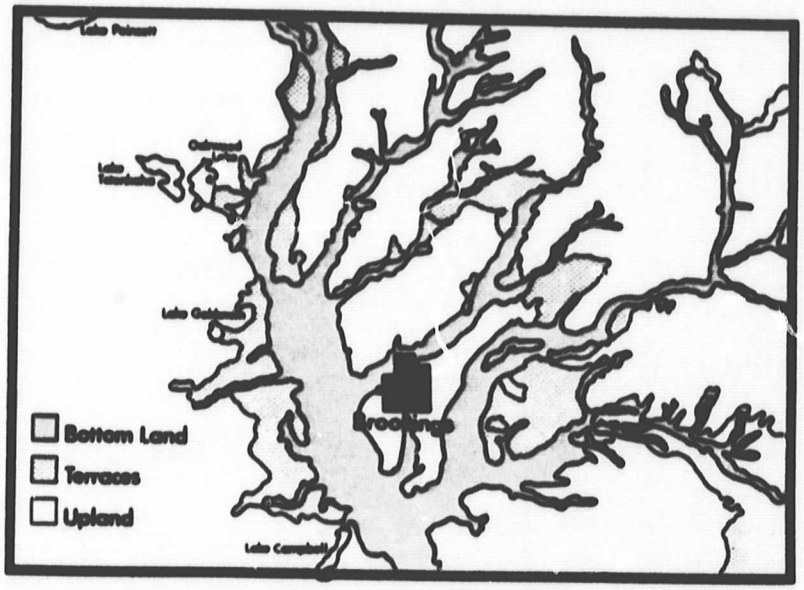

Fig. 1. Landform map of Brookings County, South Dakota, showing location of alluvial soils (bottomland) of the Big Sioux River Basin which were flooded in early April 1978.

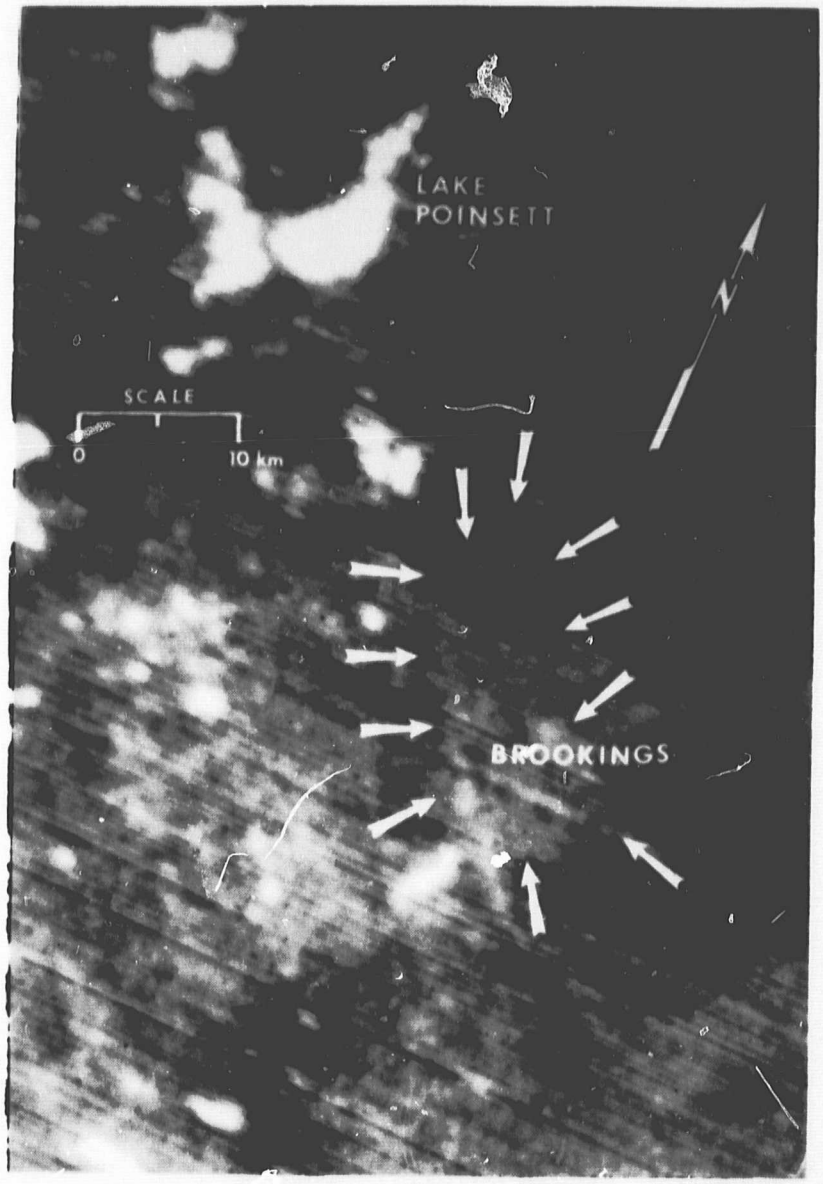

Fig. 2. Photographic enlargement of a May 14, 1978, night thermal infrared image (scene ID A-A0018-08420) showing a high soil moisture area (arrows) in southeastern South Dakota. Dark is cool.

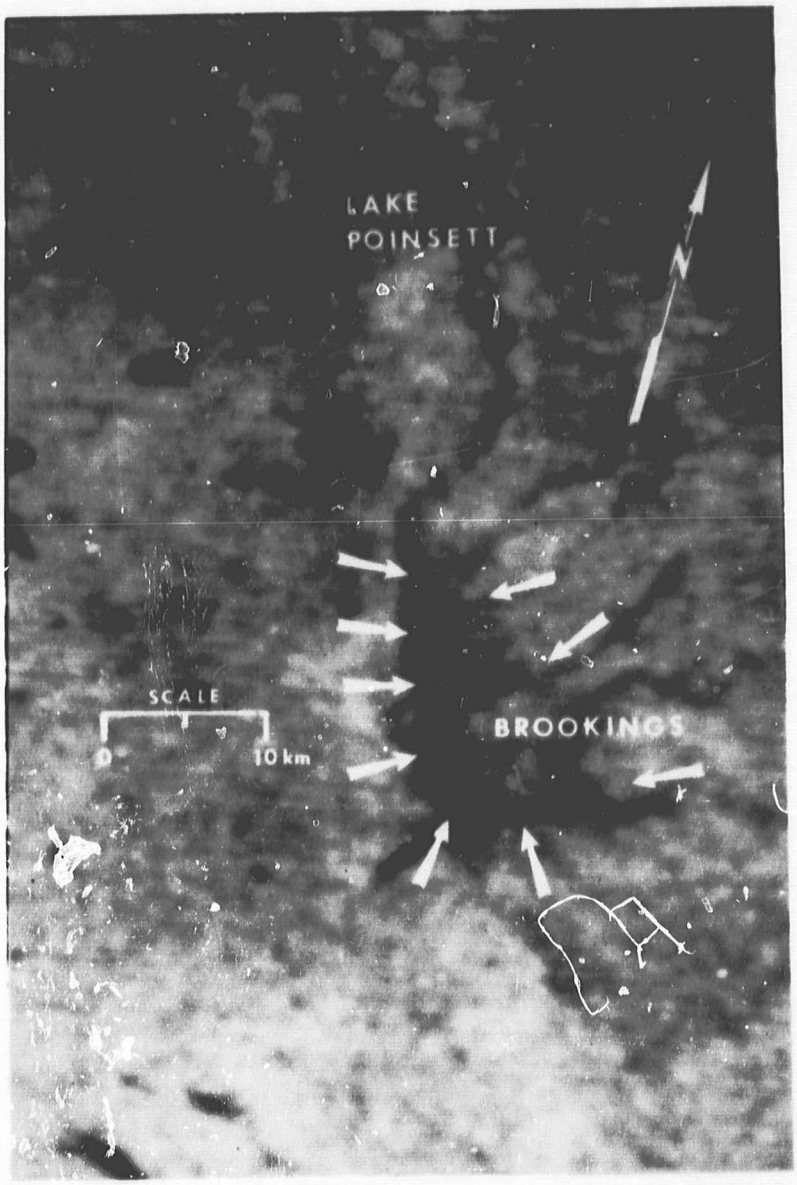

Fig. 3. Photographic enlargement of a May 15, 1978, day thermal infrared image (scene ID A-A0029-19575) showing a high soil moisture area (arrows) in southeastern South Dakota. Dark is cool.

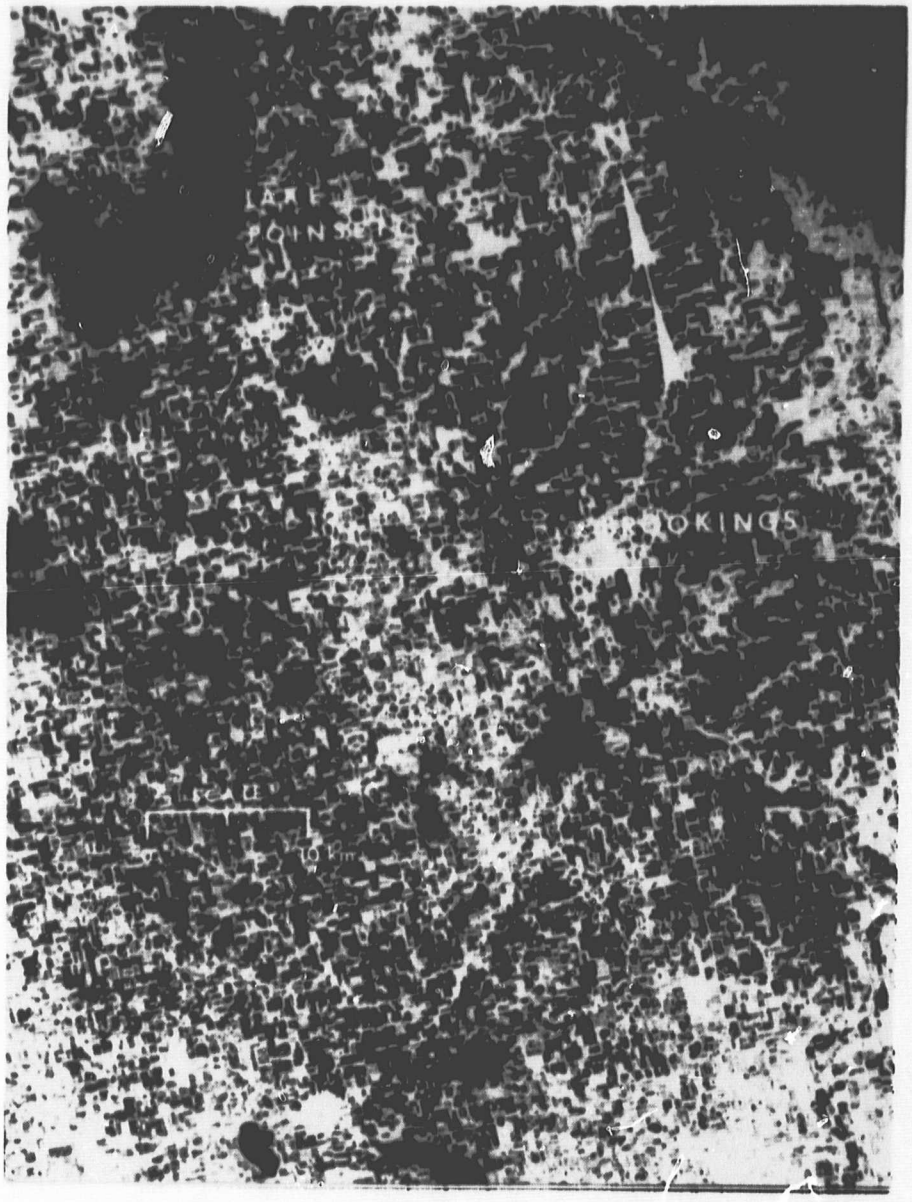

Fig. 4. Photographic enlargement of a May 13, 1978, Landsat MSS 7 image (scene ID E-21207-16083) of the same area shown in Fig. 2 and 3.

Although digital data were not available at the time of the writing of this article to quantify radiometric temperature differences associated with the soil moisture differences, results presented here demonstrated the superiority of HCMM thermal data acquired at the appropriate periods of the diurnal temperature cycle over Landsat data for assessing soil moisture differences. Final results from HCMM soil moisture investigations currently in progress will fully evaluate the utility of using HCMM and similar data for evaluating soil moisture from space.

REFERENCES

Heilman, J.L., Moore, D.G., and Beutler, G. (1978), HCMM Energy Budget Data as a Model Input for Assessing Regions of High Potential Groundwater Pollution, Interim Report No. SDSU-RSI-78-01, Remote Sensing Institute, South Dakota State University, to Goddard Space Flight Center. Contract No. NAS5-24206.

Idso, S.B., Schmugge, T.J., Jackson, R.D., and Reginato, R.J. (1975), The Utility of Surface Temperature Measurements for the Remote Sensing of Soil Water Status, J. Geophys. Res., 80:3044-3049.

Pratt, D.A., and Ellyett, C.D. (1979), The Thermal Inertia Approach to Mapping of Soil Moisture and Geology, Remote Sens. Environ. 8:151-168.

REMOTE SENSING OF CANOPY TEMPERATURE AT INCOMPLETE COVER[1/]

J.L. Heilman, W.E. Heilman, and D.G. Moore[2/]

1/ Contribution No. SDSU-RSI-J-80-05 from the Remote Sensing Institute, South Dakota State University, Brookings, SD 57007. Research supported in part by NASA under contract no. NAS5-24206, and the State of South Dakota.

2/ Associate Professor, Department of Soil and Crop Sciences, and Remote Sensing Center, Texas A&M University, College Station, Texas 77843; Graduate Assistant, Department of Physics, Iowa State University, Ames, Iowa 50010; Assistant Director, Remote Sensing Institute, South Dakota State University, Brookings, South Dakota 57007.

ABSTRACT

A field study was conducted in a barley (*Hordeum vulgare L.*) canopy to assess the potential for extracting canopy temperature information from nadir radiometric measurements at incomplete cover. Composite temperatures consisting of emitted and reflected longwave radiation from the barley and the soil background were measured by a nadir-viewing infrared radiometer. Canopy temperatures were measured by an infrared radiometer at a 30^{o} angle from the horizontal. Soil temperatures were measured with thermocouples.

Composite temperatures were 0.5 to 11.5 C higher than canopy temperatures with the largest difference occurring at low canopy cover. The correlation between composite and canopy temperature for data acquired throughout the growing season was not significant. A model which considered emitted radiation from both the canopy and the soil background, and which included reflected longwave sky irradiance was used to predict crop temperatures from nadir measurements. Predicted temperatures agreed with observed values (r^2 = 0.88), and the prediction accuracy was independent of canopy cover. When emissivity corrections were not applied, prediction accuracy varied with percent cover with largest errors occurring at low cover. Prediction accuracy also varied with canopy cover when appropriate emissivities were used but sky irradiance was ignored. Results indicate that canopy temperatures can be estimated from nadir measurements at incomplete cover if percent cover, soil temperature, soil and canopy emissivities, and sky irradiance are known.

INTRODUCTION

Remotely-sensed surface temperatures can be useful for many agricultural applications including evapotranspiration modeling, soil moisture detection, plant stress detection, yield prediction, and irrigation scheduling. Most studies which have used remote measurements have been restricted to bare soils or fully developed crop canopies because of the complexities involved in interpreting thermal data at less than full cover.

Much of the complexity results because the remote sensing instrument measures emitted and reflected radiation from vegetation and soil which generally have different temperatures and emissivities. Hatfield (1979) reported that differences between angular and vertical infrared thermometer measurements of canopy temperatures were greatest at 20 to 50% cover and decreased as canopy density increased. He speculated that differences were enhanced by emissivity variations. Millard et al. (1980) found that for canopies covering at least 85% of the soil surface, airborne measurements of plant temperatures differed from ground measurements by less than 2 C. At 50% cover, differences were as large as 9 C. Investigators have shown that even at full cover thermal radiance from the soil surface can affect remote temperature measurements of crop canopies (Blad and Rosenberg, 1976).

Incomplete plant canopies are important remote sensing targets because of the potential benefits arising from early assessment of crop condition. Jackson et al. (1979) presented a model for extracting canopy temperature information from a composite of soil and plant

temperatures measured by a sensor scanning perpendicular to canopy rows. They found that if a critical scan angle (determined from reflectance measurements) was exceeded, the temperature obtained from the scanner was that of sunlit vegetation. They also found that the extraction process was difficult for canopies having low percent cover.

We evaluated relationships among percent cover, soil temperature, and radiometric measurements of canopy temperature, and used a model of emitted canopy and soil background radiance and reflected sky irradiance to assess the potential for extracting canopy temperatures from nadir radiometric measurements. Effects of neglecting emissivity variations and sky irradiance in the model calculations were evaluated.

MATERIALS AND METHODS

Experiments were conducted on a 25 m $\times$ 300 m field of Volga loam (fine-loamy over sandy or sandy-skeletal, mixed (calcareous), frigid, Cumulic Haplaquoll) at the South Dakota State University Agricultural Engineering Research Farm located 8 km south of Brookings, South Dakota. Larker barley (*Hordeum vulgare L.*) was planted in the field at 15-cm row spacing (north-south rows) at a population of 2.5 million plants ha^{-1}. The barley was not irrigated. Surface roughness of the soil was minimal.

Surface soil temperatures (approximately 1 mm below the soil surface) were measured with copper-constantan thermocouples at two locations (A and B) within the field. For each location, three thermocouples were wired in parallel to obtain an average measurement of shaded and sunlit soil which approximated surface temperature. For bare soil, thermocouple measurements were within 1.0 C of radiometric surface temperatures

(corrected for emissivity and sky irradiance) measured with a precision radiation thermometer (Model PRT-5, Barnes Engineering Company).[3/] Composite temperatures consisting of radiance contributions from the soil surface and the barley were measured at both locations at 1330 Local Standard Time (LST) on clear days at a vertical position (zero degree look angle measured from nadir) 2 m above the canopy. The temperature resolution of the 20^{o} field of view PRT was ±0.5 C in the 8-14 μm wavelength interval. Canopy temperatures were measured with the PRT-5 at a height of 1 m above the canopy and a look angle of 30^{o} from the horizontal (Millard et al., 1980) pointing to the east and the west (perpendicular to row direction). At that angle and direction, radiance contributions from the soil were minimized (Hatfield, 1979). Canopy temperatures were corrected for emissivity and sky irradiance using a canopy emissivity of 0.98.

Emissivities of the canopy at full cover were measured using a procedure similar to that described by Fuchs and Tanner (1966). We used a painted aluminum plate with an emissivity of 0.52 rather than an anodized plate to determine sky irradiance (Blad and Rosenberg, 1976). Soil emissivities were measured on a bare soil plot adjacent to the barley field.

Soil water contents (0 to 4-cm layer) for each location were determined gravimetrically on soil samples collected at the time of the temperature measurements. Percent cover was determined using 35 mm color infrared slides of the canopy (photographed from a vertical position approximately 1 m above the canopy) projected on a random dot grid.

[3/] Mention of trade name does not imply endorsement of a particular product or company.

Figure 1 shows seasonal trends in percent cover of the barley canopy.

RESULTS AND DISCUSSION

In the discussion that follows, composite temperature refers to apparent temperatures measured by the nadir-viewing PRT-5. Canopy temperature refers to temperature measured by the PRT-5 at a 30^{0} angle from the horizontal.

During the investigation, composite temperatures were 0.5 to 11.5 C higher and surface soil temperatures 1.5 to 20 C higher than canopy temperatures (Figure 2). As expected, differences between composite and canopy temperature decreased as canopy cover increased and less emitted radiation from the warm soil background was detected by the radiometer. The correlation between composite and canopy temperature was nonsignificant ($r = 0.41$).

Millard et al. (1980) found that errors from assuming nadir-viewing thermal scanner measurements represented actual canopy temperature were a linear function of canopy cover. We found a highly significant linear relationship ($r^2 = 0.52$) between the composite-canopy temperature difference and percent cover (Figure 3). However, the considerable scatter in our data suggests that it may not be possible to assess errors in determining canopy temperature using only canopy cover information as Millard et al. (1980) suggested.

We assumed the longwave radiation flux from a canopy and the soil background could be approximated by the relationship

$$R = f_c\varepsilon_c\sigma T_c^4 + (1-f_c)\,\varepsilon_s\sigma T_s^4 + f_c(1-\varepsilon_c)B^* + (1-f_c)(1-\varepsilon_s)B^* \qquad [1]$$

where $R(W\ m^{-2})$ is longwave flux, f_c is percent cover of the canopy

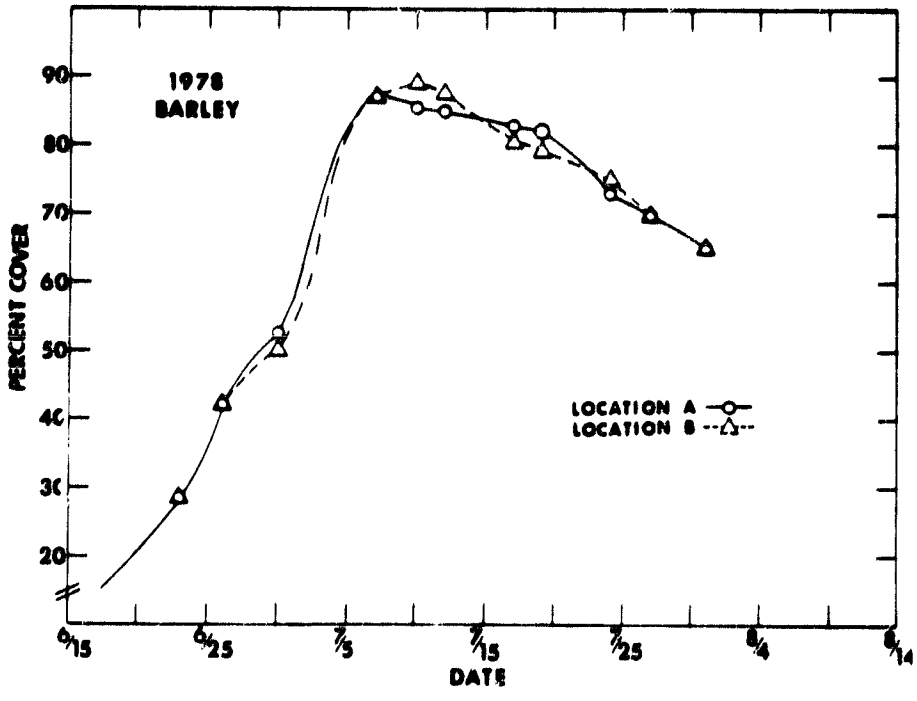

Figure 1. Seasonal variations in percent cover of the barley canopy. Jointing and heading occurred on 16 June and 19 July, respectively.

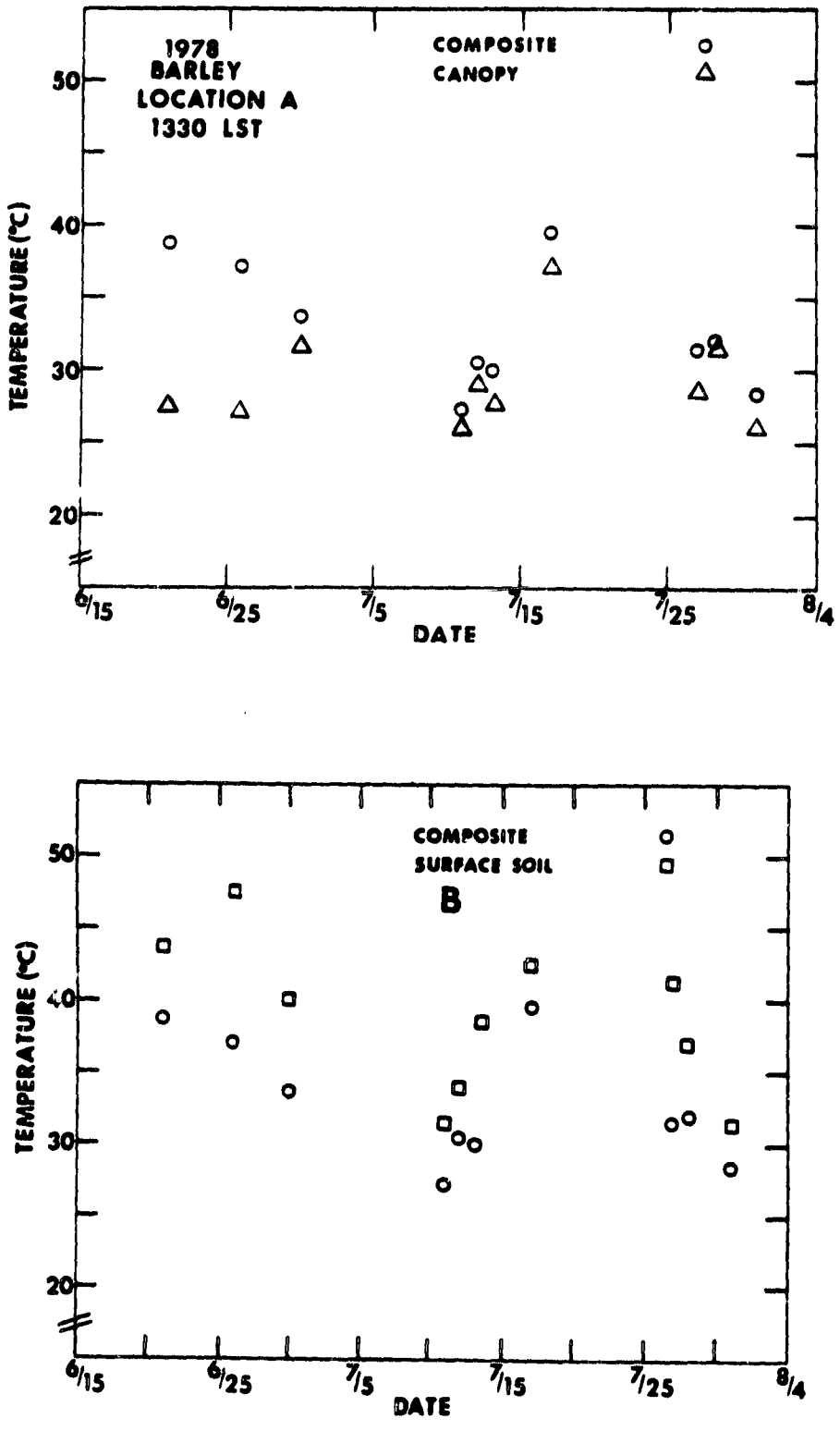

Figure 2. Comparison of composite temperatures with canopy temperature (A), and surface soil temperature (B) at 1330 LST. Data are from location A.

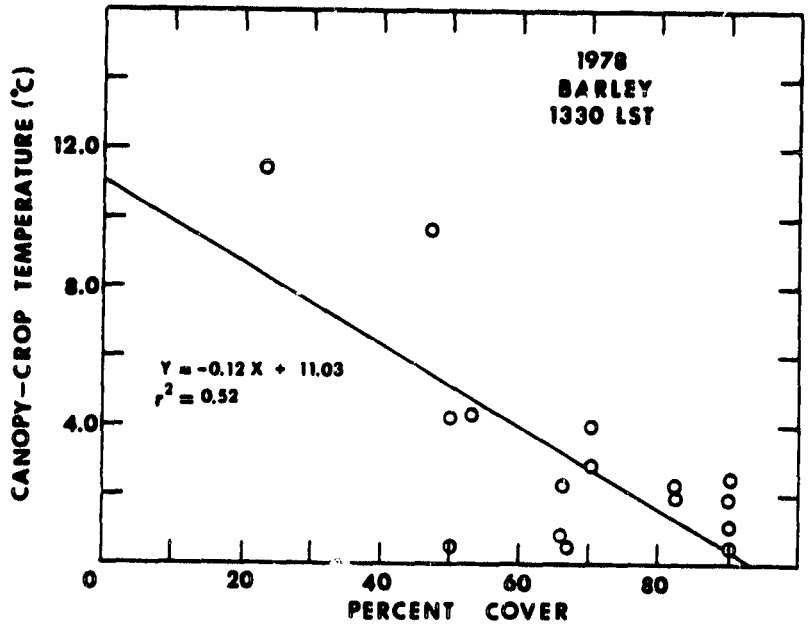

Figure 3. Composite-canopy temperature difference as a function of percent cover.

expressed as a fraction, ε_c is canopy emissivity, ε_s is soil emissivity, T_c (K) is canopy temperature, T_s (K) is surface soil temperature, σ (5.67×10^{-8} W $m^{-2}K^{-4}$) is the Stefan-Boltzmann constant, and B* (W m^{-2}) is longwave sky irradiance. The first two terms on the right-hand side of equation [1] represent longwave radiation emitted from the canopy and exposed soil background, respectively. The last two terms represent longwave sky irradiance between the canopy and the soil is ignored in equation [1]. Equation [1] also does not partition fractions of shaded and sunlit leaves, or fractions of exposed soil background which are shaded and sunlit. Canopy temperature can be expressed by rearranging equation [1] to give

$$T_c = \frac{R-(1-f_c)\varepsilon_x\sigma T_x^4-f_c(1-\varepsilon_c)B^*-(1-f_c)(1-\varepsilon_x)B^*}{f_c\varepsilon_c\sigma}^{\frac{1}{4}} \qquad [2]$$

We compared observed values of T_c with values predicted using equation [2] and measured values of f_c, T_x and B* (Fig. 4). R was calculated from measurements of composite temperature using the relationship $R = \sigma T_{comp}^4$ where T_{comp} is composite temperature. A measured value of 0.98 was used for ε_c. Soil emissivity varied with water content as shown in Figure 5. Linear regression analysis of predicted versus observed canopy temperature yielded a slope of 1.04, an intercept of -0.53, and a r^2 of 0.88. Differences of observed from predicted values ranged from -1184 to +2.50 C. The prediction accuracy of equation [2] was independent of canopy cover. The correlation between the predicted minus observed canopy temperature difference and percent cover was 0.26 (non-significant).

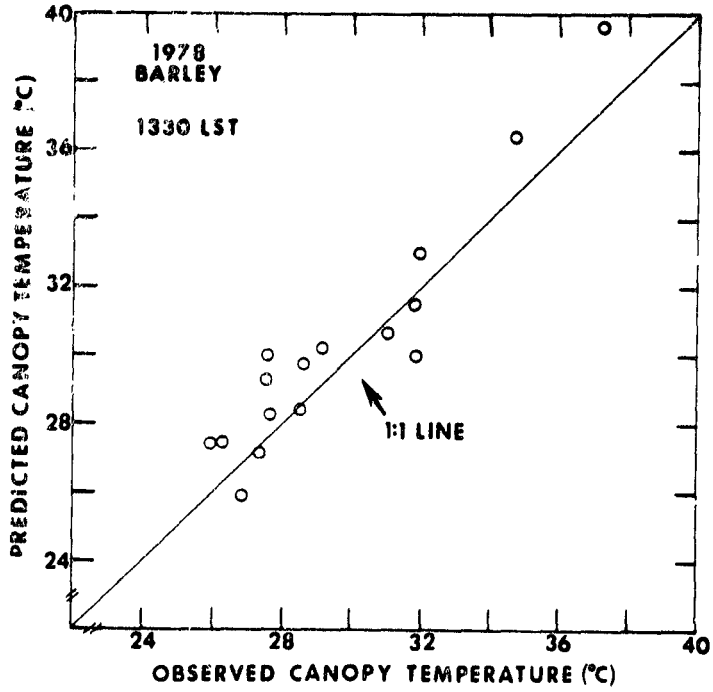

Figure 4. Comparison of predicted and observed canopy temperatures. Canopy temperatures were predicted using equation (2).

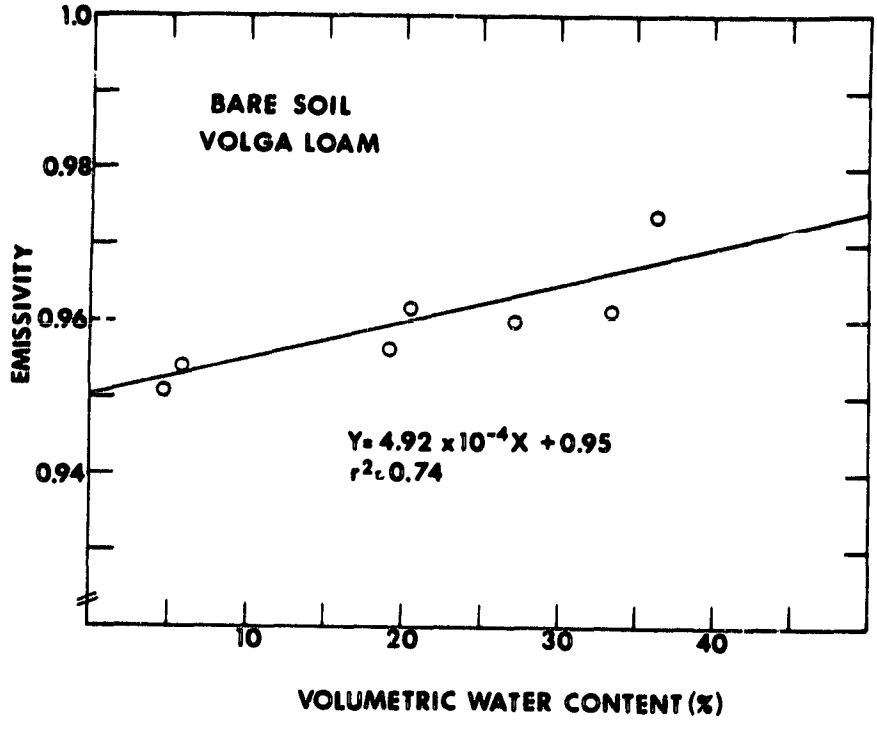

Figure 5. Relationship between measured soil emissivity and volumetric water content in the 0-4 cm layer.

Many investigators have discussed the importance of correcting radiometric data for emissivity variations. Bartholic et al. (1972) reported temperature errors ranging from 1.9 C for bare, dry soil to 0.8 for cotton which arose from assuming an emissivity of 1. Jackson et al. (1977) reported a nearly constant error of 1.7 C for wheat temperature by not correcting for emissivity. Similarly, Sutherland and Bartholic (1977) found that assuming an emissivity of 1 produced errors on the order of 1.0 C for complete canopies.

When emissivities of 1 were used for the soil and canopy in equation [2], predicted canopy temperatures ranges from 6.43 C lower to 1.70 C higher than observed values. Linear regression analysis of predicted versus observed canopy temperatures yielded a clope of 1.14, an intercept of -5.08, and a r^2 of 0.76. Prediction accuracy varied with canopy cover as shown in Figure 6 with largest errors occurring at low percent cover when radiance contributions from the soil were at a maximum. The magnitude of the error from assuming emissivities of 1 depends not only on canopy cover, but also on soil type and water content. Soil emissivities ranging from 0.90 for dry sand to 0.99 for loamy soils have been reported (Sellers, 1972; Sutherland and Bartholic, 1977; Taylor, 1979).

Prediction accuracy when measured emissivities were used in equation [2] but the B* terms were neglected also changed with canopy cover (Fig. 6). The sum of the reflected B* components ranged from 13.2 $W.m^{-2}$ at 23% cover to 5.6 $W\ m^{-2}$ at 90% cover. Differences of observed from predicted canopy temperatures ranged from 0.8 to 10.7 C. Regression analysis of predicted versus observed canopy temperatures gave a slope of 0.66, an intercept of 7.74 and a r^2 of 0.66.

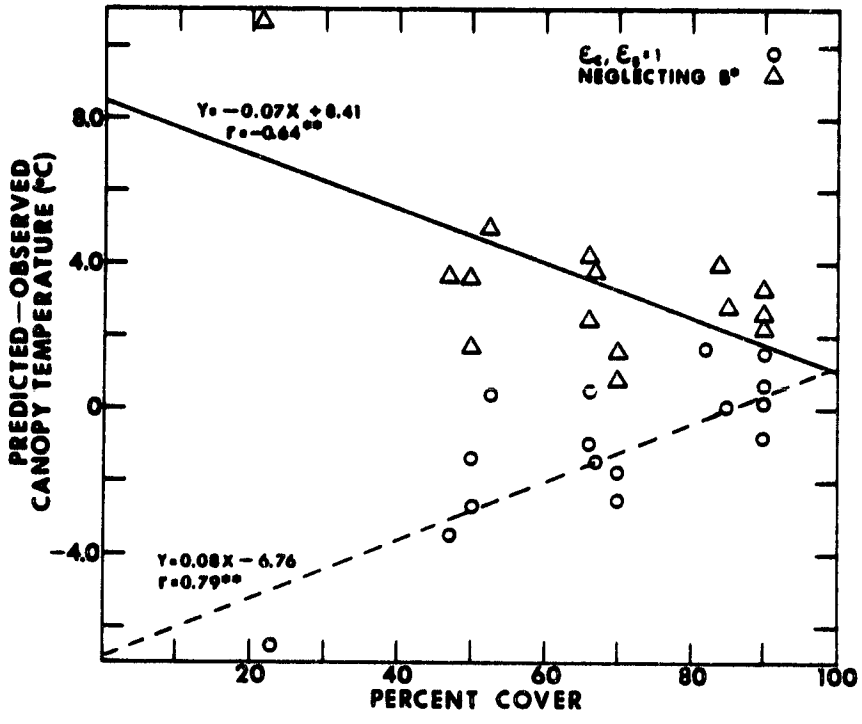

Figure 6. Predicted minus observed canopy temperatures as a function of percent cover when values of 1 were used for ϵ_c and ϵ_s (circles); and when measured values of ϵ_c and ϵ_s were used, but sky irradiance terms were neglected (triangles).

This study has shown that canopy temperatures at incomplete cover can be estimated using nadir-viewing radiometers if appropriate considerations are given to soil background radiance, emissivity and sky irradiance. Techniques are available for estimating some of the inputs to the canopy temperature model. Canopy cover can potentially be estimated from remote sensing data (Heilman et al., 1977; Tucker et al., 1978; Jackson et al., 1979). Emissivity data can be obtained from the literature for a wide range of soil types. Sky irradiance can usually be estimated from prevailing sky conditions (Soer, 1980). However, under certain conditions, sky irradiance can be highly variable and may require direct measurement (Conaway and van Bavel, 1967). Estimating the radiance contribution from the soil background remains a difficult problem. Models have been developed for estimating surface and near surface soil temperature (Behroozi-Lar et al., 1975; Pratt and Elyett, 1979; Meyer et al., 1975; van Bavel and Hillel, 1976) and they can potentially be extended to crop canopies.

LITERATURE CITED

Bartholic, J.F., L.N. Namken, and C.L. Wiegand. 1972. Aerial thermal scanner to determine temperatures of soils and of crop canopies differing in water stress. Agron. J. 64:603-608.

Behroozi-Lar, M., B.K. Huang, and H.D. Bowen. 1975. Simulation of soil temperature profile using PCAP. Paper No. 75-1037, 1975 Annual Meeting American Society of Agricultural Engineers.

Blad, B.L. and N.J. Rosenberg. 1976. Measurement of crop temperatures by leaf thermocouple, infrared thermometry and remotely sensed thermal imagery. Agron. J. 68:635-641.

Conaway, J. and C.H.M. van Bavel. 1967. Radiometric surface temperature measurements and fluctuations in sky radiant emittance in the 600 to 1300 cm^{-1} waveband. Agron. J. 59:389-390.

Fuchs, M. and C.B. Tanner. 1966. Infrared thermometry of vegetation. Argon. J. 58:596-601.

Hatfield, J.L. 1979. Canopy temperatures: the usefulness and reliability of remote measurements. Agron. J. 71:889-892.

Heilman, J.L., E.T. Kanemasu, J.O. Bagley, and V.P. Rasmussen. 1977. Evaluating soil moisture and yield of winter wheat in the Great Plains using Landsat data. Remote Sensing Environ. 6:315-326.

Jackson, R.D., R.J. Reginato, P.J. Pinter, Jr., and S.B. Idso. 1979. Plant canopy information extraction from composite scene reflectance of row crops. Appl. Optics. 18:3775-3782.

Meyer, C.R., J.A. Tunheim, and D.G. Moore. 1975. Heat-flow temperature model for remotely mapping near-surface water tables by thermography. S.D. Academy of Science. 54:23-32.

Millard, J.P., R.J. Reginato, R.C. Goettelman, S.B. Idso, R.D. Jackson, and M.J. LeRoy. 1980. Experimental relations between airborne and ground measured wheat canopy temperatures. Photogram. Eng. and Remote Sensing. 46:221-224.

Pratt, D.A. and C.D. Ellyett. 1979. The thermal inertia approach to mapping soil moisture and geology. Remote Sensing Environ. 8:151-168.

Sellers, W.D. 1972. Physical Climatology. University of Chicago Press, Chicago.

Soer, G.J.R. 1980. Estimation of regional evapotranspiration and soil moisture conditions using remotely sensed crop surface temperatures. Remote Sensing Environ. 9:27-45.

Sutherland, R.A. and J.F. Bartholic. 1977. Significance of vegetation in interpreting thermal radiation from a terrestrial surface. J. Appl. Meteorol. 16:759-763.

Taylor, S.E. 1979. Measured emissivity of soils in the southeast United States. Remote Sensing Environ. 8:359-364.

Tucker, C.J. 1979. Red and photographic infrared linear combination for monitoring vegetation. Remote Sensing Environ. 8:127-150.

van Bavel, C.H.M., and D.I. Hillel. 1976. Calculating potential and actual evaporation from a bare soil surface by simulation of concurrent flow of water and heat. Agric. Meteorol. 17:453-476.

THERMOGRAPHY FOR ESTIMATING NEAR-SURFACE SOIL MOISTURE UNDER DEVELOPING CROP CANOPIES[1/]

J. L. Heilman and D. G. Moore

1/ Contribution No. SDSU-RSI-J-79-11 from the Remote Sensing Institute, South Dakota State University. This investigation was supported by NASA under Contract NAS5-24206 and the State of South Dakota.

ABSTRACT

Previous investigations of thermal infrared techniques using remote sensors (thermography) for estimating soil water content have been limited primarily to bare soil. Ground-based and aircraft investigations were conducted to evaluate the potential for extending the thermography to approach to developing crop canopies. A significant exponential relationship was found between the volumetric soil water content in the 0-4 cm soil layer and the diurnal difference between surface soil temperature measured at 0230 and 1330 LST (satellite overpass times of NASA's Heat Capacity Mapping Mission - HCMM). Surface soil temperatures were estimated using minimum air temperature, percent cover of the canopy and remote measurements of canopy temperature. Results of the investigation demonstrated that thermography can potentially be used to estimate soil temperature and soil moisture throughout a complete growing season for a number of different crops and soils.

INTRODUCTION

Remotely sensed surface temperatures have been investigated for estimating soil water content (Idso et al., 1975; Idso and Ehler, 1976; Schmugge et al., 1978). Soil water contents have been related to differences between the daily maximum and minimum soil or crop temperatures. The investigations generally have been limited to bare soils or fully developed crop canopies because of difficulties in

interpreting thermal data at less than full cover when significant emittance contributions from both soil and vegetation occur. The ability to derive useful information from remote temperature measurements for conditions other than bare soil or fully developed canopies would greatly expand the usefulness of the remote sensing techniques.

Investigators have shown that even at full cover, thermal emittance from the soil surface can affect remote temperature measurements of crop canopies (Blad and Rosenberg, 1976). Thus, surface soil temperatures can potentially be estimated from remote measurements of land surface emittance where a crop canopy is the primary source of radiation.

We conducted a ground based and aircraft investigation to evaluate the potential for estimating soil surface temperature and soil moisture from measurements of total area emittance at various stages of crop canopy development. The investigation was conducted to examine data collected during times of the diurnal temperature cycle corresponding to data collection by NASA's Heat Capacity Mapping Mission (HCMM), launched in April 1978. The satellite, which carries a two-channel radiometer (0.5-1.1 and 10.5-12.5 μm) in a sun-synchronous orbit, collects data at midlatitudes at approximately 0230 and 1330 LST during the diurnal cycle with repeat coverage of 5 or 16 days dependings on latitude.

MATERIALS AND METHODS

Plot Study

Experiments were conducted on a 25 m x 300 m field of Volga loam (fine, loamy over sandy, mixed (calcarious), frigid, Cumulic Haplaquoll)

at the South Dakota State University Agricultural Engineering Research Farm located 8 km south of Brookings, South Dakota. Larker barley (Hordeum vulgare L.) was planted in the field at 15 cm row spacings (north-south rows) and a population of 2.5 million plants ha^{-1}. Rainfall in the Brookings area averages 558 mm $year^{-1}$. No supplemental water was applied to the barley. Surface roughness of the soil was minimal.

Surface soil temperatures (1 mm below the soil surface) were measured with copper-constantan thermocouples at two locations (A and B) within the field. For each location, three thermocouples were wired in parallel to obtain an average measurement which approximated surface temperature. Apparent canopy temperatures consisting of emittance contributions from the soil surface and the barley (shaded and sunlit leaves) were measured with a portable infrared radiometer (Model PRT-5, Barnes Engineering Co.) at a vertical position (zero degree look angle measured from nadir) at a height of 2 m above the canopy. The temperature resolution of the 20^{o} field of view PRT-5 was $\pm 0.5^{o}$ C in the 8-14 μm wavelength interval. Apparent crop temperatures were measured with the PRT-5 at a height of 1 m above the canopy and a look angle of $\sim 60^{o}$ to minimize emittance contributions from the soil. Temperatures were measured at 0230 and 1330 LST.

The temperatures measured with the PRT-5 were not corrected for emissivity. Emissivities, determined using a procedure similar to that described by Fuchs and Tanner (1966), ranged from 0.96 for bare, dry soil to 0.98 for the fully developed barley canopy. For the range of temperatures and percent cover encountered, the maximum error from not correcting for emissivity was 1.5^{o} C.

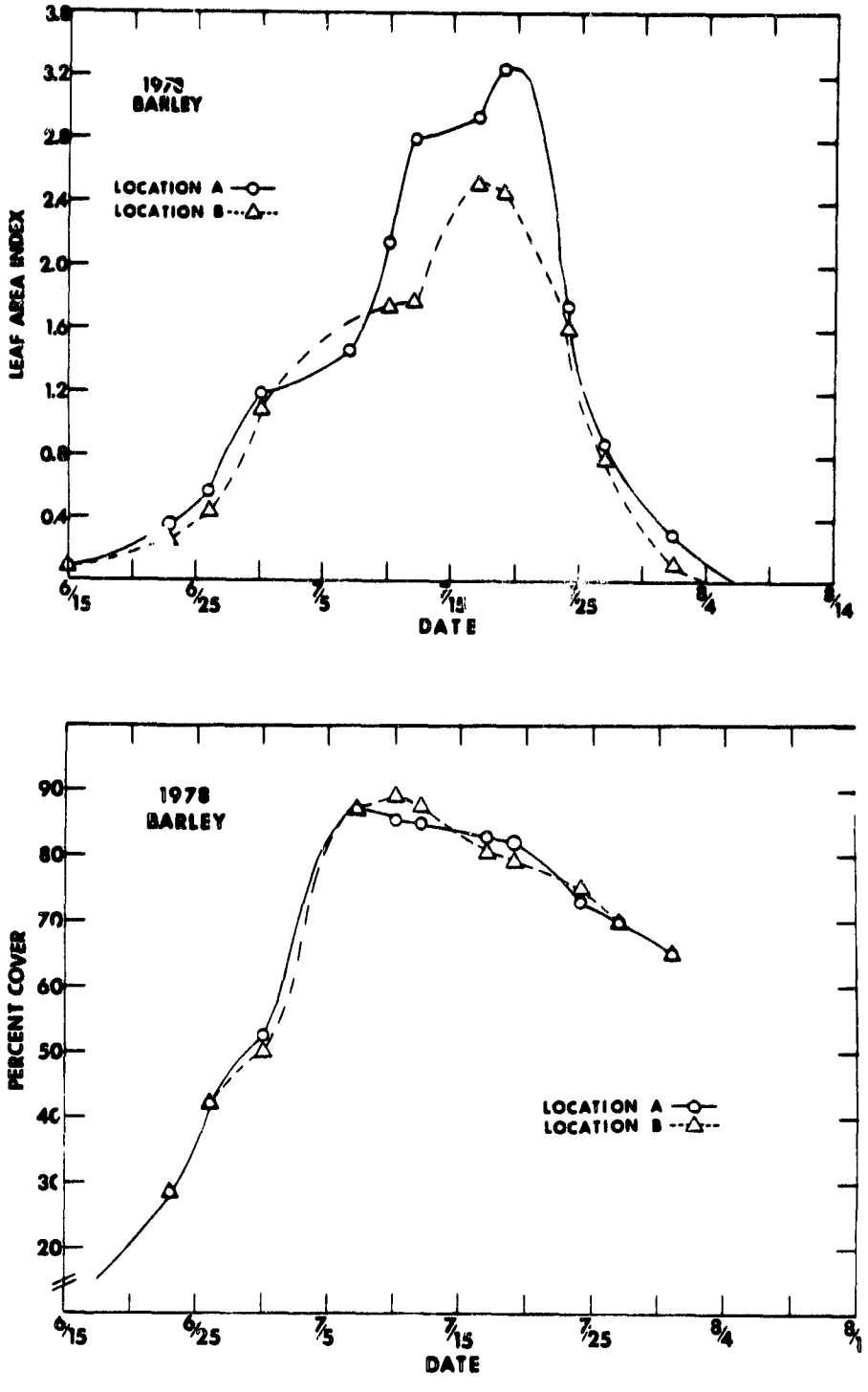

Fig. 1. Seasonal variations in leaf area index (A) and percent cover (B) of the barley canopy. Jointing and heading occurred on 16 June and 19 July, respectively.

Soil water contents (0-4 cm layer) for each location were determined gravimetrically on soil samples collected at the time of the temperature measurements. The average of soil water contents measured at 0230 and 1330 LST was used to represent the 24 h average. Jackson et al. (1976) reported that the average of the daily maximum and minimum water content closely approximated the 24 h average.

Temperature and soil water content measurements were initiated when the canopy cover reached 30%. Data were collected for 22 dates during the 45-day investigation.

Plant samples for determining leaf area index (leaf area/soil area) were taken every 5-7 days. Leaf areas (green leaves only) were measured with an optical planimeter (Lambda Instrument Corp.). Percent cover was determined using 35 mm color infrared slides of the canopy (photographed from a vertical position ~1 m above the canopy) projected on a random dot grid. Daily values of lead area index (LAI) and percent cover were estimated from graphs of observed LAI and percent cover versus date (Fig. 1). We did not estimate percentages of shaded and sunlit leaves, or percentages of shaded and sunlit soil. Maximum and minimum air temperatures were obtained from the Brookings National Weather Service Station (~1s km from the research site). All data were subjected to regression analyses.

Aircraft Study

Apparent canopy temperatures of corn, soybean, millet and pasture were collected along a 24 km flight line northwest of Brookings by a quantitative thermal scanner (Daedalus Enterprises, Inc., Ann Arbor,

Michigan) flown in the Remote Sensing Institute's twin-engine Beechcraft at an altitude of 3650 m above ground level. The 1.6 mrad scanner detector has a neΔt of 0.5^{o} C. Data were collected at 1330 and 0230 LST on 5 and 6 September 1978. Scanner data were not corrected for atmospheric attenuation of emissivity variations. Sky conditions were clear for all flights. Errors from neglecting emissivity variations and atmospheric effects were <1^{o} C.

Soil water contents (0-4 cm layer) were gravimetrically sampled in each of the fields at the time of the aircraft overflights. Percent cover was estimated using the same procedure used in the plot study. Data from the aircraft study were used to test the predictive equations developed from the plot study on barley.

RESULTS AND DISCUSSION

Soil Water Content Versus Temperature Relationships

The amplitude of the diurnal soil surface temperature wave is a function of thermal inertia and meteorological factors (solar radiation, air temperature, humidity, etc.) Thermal inertia - an indication of a soil's resistance to temperature change - is defined as $pc\lambda^{1/2}$, where p is density, c specific heat and λ thermal conductivity. Since p, c and λ of a soil increase as soil water content increases, the resulting amplitude of the diurnal temperature wave decreases.

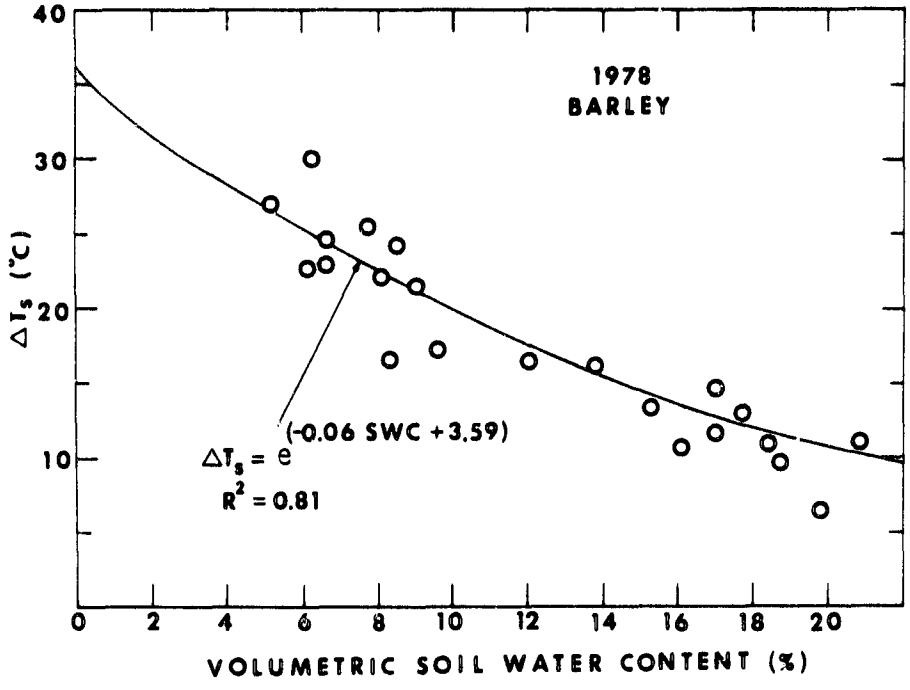

Fig. 2. Relationship of the different (ΔT_s) between soil surface temperatures measured at 1330 and 0230 LST and the average 24 h volumetric soil water content (SWC) in the 0 to 4 cm layer of the profile.

When the soil surface is wet, evaporation is a major factor controlling surface heat loss. After the surface layer dries and the soil water supply cannot meet the evaporative demand, surface heat loss is by conductive transfer (soil heat flux) and is largely influenced by thermal inertia. Nocturnal cooling is highly related to thermal inertia. Thus, the diurnal surface temperature range can be an indication of soil water content. Idso et al. (1975) found a linear relationship between the diurnal range of surface soil temperatures and soil water content in the 0-4 cm layer of soil, and reported that the temperature versus water content relationship was a function of soil type. However, they also found that if soil water content was expressed in units of pressure potential, this dependence was minimal.

Vegetation cover alters the solar radiation at the soil surface and thus affects soil evaporation and soil temperatures. Therefore, dynamic growth and development of vegetation would be expected to complicate the temperature versus water content relationship.

Initially, we evaluated the relationship of day minus night surface soil temperatures (ΔT_s) versus soil water content at various stages of canopy development. Leaf area index and percent cover of the barley canopy ranged from 0.3 to 3.2 and 30-90%, respectively. The exponential equation

$$\Delta T_s = e^{(-0.06SWC+3.59)} \qquad (1)$$

with an r^2 of 0.81 and a standard deviation from regression of 2.54° C, was found to best represent the relationship between ΔT_s and the

average 24 h volumetric soil water content (SWC) in the 0-4 cm layer of the soil profile (Fig. 2). The exponential form fit the data better than linear (r^2 = 0.71), power (4^2 = 0.76) or quadratic (r^2 = 0.77) curves.

Idso et al. (1976) proposed a procedure for compensating for environmental variability in the thermal inertia approach by normalizing ΔT_s measurements with respect to an arbitrary standard diurnal air temperature variation. We found no significant improvement in the ΔT_s versus SWC relationship using the same normalization procedure.

The temperature versus water content relationship [Eq. (1)] applies only to Volga loam. However, Idso et al. (1975) converted soil water content to a pressure potential and found a more universal relationship that appeared to be independent of soil type. Schmugge et al. (1978) reported that in the absence of pressure potential data, textural differences in temperature versus water content relationships could be reduced by expressing soil water content as a percent of field capacity. The temperature versus soil water content relationships have limited usefulness unless soil temperatures can be estimated from remote measurements under all crop-cover conditions.

Estimating Soil temperature from measurements of canopy temperature

During the investigation, surface-soil temperatures at 0230 LST were 1.1-2.2^{o} C higher than apparent crop temperatures (Fig. 3a). Differences between canopy and crop temperatures, even at full cover, probably were the result of significant amounts of thermal radiation from the soil surface being detected by the infrared radiometer at 0230 LST (Blad and Rosenberg, 1976).

At 1330 LST, radiometric measurements of apparert canopy temperature were 0.5-17° C higher, and surface-soil temperatures 1.5-20° C higher, than apparent crop temperatures (Fib. 3b). Greatest differences between canopy and crop temperatures at full cover occurred on days with high temperatures and high evaporative demand. On those days, some silting of leaves occurred, which exposed more of the soil background to incoming solar radiation.

Because emittance contributions from the soil surface apparently were detected by the infrared radiometer, equations were developed from regression analyses to estimate soil temperatures from remote measurements of canopy temperature. For the 0230 LST measurements, the resulting equation was

$$T_{s(0230)} = 0.40\ PRT_{(0230)} + 0.60T_{a\ min} + 5.10, \qquad (2)$$

with an R^2 of 0.78 and a standard deviation from regression of 1.31° C Here $T_{s(0230)}$ (°C) is surface soil temperature, $PRT_{(0230)}$ measurement of canopy temperature, and $T_{a\ min}$ is the minimum NWS air temperature For the 1330 LST measurement, the surface soil temperatures were related to the PRT measurements of canopy temperature and an exponential function of percent cover (PC). The resulting equation was

$$T_{s(1330)} = 0.79\ PRT_{(1330)} \times e^{(-0.80PC)} + 20.35 \qquad (3)$$

with an r^2 of 0.86 and a standard deviation from regression of 2.63° C where PC is expressed as a fraction. We found no improvement in estimating soil temperature by including leaf area index, solar radiation or maximum air temperature in the analyses. Fig. 4 compares predicted soil temperature with observed values.

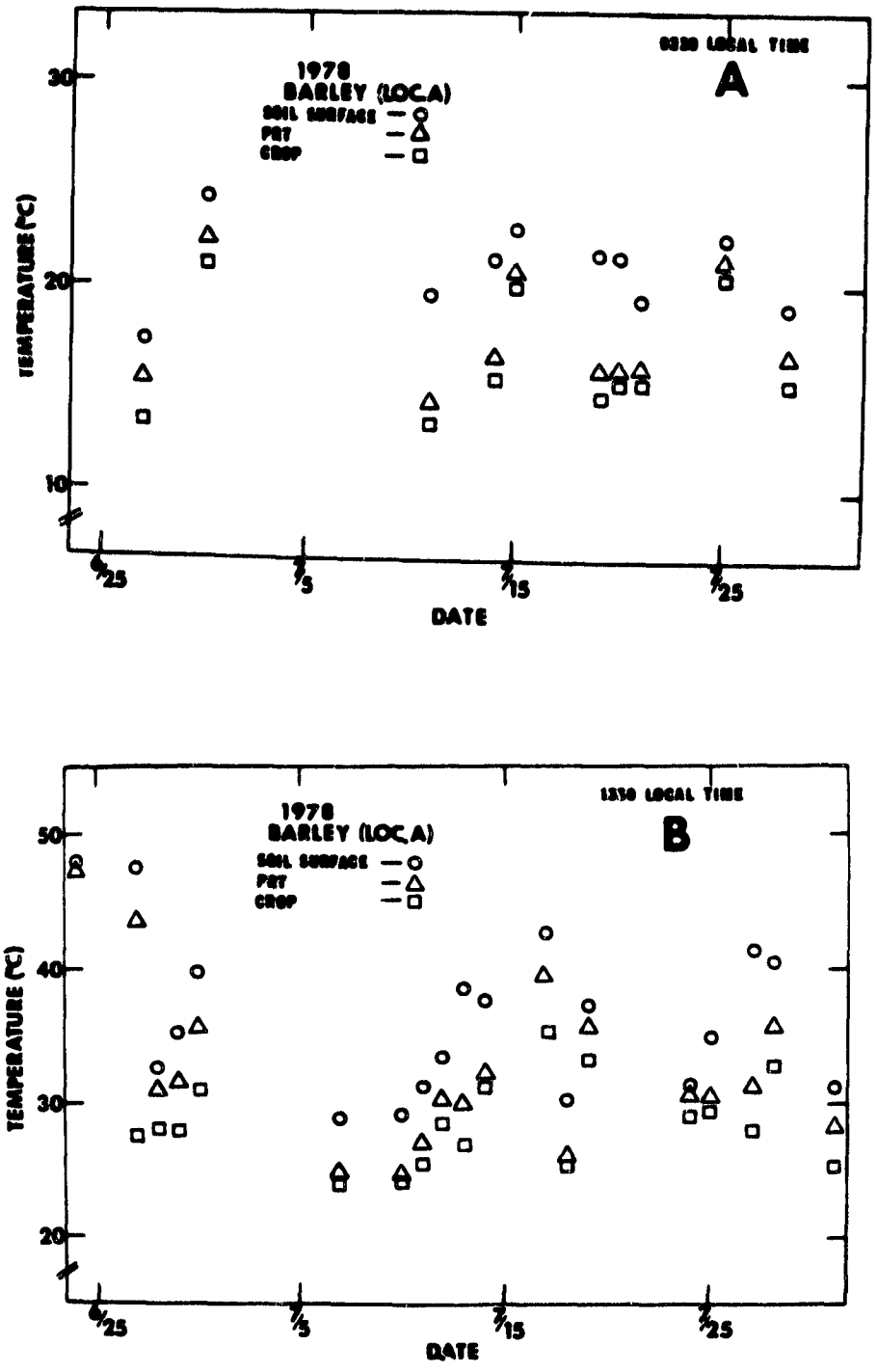

Fig. 3. Comparison of soil-surface (1 mm below surface), apparent canopy (PRT and apparent crop temperatures measured at 0230 (A) and 1330 LST (B). Canopy temperatures included emittance contributions from the crop and soil background.

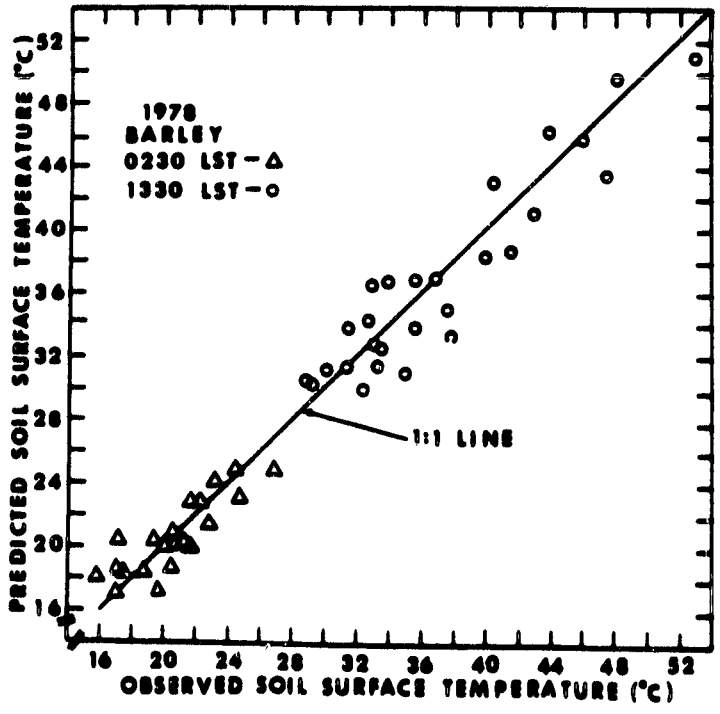

Fig. 4. Comparison of predicted and observed values of surface soil temperature at 0230 and 1330 LST. Temperatures were predicted using Eqs. (2) and (3).

Measurements of canopy temperature used to derive (2) and (3) ranged from 13 to 22^{o} C for (2), and from 24 to 52^{o} C for (3). Percent cover ranged from 0.3 to 0.9.

Evaluation of results

Fig. 5 compares observed soil water contents with values predicted using Eqs. (1)-(3), and the aircraft thermal scanner measurements of apparent corn, soybean, millet and pasture canopy temperatures. Eq. (1) was converted to express soil water content as a percent of field capacity to minimize differences associated with soil texture (Schmugge et al., 1978). Percent canopy cover ranged from 50 to 80% for pasture and from 90 to 95% for corn, soybean and millet. Soil textures ranged from sandy loam to silty clay loam. Differences of observed from predicted values ranged from -24.5 to +15.3% of field capacity. The average differences was 1.6% of field capacity. The less accurate estimates of soil moisture for corn, soybean and millet were probably due to their high percent cover.

CONCLUDING REMARKS

The results of this investigation indicate that thermography for extimating soil water content can potentially be extended to developing crop canopies. The diurnal difference between surface soil temperatures measured at HCMM overpass times is correlated with surface soil water content. Surface soil temperatures can be

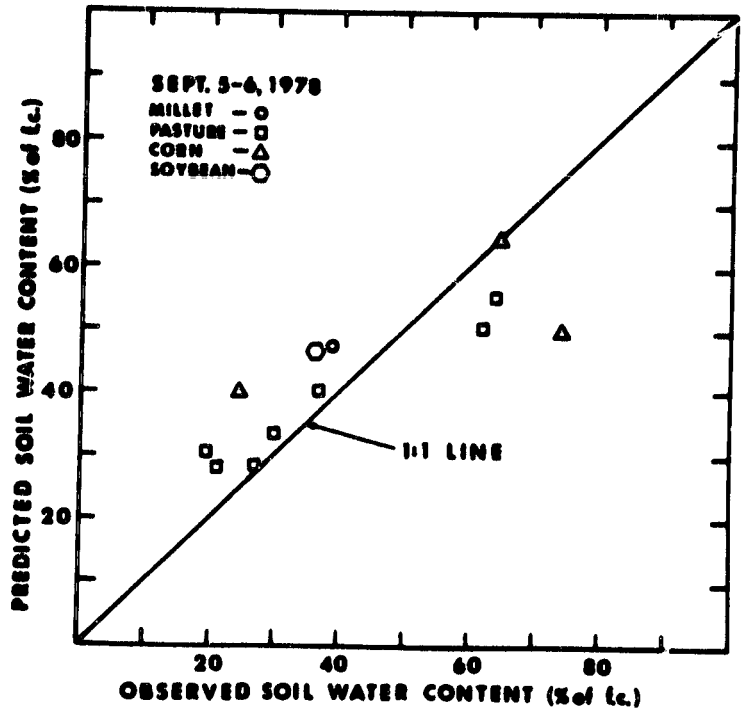

Fig. 5. Comparison of predicted and observed values of 24 h average soil water content in the 0 to 4 cm layer of the soil profile. Predictions were made using Eqs. (1), (2) and (3), and aircraft thermal scanner measurements of canopy temperature.

estimated from remote measurements of canopy temperature if minimum air temperature and percent cover of the canopy are known. Remote sensing evaluation of crop cover has been demonstrated (Heilman et al., 1977; Kanemasu et al., 1977; Tucker, 1979) for certain species.

REFERENCES

Blad, B.L., and N.J. Rosenberg, 1976: Measurement of crop temperature by leaf thermocouple, infrared thermometry and remotely sensed thermal imagery. Agron. J., 68, 635-641.

Fuchs, M.E., and C.B. Tanner, 1966: Infrared thermometry of vegetation, Agron. J., 58, 596-601.

Heilman, J.L., E.T. Kanemasu, J.O. Bagley and V.P. Rasmussen, 1977: Evaluating soil moisture and yield of winter wheat in the Great Plains using Landsat data. Remote Sens. Environ., 6, 315-326.

Idso, S.R., and W.L. Ehrler, 1976: Estimating soil moisture in the root zone of crops: a technique adaptable to remote sensing. Geophys. Res. Lett., 3, 23-25.

--------, T.J. Schmugge, R.D. Jackson and R.J. Reginato, 1975: The utility of surface temperature measurements for the remote sensing of surface soil water status, J. Geophys. Res., 80, 3044-3049.

--------R.D. Jackson and R.J. Reginato, 1976: Compensating for environmental variability in the thermal inertia approach to remote sensing of soil moisture. J. Appl. Meteor., 15, 811-817.

Jackson, R.D., R.J. Reginato and S.B. Idso, 1976: Timing of ground truth data acquisition during remote assessment of soil-water content. Remote Sens. Environ., 44, 249-255.

Kanemasu, E.T., J.L. Heilman, J.O. Bagley and W.L. Powers, 1977: Using Landsat data to estimate evapotranspiration of winter wheat. Environ. Management, 1, 515-520.

Schmugge, T., B. Blanchard, A. Anderson and J. Wang, 1978: Soil moisture sensing with aircraft observations of the diurnal range of surface temperature. Water Resour. Bull, 14, 169-178.

Tucker, C.J., 1979: Red and photographic infrared linear combination for monitoring vegetation. Remote Sens. Environ., 8, 127-150.

SOIL MOISTURE APPLICATIONS OF THE HEAT CAPACITY MAPPING MISSION

J.L. Heilman and D.G. Moore[1/]

[1/] Research Soil Physicist and Assistant Director, Remote Sensing Institute, South Dakota State University, Brookings, South Dakota 57007.

ABSTRACT

Results of ground, aircraft, and satellite investigations are presented that demonstrate the potential for using data from NASA's Heat Capacity Mapping Mission (HCMM) satellite to provide information on near-surface soil moisture. The satellite, which carries a two-channel radiometer (0.5 to 1.1 and 10.5 to 12.5 μm) in a sun-synchronous orbit, collects data at approximately 0230 and 1330 local standard time with repeat coverage of five or 16 days depending on latitude. Near-surface soil moisture influences surface temperature through conductive heat transfer (affected by thermal inertia) and evaporation. Thus, HCMM data acquired near maximum and minimum periods of the diurnal temperature cycle can provide useful soil moisture information. Hydrologic interpretations of HCMM data are complicated by vegetation, evapotranspiration, topography, atmospheric absorption and other environmental variables such as solar radiation, temperature, wind, etc.

KEY TERMS: HCMM, Thermal Inertia, Energy Balance, Soil Moistur

INTRODUCTION

Virtually all physical processes occurring at the earth's surface or in the atmosphere involve transformations or transfers of energy. Energy balance interactions have important hydrologic implications since water and energy balances are intimately related (evapotranspiration requires a source of energy). Distribution of precipitation affects the thermal regime of the surface through changes in evapotranspiration and thermal properties of soil and vegetation. Surface temperatures are also influenced by distribution and flow of shallow aquifers.

Surface temperatures can provide information on the nature of surface and subsurface hydrology. However, spatial and temporal variations in surface temperature are difficult to evaluate on the ground. The spatial criterion can be fulfilled by remote sensing from aircraft and satellite. Monitoring of dynamic hydrologic features, such as soil moisture, which requires repetitive coverage is feasible only with satellites.

NASA's Heat Capacity Mapping Mission (HCMM) launched on April 26, 1978, is the first satellite designed to evaluate remote sensor-derived temperature measurements of the earth's surface at times when the temperature variation is at a maximum. Thus, the HCMM represents a potentially useful tool for hydrologic studies.

Ground, aircraft, and satellite investigations were conducted in eastern South Dakota to evaluate the potential for using HCMM data to monitor soil moisture and depth to shallow groundwater. Many of the results are preliminary since investigations are still in progress.

Eastern South Dakota is characterized by shallow perched water tables and significant spatial and temporal variations in soil moisture and agricultural land use. Most topographic features in the area are related to glaciation or stream erosion. The complexities of the groundwater regime and land use patterns in eastern South Dakota provide a wide range of conditions in which HCMM data can be evaluated.

HEAT CAPACITY MAPPING MISSION

The HCMM carries a two-channel radiometer (0.55 to 1.1 and 10.5 to 12.5 μm) in a sun-synchronous orbit (orbital altitude is 620 km). Spatial resolutions are 0.5 x 0.5 km at nadir for the visible channel and 0.6 x 0.6 km at nadir for the thermal infrared channel. The neΔt of the thermal channel is 0.4°K at 280°K. Swath width is 716 km. HCMM collects data at 2:30 a.m. and 1:30 p.m. local standard time at mid-latitudes with a repeat cycle of five of 16 days depending on latitude.

Standard data products include visible, day IR, and night IR imagery (1:4,000,000 scale), and associated computer compatible tapes. An example of a night thermal IR image is shown in Fig. 1. Special data products include day-night temperature difference and apparent thermal inertia (ATI). ATI, which has many attributes of true thermal inertia, is defined at $C(1-a)/\Delta T$ where C is a constant related to latitude and solar declination, a is apparent albedo obtained from daytime HCMM reflectivity measurements, and ΔT is the day-night radiometric temperature difference observed by HCMM.

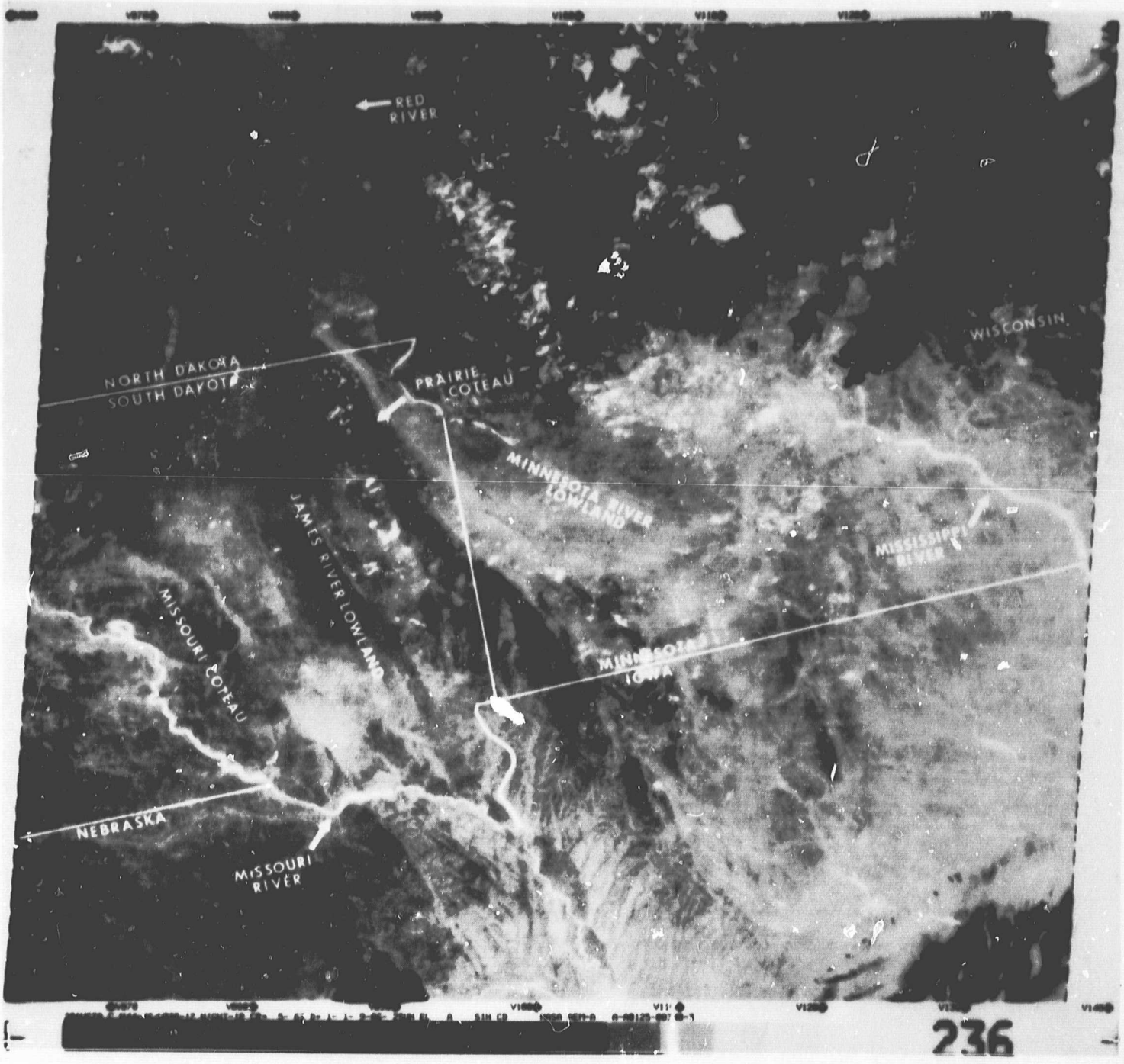

Figure 1. An August 29, 1978, night HCMM thermal infrared image (scene ID A-A0125-08340) of portions of the upper Midwest. (Approximate scale 1:4,000,000, dark is cool). neΔT = 0.4^{o}C; IFOV = 0.6 x 0.6 km; overpass time = 0234 local standard time.

INTERPRETATION EXAMPLES

Diurnal variations of surface soil temperatures are principally related to thermal inertia, evaporation, land use, and meteorological factors (solar insolation, air temperature, humidity, etc.). Thermal inertia, an indication of a soil's resistance to temperature change, is defined as $(C\lambda)^{\frac{1}{2}}$ where C is volumetric heat capacity and λ is thermal conductivity. Since C and λ increase as soil water content increases, the resulting amplitude of the diurnal soil temperature wave decreases.

When the soil surface is wet, evaporation is a major factor controlling surface heat loss since more energy is partitioned into latent heat of vaporization and is not available for heating the soil. After the surface layer dries and the soil water supply cannot meet the evaporative demand, surface temperature of a bare soil is largely related to thermal inertia. Nocturnal cooling is highly dependent on thermal inertia. Thus, the amplitude of diurnal soil temperature variations can be an indication of near-surface soil water content.

Idso et al. (1975) found a linear relationship between the diurnal range of surface soil temperatures (bare soil) and near-surface soil water content, and reported that the temperature versus water content relationship was a function of soil type. The textural dependence can be minimized by expressing soil water content in units of pressure potential or as a percent of field capacity (Idso et al., 1975; Schmugge et al., 1978). Meteorological variability can be reduced

by normalizing the amplitude of the diurnal surface soil temperature wave with respect to a standard diurnal air temperature variation (Idso et al., 1976).

Vegetation alters solar insolation at the soil surface and thus affects soil temperature. Therefore, growth and development of vegetation would be expected to complicate temperature versus soil water content relationships. Since crop canopies are the primary source of land surface emittance during most of the growing season in South Dakota, the use of HCMM data for hydrologic investigations requires that vegetation be considered in the analysis.

A ground study was conducted in a barley canopy planted in a 25 x 300 m field of Volga loam to evaluate soil temperature (measured at HCMM overpass times by thermocouples 1-mm below the soil surface) versus water content relationships at various stages of canopy development (Heilman and Moore, 1980). Percent cover of the developing barley canopy ranged from 30 to 90 percent over the 45-day study. The exponential equation

$$\Delta T_s = e^{(-0.06\ SWC + 3.59)} \qquad (1)$$

with an r^2 of 0.81 was found to best represent the relationship between day minus night surface soil temperatures (ΔT_s) and the average 24-hr volumetric soil water content (SWC) in the 0 to 4-cm layer of the soil profile (Fig. 2).

The relationship in (1) has limited usefulness unless ΔT_s can be estimated from remote measurements under a wide range of crop-cover

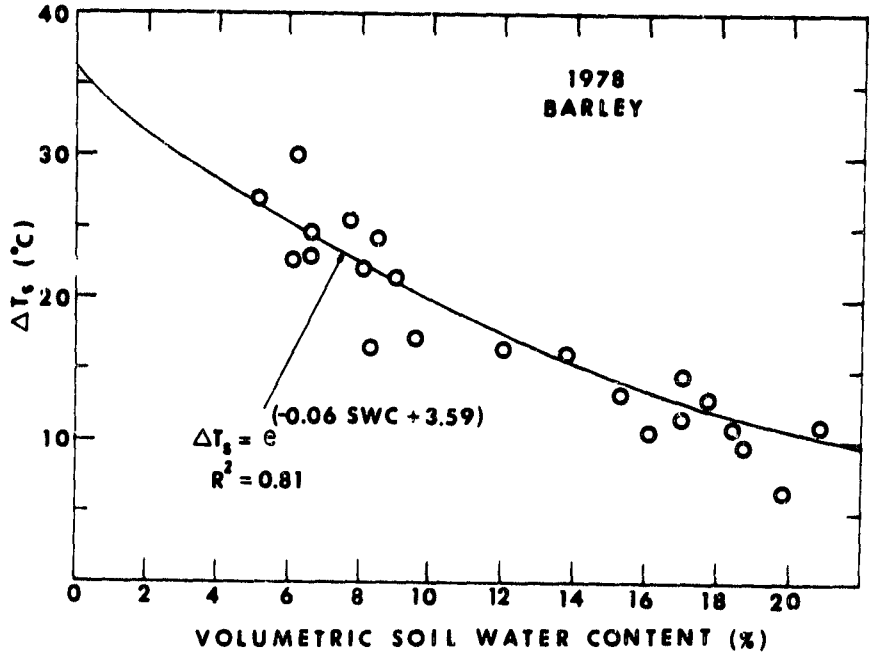

Figure 2. Relationship of the difference (ΔT_s) between soil surface temperatures measured at HCMM overpass times and the average 24-hr volumetric soil water content (SWC) in the 0 to 4-cm layer of the profile. Temperatures were measured by thermocouple 1 mm below the surface in a field of Volga loam (Heilman and Moore, 1980).

conditions. The ground study found that apparent canopy temperatures measured 2 m above the canopy by a 20° FOV infrared radiometer (Model PRT-5, Barnes Engineering Co.) at a vertical position (zero degree look angle measured from nadir) at HCMM overpass times contained significant emittance contributions from both the soil and the crop canopy throughout the growing season. Therefore, equations were developed from regression analyses of surface-soil and apparent-canopy temperatures to estimate surface-soil temperature from remote measurements. For 0230 LST measurements, the equation

$$T_{s(0230)} = 0.40\ T_{c(0230)} + 0.60\ T_{a\ min} + 5.10 \qquad (2)$$

with an R of 0.78 was obtained where $T_{s(0230)}$ (°C) is surface soil temperature, and $T_{a\ min}$ (°C) is the minimum air temperature obtained from the nearest National Weather Service station. For the 1330 LST measurement, surface soil temperature was related to apparent canopy temperature and an exponential function of percent cover (PC). The equation

$$T_{s(1330)} = 0.79\ T_{c(1330)} \times e^{(-0.80\ PC)} + 20.35 \qquad (3)$$

with an r^2 of 0.86 was obtained where PC is expressed as a fraction.

Equations (1), (2), and (3) were tested using simulated HCMM data (aircraft thermal scanner data collected at an altitude of 3650 m AGL) collected over corn, soybean, millet, and pasture (Heilman and Moore, 1980). Percent canopy cover ranged from 50 to 80 percent for pasture and from 90 to 95 percent for corn, soybean, and millet. Soil textures ranged from sandy loam to silty clay loam.

Figure 3 compares observed soil water content with values predicted using equations (1) through (3) and simulated HCMM measurements of apparent canopy temperature. Equation (1) was converted to express soil water content as a percent field capacity to minimize textural differences (Schmugge et al., 1978). The average difference of observed from predicted values was 1.6 percent of field capacity.

Preliminary analyses of actual HCMM data of eastern South Dakota indicates that high soil moisture areas can be detected using HCMM thermal imagery. In early April 1978 heavy spring runoff and ice blockage caused significant flooding of alluvial areas in a portion of the Big Sioux River Basin in southeastern South Dakota (Fig. 4). Flood waters had receded by mid-May, but an area of high soil moisture (at or near field capacity) remained. Soil moisture in the surrounding upland soils was generally less.

The high moisture area appeared cooler than surrounding areas on May 15 day thermal imagery (Fig. 5). Temperature differences between the flood plain and surrounding areas were probably the result of thermal inertia and evaporation differences associated with soil moisture differences. Landsat imagery (Fig. 6) confirmed that no standing water was present in the fields. Adjacent alluvial areas did not appear different from uplands, indicating that the anomaly was not associated with inherent thermal inertia of the soil but with a moisture difference.

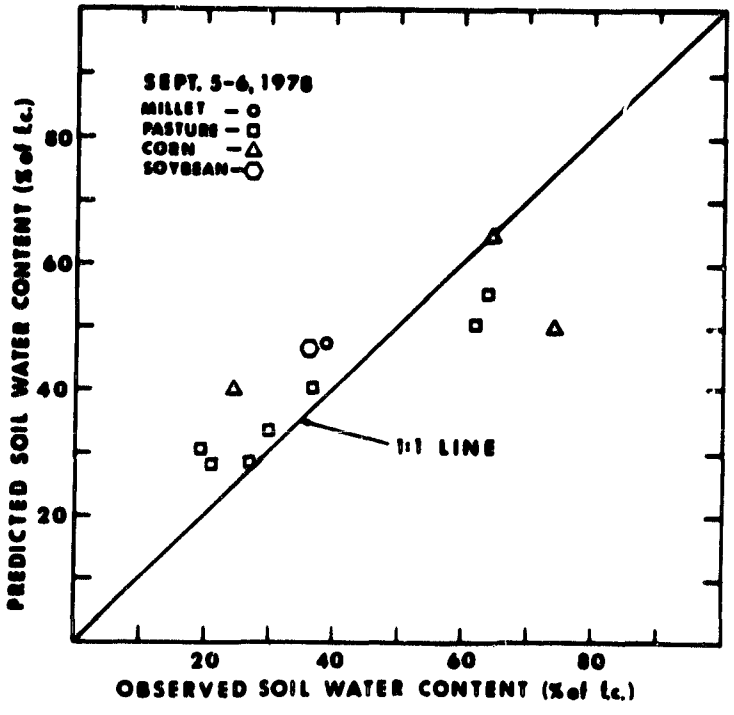

Figure 3. Comparison of predicted and observed values of 24-hr average soil water content in the 0 to 4-cm layer of the soil profile. Predictions were made using equations (1), (2), and (3) and simulated HCMM measurement of canopy temperature (Heilman and Moore, 1980).

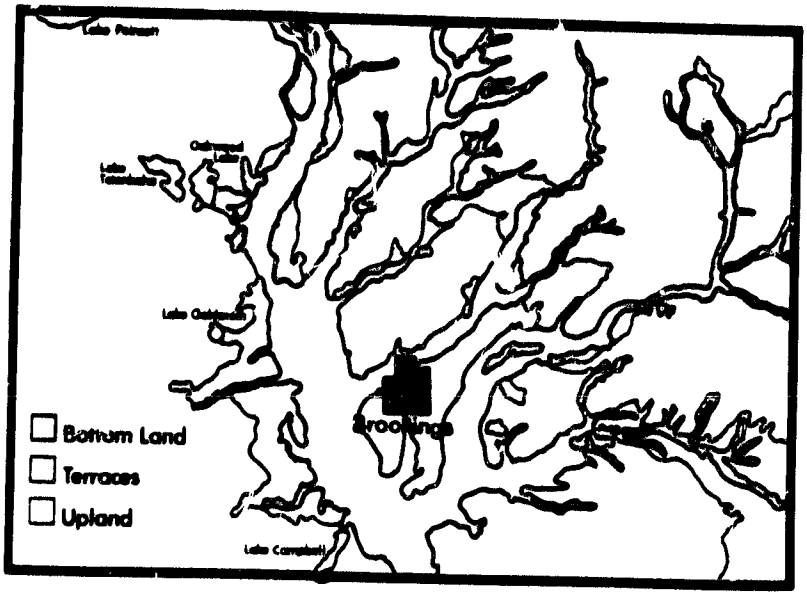

Figure 4. Landform map of Brookings County, South Dakota, showing location of alluvial soils (bottomland) in the Big Sioux River Basin which were flooded in early April 1978 (Heilman and Moore, 1981).

ORIGINAL PAGE
BLACK AND WHITE PHOTOGRAPH

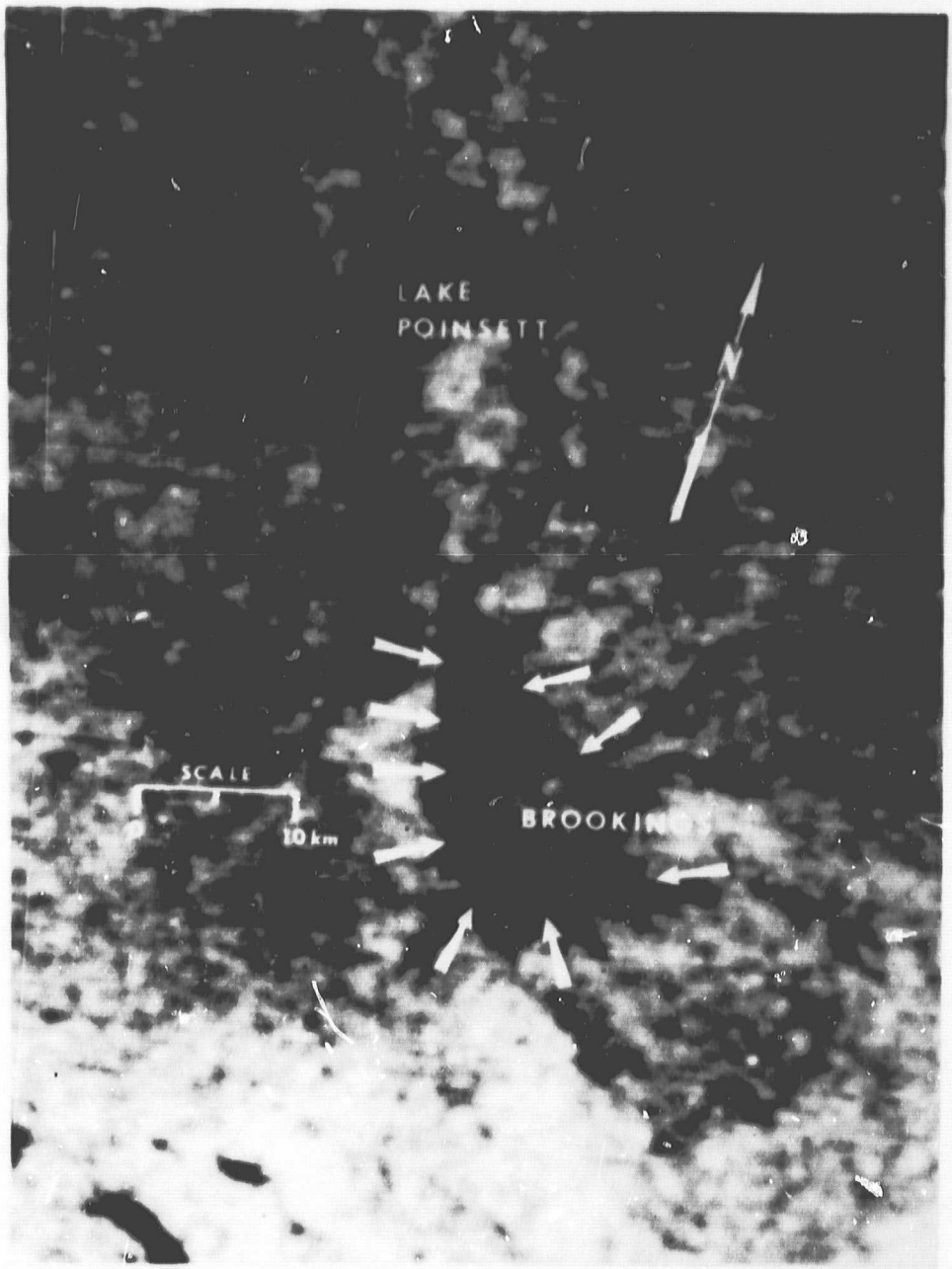

Figure 5. Enlargement of May 15, 1978, day HCMM thermal infrared data (scene ID A-A0029-19575) showing a high soil moisture area (arrows) in eastern South Dakota (Heilman and Moore, 1981). Dark is cool.

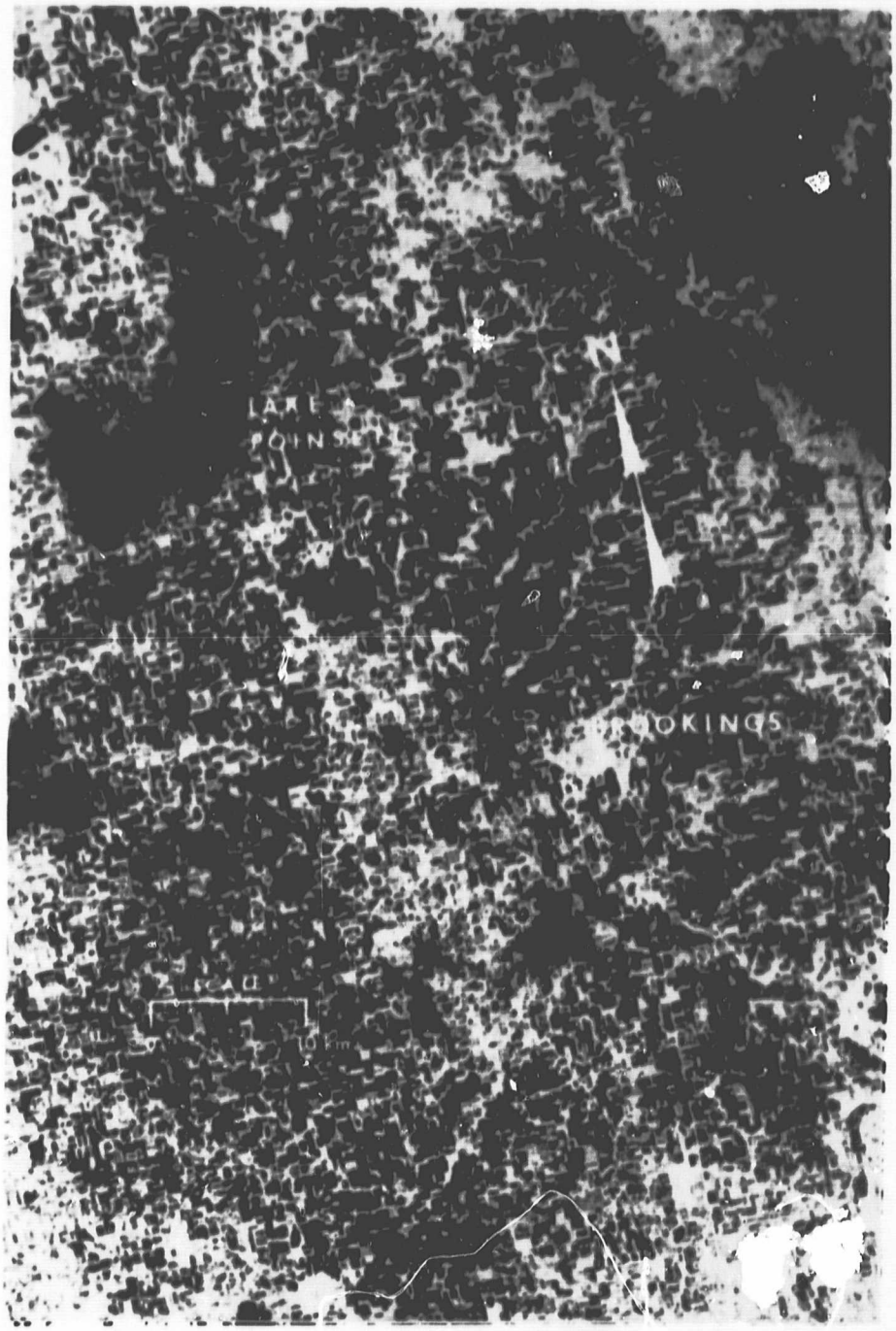

Figure 6. Photographic enlargement of a May 13, 1978, Landsat color composite (scene ID E-21207-16083) of the same area shown in Figure 5. Note that no standing water is visible in the flood plain of the Sioux River Basin.

These results indicate a potential for evaluating soil moisture using HCMM data. Final results from HCMM soil moisture investigations currently in progress will continue to evaluate the utility of using HCMM and similar data for quantifying soil moisture differences from space.

DISCUSSION

Although the potential for using HCMM and similar data in soil moisture investigations has been demonstrated, there are limitations in the use of such data which must be considered. Environmental factors which influence energy balance interactions must be considered when using thermal data. Due to its large heats of fusion and vaporization, water undergoing phase transformations acts as a heat source or sink. Changes in heat content will not be represented by a corresponding temperature change if a phase transformation occurs. Thus, conditions favoring high evapotranspiration rates or dew or frost formation are not favorable for remote sensing of near-surface soil moisture.

Wind patterns may obscure thermal anomalies created by soil moisture (Fig. 7). Topographic variations and vertical extrusions affect the boundary layer and thus affect sensible and latent heat transport.

Atmospheric constituents (clouds, aerosols, water vapor, etc.) influence surface temperature by attenuating incoming solar radiation and affecting radiative cooling of the surface. Since atmospheric counter-radiation is emitted by atmospheric constituents, radiative

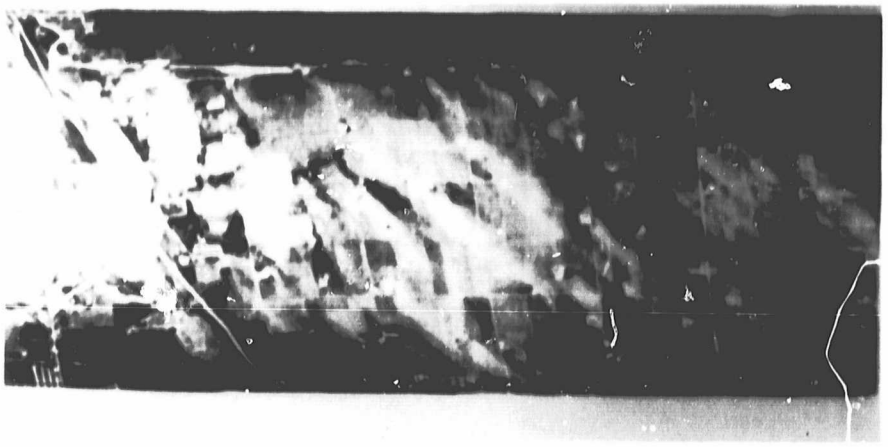

Figure 7. Wind patterns on night thermal imagery of an area south of and including Sioux Falls. Wind was from the northeast at a speed of 10 knots. Approximate scale 1:55,000; dark is cool.

cooling will be greater under a clear sky. Atmospheric components also affect the amount of longwave radiation emitted by the surface that is detected by HCMM or other thermal sensors.

Thermal remote sensing has an advantage of relating to subsurface properties since surface temperatures and emittances are a function of both surface and subsurface properties. These preliminary results indicate that observations at appropriate periods within the diurnal cycle can provide information on soil moisture. These and other preliminary results appear promising for development of interpretation models to advance the use of thermography.

ACKNOWLEDGMENTS

Partial support for the investigations was provided by NASA under contract No. NAS5-24206 and the State of South Dakota. Contribution No. SDSU-RSI-J-80-03 from the Remote Sensing Institute, South Dakota State University.

LITERATURE CITED

Heilman, J.L., and D.G. Moore. 1980a. Thermography for estimating near-surface soil moisture under developing crop canopies. J. Appl. Meteor. 19:324-328.

Heilman, J.L., and D.G. Moore. 1981. HCMM detection of high soil moisture areas. Remote Sensing Environ. (In press)

Idso, S.B., T.J. Schmugge, R.D. Jackson, and R.J. Reginato. 1975. The utility of surface temperature measurements for the remote sensing of surface soil water status. J. Geophys. Res. 80:3044-3049.

Idso, S.B., R.D. Jackson, and R.J. Reginato. 1976. Compensating for environmental variability in the thermal inertia approach to remote sensing of soil moisture. J. Appl. Meteor. 15:811-817.

Schmugge, R., B. Blanchard, A. Anderson, and J. Wang. 1978. Soil moisture sensing with aircraft observations of the diurnal sensing with aircraft observations of the diurnal range of surface temperature. Water Resour. Bull. 14:169-178.

EVALUATING NEAR-SURFACE SOIL MOISTURE USING HEAT CAPACITY MAPPING MISSION (HCMM) DAT[1/]

J. L. Heilman
Remote Sensing Center
Texas A & M University
College Station, TX 77843

D. G. Moore
Remote Sensing Institute
South Dakota State University
Brookings, SD 57007

1/ Contribution No. SDSU-RSI-J-80-08 from the Remote Sensing Institute, South Dakota State University. This investigation was supported by NASA under contract NAS5-24206.

ABSTRACT

Four dates of Heat Capacity Mapping Mission (HCMM) data were analyzed to evaluate the utility of HCMM thermal data for estimating near-surface soil moisture in a complex agricultural landscape. Because of large spatial and temporal ground cover variations, HCMM radiometric temperatures consisted of radiance contributions from different canopies and their respective soil backgrounds. However, when surface soil temperatures were empirically estimated from HCMM temperatures and percent cover of each pixel, a highly significant correlation ($r = 0.74^{**}$) was obtained between the estimated soil temperatures and near-surface soil water content.

INTRODUCTION

Remotely sensed surface temperatures have been investigated for estimating soil water content in the surface layer of soil (Idso et al., 1975; Reginato et al., 1976; Heilman and Moore, 1980). Generally the investigations have been limited to bare soil or fully developed crop canopies because of difficulties in interpreting data at less than full cover when significant radiance contributions occur from both vegetation and soil. Heilman and Moore (1980) found that thermal techniques could potentially be extended to conditions of partial canopy cover.

Investigations have also been limited to ground or aircraft studies since high resolution thermal data from satellites were unavailable for the appropriate periods of the diurnal temperature cycle. The Heat Capacity Mapping Mission (HCMM) satellite, launched in April 1978, was the first satellite devoted to acquiring high resolution thermal data at optimum periods of the diurnal cycle. The HCMM carried a two-channel radiometer (0.55 to 1.1 and 10.5 to 12.5 μm) in a sun-synchronous orbit at an altitude of 620 km. Spatial resolutions were 0.5 x 0.5 km at nadir for the visible channel and 0.6 x 0.6 km at nadir for the thermal channel. The $NE\Delta t$ of the thermal channel was 0.4 K at 280K. The HCMM collected data at approximately 0230 and 1330 local standard time (LST) with a repeat cycle of 5 or 16 days depending on latitude.

An investigation was conducted to evaluate the utility of using HCMM data to evaluate near-surface soil moisture for a complex agricultural landscape.

MATERIALS AND METHODS

The study was conducted in an 8 x 24 km area within the Big Sioux River Basin in Brookings County in southeastern South Dakota. Surficial deposits in the drainage basin are predominantly of glacial origin, and consist of end moraine, ground moraine, and outwash deposits (Ellis et al., 1969).

The large study area was required to obtain a wide variation of soil textures and agricultural land use. Soils in the basin range from poorly drained silty clay loams in the flood plain to well drained sandy loams in the slightly elevated terraces. Major agricultural land use categories are small grains, row crops, hayland, and pasture with field sizes generally less than 16 ha.

Soil water contents (0 to 4 cm layer were determined gravimetrically on samples collected on HCMM overpass days in fields representative of soil and land use variations in the basin. Three samples were collected per field and averaged. Sampling occurred between 1000 and 1400 LST. The soil water content for each field was used to represent an entire HCMM pixel, although each pixel ultimately contained more than one land use.

The number of sampling locations varied because of logistical problems associated with collecting samples over a large area in a short period of time. Table 1 summarizes the soil moisture data collections.

Percent cover at each location was determined using 35 mm slides of the canopies (photographed from a vertical position approximately 1 m above the canopies) projected on a random dot grid. When the canopies

Table 1. Number of fields sampled for soil moisture on cloud-free days of HCMM overpass selected for analysis. Three samples were collected in each field.

Date	No. of Fields	Land Cover
June 5, 1978	4	corn, pasture
July 13, 1978	2	corn
August 8, 1978	4	corn, pasture
September 4, 1978	13	corn, pasture, stubble

Table 2. HCMM scenes analyzed in soil moisture study

Date	Time	Scene I.D.
June 5, 1978	1330 LST	AA0040-19500
July 13, 1978	1330 LST	AA0070-19570
August 8, 1978	1330 LST	AA0104-19400
September 4, 1978	1330 LST	AA0131-19420

were too tall for the photographic procedure, percent cover was estimated from visual inspection. These data were used to prepare average percent cover curves for the growing season for each land use category. Daily maximum air temperatures were obtained from the Brookings National Weather Service Station.

Four dates of daytime HCMM data representative of the growing season were selected for analyses (Table 2). Cloud-free day/night data were available only for July 13, but insufficient soil moisture data were collected on that date to relate diurnal temperature variations to soil water content.

Radiometric temperatures were extracted for each pixel containing a field where soil samples were collected by overlaying computer gray maps of HCMM data with a Brookings County map containing the sampling sites. Radiometric temperatures were corrected for atmospheric effects by comparing HCMM and ground measurements of Missouri River reservoir temperatures in central and southeastern South Dakota. Radiometric temperatures were not corrected for emissivity variations.

Percentage of each land use category for each pixel was determined using photointerpretation of a May 13, 1978, Landsat color composite (scene I.D. E-21207-16803) superimposed on HCMM gray maps via a Bausch & Lomb Zoom Transferscope. Percentage of each land use within each pixel, and the average percent cover curves for each land use category were used to calculate a pixel percent cover for each date of HCMM data.

RESULTS AND DISCUSSION

Surface soil temperature variations are a function of soil thermal properties, land cover, evaporation, albedo, meteorological and other factors (air temperature, solar radiation, wind, etc.). When the soil surface is wet, evaporation is a major factor controlling heat loss. After the surface layer dries and the soil water supply cannot meet the evaporative demand, surface heat loss is largely influenced by thermal inertia. Thermal inertia, defined as $(\rho c \lambda)^{1/2}$ where ρ is density, c specific heat, and λ thermal conductivity, is an indication of a soil's resistance to temperature change. Since ρ, c, and λ of a soil increase as soil water content increases, the resulting amplitude of the diurnal surface temperature wave decreases. Thus, soil surface temperatures at maximum and minimum periods of the diurnal temperature cycle can be an indication of soil water content.

Idso et al. (1975) found linear relationships between the diurnal range of surface soil temperatures (bare soil) and soil water content in the 0 to 4-cm layer of soil, and between the surface soil - air temperature difference and soil water content for the same depth interval. The temperature versus water content relationships were a function of soil type. However, Idso et al. also found that if soil water content was expressed in pressure potential units, this dependence was minimal.

Unfortunately, bare soil conditions seldom exist for any length of time in agricultural areas. Thus, remote sensing techniques must be developed for a wide range of ground cover conditions. HCMM radiometric

temperatures (corrected for atmospheric effects but without consideration given to ground cover variations) did not correlate ($r = 0.16$) with soil water content for the four dates analyzed. Generally, each pixel contained more than a single land use. Thus, the radiometric temperatures consisted of a combination of radiance contributions from different canopies and their respective soil backgrounds. Estimated percent cover for the pixels ranged from 10 to 95 percent during the study.

Heilman and Moore (1980) found that soil surface temperatures beneath crop canopies were correlated with near-surface water content, and developed a procedure for estimating soil surface temperatures under crop canopies from remote measurements of a composite temperature. They used the euation

$$T_s = 0.79\ T_c e^{(-0.80\ PC)} + 20.35 \qquad (1)$$

where T_s (^oC) is predicted soil surface temperature, T_c (^oC) is a composite temperature consisting of radiance contributions from the crop and soil background, and PC is percent cover expressed as a fraction.

Equation (1) was used to estimate surface soil temperatures from HCMM temperatures and pixel percent cover. Regression analyses were used to correlate T_s with soil water content (SWC). The following equation was

$$T_s = 58.35\ SWC^{-0.18} \qquad (2)$$

with a r of 0.74 (significant at the 0.01 level) and a $S_{y.x}$ of 2.1 ^oC (Figure 1).

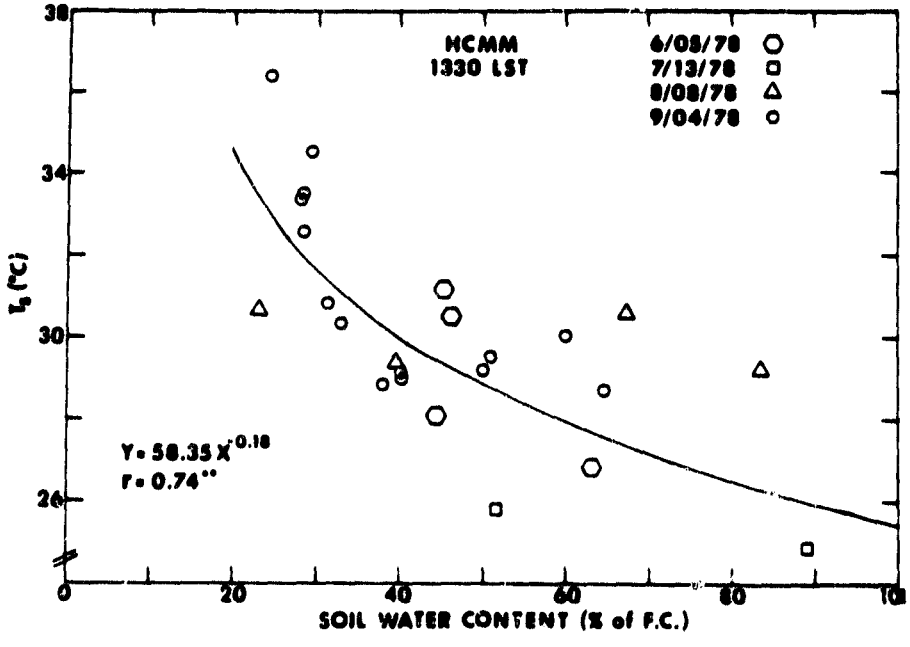

Figure 1. Relationship between predicted soil surface temperatures (T_s) and soil water content in the 0 to 4-cm layers of the soil profile. Predictions were made using equation (1) and HCMM radiometric temperatures. Soil water contents are an average of three measurements.

Soil water content was expressed as a percent of field capacity to minimize differences associated with soil texture (Schmugge et al., 1978).

Soil surface temperatures are affected by day-to-day environmental variations (wind, humidity, air temperature, etc.). We attempted to compensate for some of that variability by relating differences between T_s and maximum air temperature to soil water content (Idso et al., 1975). Table 3 lists maximum air temperatures for the four analysis dates. However, we found no significant improvement using that procedure.

Results of this study indicate that thermal data acquired from spacecraft can be correlated with near-surface soil moisture if considerations are given to spatial and temporal groundcover variations. Remote sensing of crop cover using multispectral reflectance data has been successfully demonstrated (Heilman et al., 1977; Kanemasu et al., 1977; Jackson et al., 1979; Tucker et al., 1979; Holben et al., 1980).

Reflective and thermal data have the advantage of high spatial resolution, but their usefulness is lost in the presence of clouds. Microwave sensors have the ability to penetrate non-raining clouds. However, the spatial resolution of passive sensors is limited by antenna size, while active microwave sensing is strongly influenced by look angle and surface roughness (Schmugge, 1978). Thus, the combined use of reflective, thermal, and microwave sensors may be the logical approach for assessing soil moisture from satellites. Investigations of simultaneous observations in the various spectral regions should be pursued to determine where each data set is unique and/or where the multiple estimates can be used to improve accuracies.

Table 3. Maximum air temperature for the four dates of analysis.

Date	T_{max} (C)
June 5	25.0
July 13	26.1
August 8	31.7
September 4	31.1

References

Ellis, M.E., Adolphson, D.G., Wesc, R.E., 1969, USGS Hydrology Investigation Atlas 311.

Heilman, J.L., Kanemasu, E.T., Bagley, J.O., and Rasmussen, V.P., 1977, Remote Sens. Environ. 6:315-326.

Heilman, J.L., and Moore, D.G., 1980, J. Appl. Meteor. 19:324-328.

Holben, B.N., Tucker, C.J., and Fang, C.J., 1980, Photogram. Engr. and Remote Sensing 46:651-656.

Idso, S.B., Schmugge, T.J., Jackson, R.D., and Reginato, R.J., 1975, J. Geophys. Res. 80:3044-3049.

Jackson, R.D., Reginato, R.J., Pinter, P.J., Idso, S.D., 1979, Appl. Optics 18:3775-3782.

Kanemasu, E.T., Heilman, J.L., Bagley, J.O., and Powers, W.L., 1977, Environ. Management 1:515-520.

Reginato, R.J., Idso, S.B., Vedder, J.F., Jackson, R.D., Blanchard, M.B., and Goettleman, R., 1976, J. Geophys. Res. 81:1617-1620.

Schmugge, T., 1978, J. Appl. Meteor. 17:1549-1557.

Schmugge, T., Blanchard, B., Anderson, A., and Wang, J., 1978, Water Resour. Bull. 14:169-178.

Tucker, C.J., Elgin, J.H., Jr., Mc Murtrey, J.E. III and Fang, C.J., 1979, Remote Sens. Environ. 8:237-248.

CHAPTER III: DETECTION OF NEAR-SURFACE WATER TABLES

Section 1. Groundwater Applications of the Heat Capacity Mapping Mission. Heilman, J.L., and D.G. Moore. In Satellite Hydrology, ed. Deutsch, M., D.R. Wiesnet, and A. Rango. Proc. of Fifth Annual William T. Pecora Memorial Symposium on Remote Sensing, Am. Water Resources Association, Minneapolis, Minn. (pp. 446-450).

Section 2. Evaluating Water Table Depth Using Heat Capacity Mapping Mission (HCMM) Data. Heilman, J.L. and D.G. Moore. (Submitted to Photogrammetric Engineering and Remote Sensing.)

GROUNDWATER APPLICATIONS OF THE HEAT CAPACITY MAPPING MISSION

J.L. Heilman and D.G. Moore[1/]

[1/] Research Soil Physicist and Assistant Director, Remote Sensing Institute, South Dakota State University, Brookings, South Dakota 57007.

ABSTRACT

Results of ground, aircraft, and satellite investigations are presented that demonstrate the potential for using data from NASA's Heat Capacity Mapping Mission (HCMM) satellite to provide information on perched water tables. The satellite, which carries a two-channel radiometer (0.5 to 1.1 and 10.5 to 12.5 μm) in a sun-synchronous orbit, collects data at approximately 0230 and 1330 local standard time with repeat coverage of five or 16 days depending on latitude. Perched water tables influence surface and subsurface soil temperatures because of a heat sink effect created by the high heat capacity of water. HCMM data acquired at appropriate periods of the diurnal and annual temperature cycle can provide useful information on shallow groundwater. Hydrologic interpretations of HCMM data are complicated by thermal inertia-heat sink interactions, vegetation, evapotranspiration, topography, atmospheric absorption and other environmental variables such as solar radiation, temperature, wind, etc.

KEY TERMS: HCMM, Thermal Inertia, Energy Balance, Soil Moisture, Groundwater, Perched Water Tables

INTRODUCTION

This paper discusses the groundwater portion of a hydrologic investigation of eastern South Dakota using data from the Heat Capacity Mapping Mission (HCMM) satellite. Background material and information about the HCMM are presented in the paper "Soil Moisture Applications of the Heat Capacity Mapping Mission" in the preceding soil moisture section.

INTERPRETATION EXAMPLES

Surface soil temperatures are controlled by meteorological factors and soil/water/vegetation properties at depths within the diurnal damping depth, and also by the ability of underlying soil material to store and transfer heat. For example, the high heat capacity of groundwater within the depth of annual soil temperature variation produces a heat sink in summer and a heat source in winter which reduces annual temperature variations (Cartwright, 1968). Temperatures are influenced by aquifer thickness, rate of horizontal and vertical water movement, and depth to the water table.

Variations in groundwater depth do not significantly affect the amplitude of the diurnal temperature curve, but do shift the curve up or down in absolute magnitude (Huntley, 1978). Figure 1 illustrates the effect of depth to groundwater on subsurface soil temperatures measured in the Big Sioux River Basin in southeastern South Dakota.

A highly significant positive correlation ($r = 0.68^{**}$) was found between 50-cm soil temperature and depths to groundwater of three meters or less.

Myers and Moore (1972) and Moore and Myers (1972) evaluated aerial thermography of the Sioux Basin and found that apparent thermal anomalies related to shallow groundwater could be detected during predawn hours in August and early September, the period of the maximum downward temperature gradient in South Dakota (Fig. 2). In addition, they found that the thickness of saturated sands and gravels corresponded closely to an apparent cool anomaly. During the daytime, they found that thermal patterns produced by differential ET rates, ground shadings, reflectances, and other factors masked thermal patterns produced by subsurface conditions (Fig. 2).

Similar results are visible on HCMM imagery. The Big Sioux Basin appears cooler than surrounding areas on August night thermal imagery, primarily because of the heat sink created by shallow aquifers within the Basin (Fig. 3). The Big Sioux Basin is not visible on day thermal or visible imagery because of the masking effect associated with land use (Figs. 4 and 5). Investigations are in progress to evaluate HCMM and similar data for evaluating depth to groundwater for the shallow water tables.

DISCUSSION

An important consideration in the use of HCMM and similar data in groundwater studies is the interaction of soil moisture and

groundwater. An increase in near-surface soil moisture produces lower soil temperatures during the day and higher temperatures at night, whereas, shallow groundwater produces lower soil temperatures throughout the diurnal cycle. Thus, soil moisture and groundwater affect surface temperature in the same direction during the day and in opposite directions at night during the late-summer period of maximum downward temperature gradients. Other limitations in the use of HCMM data are discussed in the previous soil moisture paper.

Observations at appropriate periods of the diurnal and annual temperature cycle may reveal information on shallow water tables within the range of the annual damping depth (10 to 15 m in northern latitudes of South Dakota). These results appear promising for development of interpretation models to advance the use of HCMM and similar data.

ACKNOWLEDGMENTS

Partial support for the investigation was provided by NASA under contract No. NAS5-24206, USGS under contract No. 14-08-0001-12510, and the State of South Dakota. Contribution No. SDSU-RSI-J-80-04 from the Remote Sensing Institute, South Dakota State University.

LITERATURE CITED

Cartwright, K. 1968. Temperature prospecting for shallow glacial and alluvial aquifers in Illinois. Illinois State Geological Survey Circular 433, Urbana, Illinois.

Huntley, D. 1978. On the detection of shallow aquifers using thermal infrared imagery. Water Resour. Res. 14:1075-1083.

Moore, D.G. and V.I. Myers. 1972. Environmental factors affecting thermal groundwater mapping. Interim report RSI-72-06 to USGS. Contract No. 14-08-0001-12510, Washington, D.C.

Myers, V.I. and D.G. Moore. 1972. Remote sensing for defining aquifers in glacial drift. Proc. of 8th International Symp. of Remote Sensing of Environment, Ann Arbor, Michigan. pp.715-728.

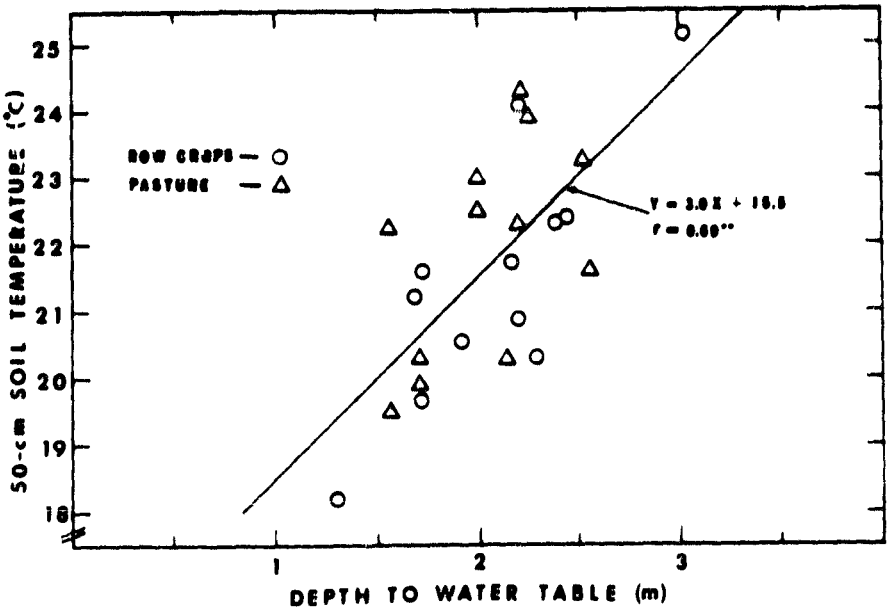

Figure 1. Relationship of 50-cm soil temperatures to depth to groundwater for row crops and pasture. Temperatures were measured in the Big Sioux River Basin during daylight hours on September 5-7, 1978.

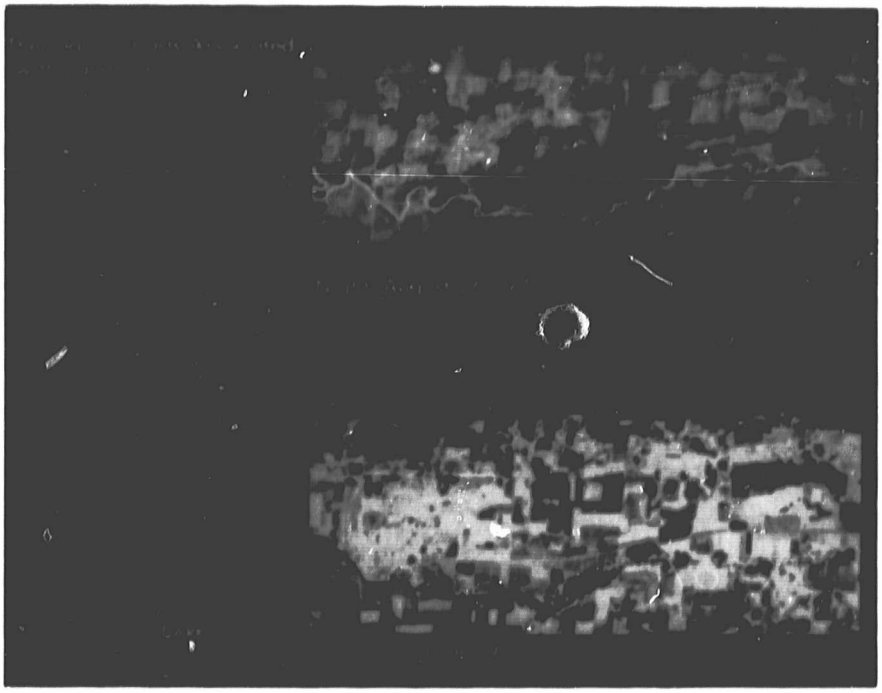

Figure 2. Day and night thermal imagery of the Sioux Basin north of Sioux Falls. The night image (b) shows a broad cool pattern within the flood plain associated with subsurface conditions. Daytime (a) thermal patterns mask anomalies associated with subsurface conditions. The flood plain is delineated by the dotted line; numbers are thickness (m) of saturated sands and gravels. Approximate scale 1:60,000, dark is cool. (After Moore and Myers. 1972; Myers and Moore, 1972).

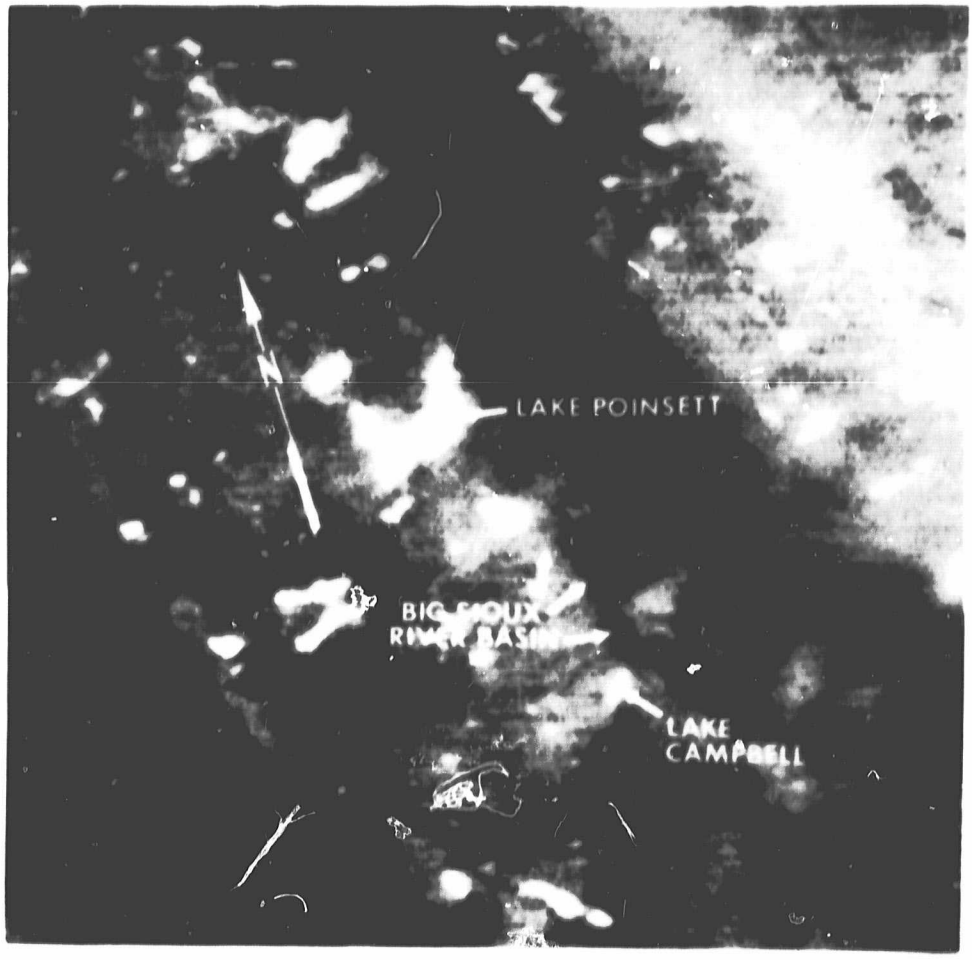

Figure 3. Photographic enlargement of an August 29, 1978, night HCMM thermal infrared image (scene ID A-A0125-08340) showing the Big Sioux Basin. Note that the Basin appears cooler than surrounding areas, due primarily to the heat sink produced by shallow groundwater within the Basin. (Approximate scale 1:1,000,000; dark is cool).

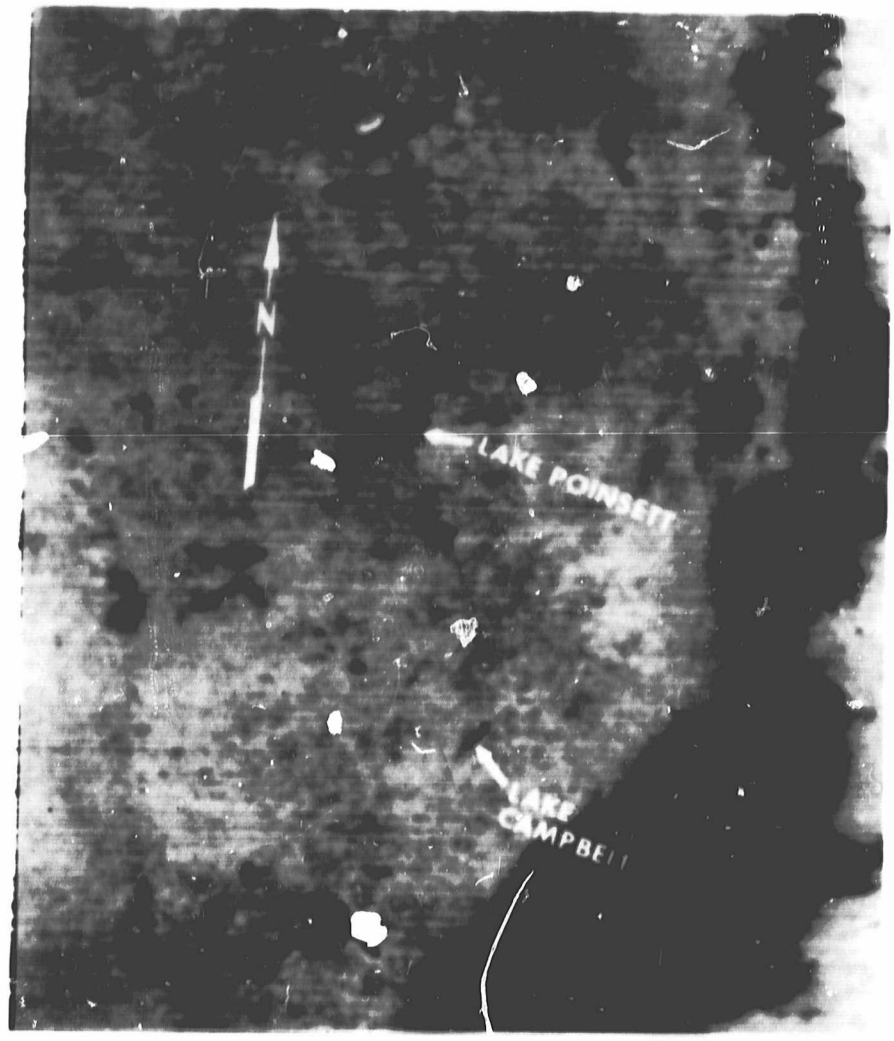

Figure 4. A September 4, 1978, photographic enlargement of a HCMM day thermal infrared image (scene ID A-A0131-19420) of the same area shown in Figure 3. Note that the Big Sioux River Basin is not visible because of emittance variation associated with land use. (Approximate scale 1:1,000,000; dark is cool).

Figure 5. A September 4, 1978, positive photographic enlargement of a HCMM day visible image of the same area shown in Figures 3 and 4. Note that the Big Sioux River Basin is not visible. (Approximate scale 1:1,000,000).

EVALUATING WATER TABLE DEPTH USING HEAT CAPACITY MAPPING MISSION (HCMM) DATA[1]

J. L. Heilman
Remote Sensing Center
Texas A & M University
College Station, TX 77843

D. G. Moore
Remote Sensing Institute
South Dakota State University
Brookings, SD 57007

1/ Contribution No. SDSU-RSI-J-80-07 from the Remote Sensing Institute, South Dakota State University. This investigation was supported by NASA under contract NAS5-24206.

INTRODUCTION

Soil temperatures are controlled not only by meteorological factors and thermal properties within the depth of diurnal temperature variation, but also by thermal properties of the underlying material. For example, Cartwright (1968a,b, 1970, 1974) found that water tables within the depth of annual soil temperature variation create a heat sink during the summer which produces cooler soil temperatures throughout the diurnal temperature cycle. This heat sink does not affect the amplitude of the diurnal temperature variation (Huntley, 1978). The magnitude of the temperature anomaly associated with shallow water tables is dependent upon aquifer thickness, rate of horizontal and vertical water movement, and water table depth.

Existence of temperature anomalies produced by shallow water tables has led investigators to evaluate the potential of thermal remote sensing for locating shallow aquifers. Chase (1969) found that apparent cool anomalies on thermal infrared imagery corresponded with shallow groundwater. Myers and Moore (1972) found a correlation between predawn radiometric temperatures and aquifer thickness. Huntley (1978) reported that surface temperature anomalies related to water table depth variations could be separated from reflectance and thermal inertial variations, but not from variations in evaporation rates.

We evaluated the utility of using Heat Capacity Mapping Mission (HCMM) radiometric temperatures to estimate water table depth. The HCMM, launched in April 1978, carries a two-channel radiometer (0.55 - 1.1 and 10.5 - 12.5 μm)

in a sun-synchronous orbit (orbital altitude is 620 km). Spatial resolutions are 0.5 x 0.5 km for the visible channel and 0.6 x 0.6 km at nadir for the thermal channel. The $NE\Delta T$ for the thermal channel is 0.4 K at 280 K. Swath width is 716 km. The HCMM collects data at approximately 0230 and 1330 local standard time (LST) with a repeat cycle of 5 or 16 days depending on latitude.

MATERIALS AND METHODS

The study was conducted in the Big Sioux River Basin in Brookings County in southeastern South Dakota (Figure 1). Surficial deposits in the drainage basin are predominantly of glacial origin, and consist of end moraine, ground moraine, and outwash deposits (Ellis et al., 1969). Most groundwater in the basin is obtained from shallow outwash deposits (within 10 m of the surface) and from sand and gravel lenses in morainal deposits.

The Big Sioux River is in contact with the outwash deposits, and groundwater discharge forms the base flow of the river. Most of the aquifer recharge occurs from runoff from snowmelt and early spring rains. Groundwater levels in the basin usually rise from late March through May, and decrease from June through September.

Soils in the basin are generally poorly drained in the flood plain and well drained in the slightly elevated terraces. Major agricultural land use categories in the basin are small grains (oats, spring wheat, barley), row crops (corn, soybeans), hayland and pasture.

Water table elevations in the basin were measured in U.S. Geological Survey observation wells (Figure 1). Soil water contents (0 to 4-cm

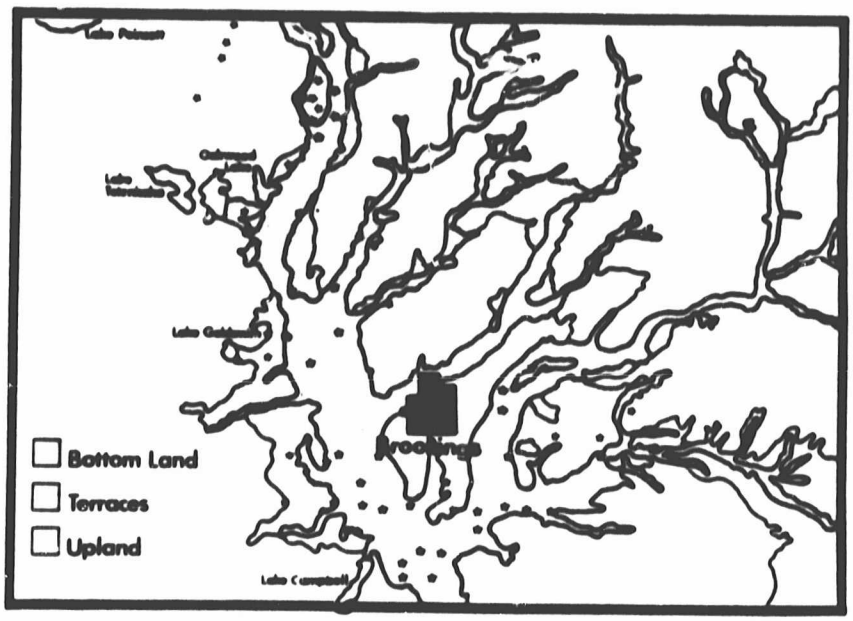

Figure 1. Landform map of Brookings County, South Dakota showing the flood plain (bottomland) and terraces of the Big Sioux River Basin. The stars indicate locations of U.S. Geological Survey groundwater observation wells.

layer) at selected locations were determined gravimetrically on soil samples collected on days of HCMM overpass.

Percent cover at several locations representative of the major land use categories were determined using 35 mm slides of the canopies (photographed from a vertical position approximately 1 m above the canopies) projected on a random dot grid. When canopies were too tall for the photographic procedure, percent cover was estimated from visual inspection. These data were used to prepare average percent cover curves for each category.

Radiometric temperatures from five HCMM scenes (Table 1) were extracted for each pixel encompassing an observation well by overlaying computer gray maps of HCMM data with a Brookings County map containing the well locations. Radiometric temperatures were corrected for atmospheric effects by comparing HCMM and ground measurements of Missouri River reservoir temperatures in central and southeastern South Dakota. Radiometric temperatures were not corrected for emissivity variations.

Table 1. HCMM scenes analyzed in water table study.

Date	Time	Scene I.D.
June 5, 1978	1330 LST	AA0040-19500
July 13, 1978	1330 LST	AA0070-19570
July 13, 1978	0230 LST	AA0078-09020
August 8, 1978	1330 LST	AA0104-19400
September 4, 1978	1330 LST	AA0131-19420

Percentage of each land use category for each pixel containing an observation well was determined using photointerpretation of a May 13, 1978, Landsat color composite (scene I.D. E-21207-16803) superimposed on HCMM computer gray maps via a Bausch & Lomb Zoom Transfer Scope. Percentage of each land use within a pixel, and the average percent cover curves for each land use category were used to calculate a percent cover for each pixel for every date of HCMM data analyzed.

RESULTS AND DISCUSSION

In an earlier paper we reported a highly significant relationship ($r = 0.68^{**}$) between 50-cm soil temperatures and water table depths of 3 m or less in the flood plain of the Big Sioux River Basin (Heilman and Moore, 1980). Subsequent analysis of additional temperature data indicated that the relationship could be extended to water tables as deep as 5 m. Water table depths in terraces and uplands were greater than 9 m and did not correlate with 50-cm soil temperatures. Thus depths greater than 5 m were excluded in the analyses of HCMM data.

Myers and Moore (1972) found that on daytime thermal imagery, thermal anomalies related to shallow water tables were overshadowed by vegetation differences (primarily differential evapotranspiration rates and shading). Similar results were found with the HCMM data (Table 2). HCMM temperatures at 1330 LST did not correlate with water table depth, primarily because the temperatures measured were mainly those of vegetation, or a composite of vegetation and soil.

Table 2. Coefficients of determination (r^2) between HCMM radiometric temperatures and water table depth.

Date	Time	r^2
June 5	1330 LST	0.02
July 13	1330 LST	0.02
July 13	0230 LST	0.03
August 8	1330 LST	0.06
September 4	1330 LST	0.02

Myers and Moore (1972) also reported that effects of vegetation were minimized at night and thus were able to obtain significant relationships between radiometric temperature and aquifer thickness using predawn thermography. We did not find any significant correlation between HCMM temperatures and water table depth for the July 13 0230 LST data (Table 2), possibly because of the small variation in radiometric temperature (less than 2 C) within the Sioux River Basin.

Heilman and Moore (1980) found that surface soil temperatures beneath a crop canopy could be estimated from remote measurements of composite temperature using the equation

$$T_s = 0.79\ e^{(-0.80\ PC)} + 20.35 \qquad (1)$$

where T_s(C) is surface soil temperature, T_c(C) is a composite radiometric temperature consisting of radiance contributions from the soil and the crop, and PC is present cover expressed as a fraction. Equation (1) was developed for measurements at 1330 LST.

We used equation (1) to estimate soil surface temperatures from HCMM temperatures (corrected for atmospheric effects) and pixel percent cover,

and found linear relationships between the predicted soil temperatures and water table depth (Figs. 2-5). Highest correlations occurred for the August 8 and September 4 data. Summertime soil temperature gradients in South Dakota are at a maximum in August and early September.

Although the correlations improved in August and September, the slopes and intercepts of the four relationships in Figs. 2-5 were not significantly different at the 0.01 level. Thus, data for the four dates were pooled, and the equation

$$T_s = 26.90 + 1.30\ D \qquad (2)$$

with a r^2 of 0.45 was obtained where D(m) is water table depth (Fig. 6).

Predicted soil temperatures were correlated not only with water table depth, but also with soil moisture (Fig. 7). Multiple regression analysis of the September 4 data yielded the equation

$$T_s = 26.60 - 0.05\ SWC + 2.50\ D \qquad (3)$$

with a r^2 of 0.87 where SWC(%) is the volumetric soil water content in the 0 to 4-cm layer. Increasing soil water content reduces the amplitude of the diurnal surface temperature variation through thermal inertia and evaporation effects which cannot be separated from heat sink effects using a single daytime measurement (Huntley, 1978).

Results of this investigation demonstrate a potential for using satellite thermography to detect regions of shallow water tables and estimate water table depth if appropriate considerations are given to the effect of vegetation on the surface thermal regime. However, techniques for separating water table influences from those of soil moisture must be developed before satellite thermography can be a useful tool for groundwater studies.

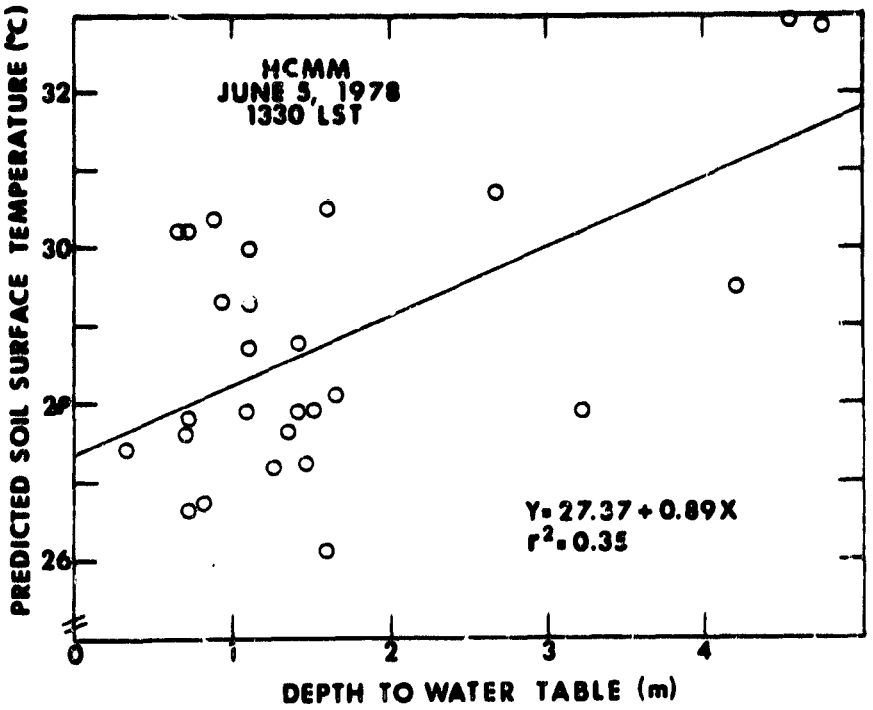

Figure 2. Relationship between predicted soil surface temperature and water table depth on June 5, 1978.

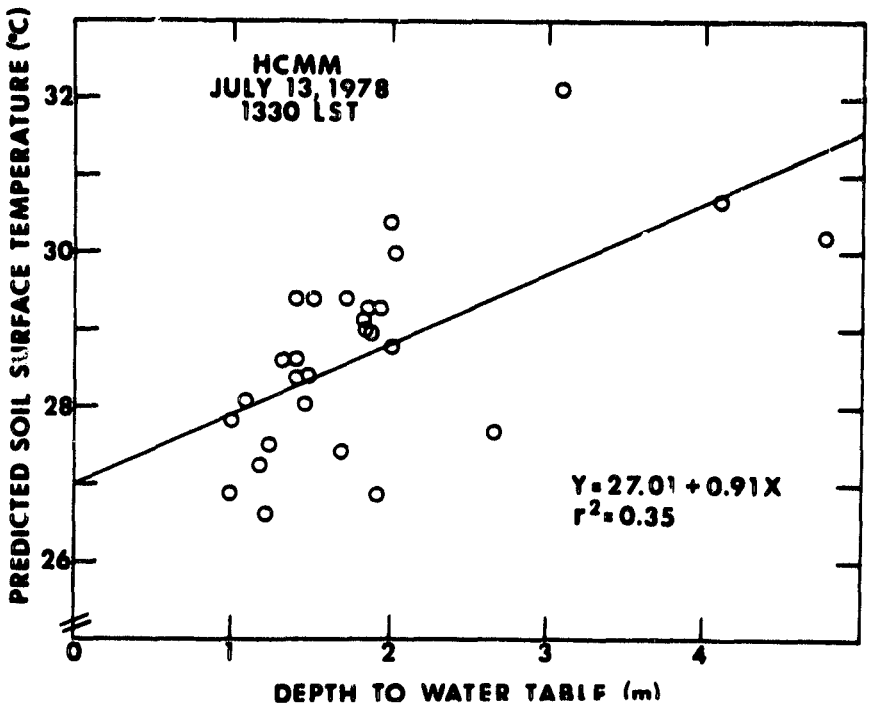

Figure 3. Relationship between predicted soil surface temperature and water table depth on July 13, 1978.

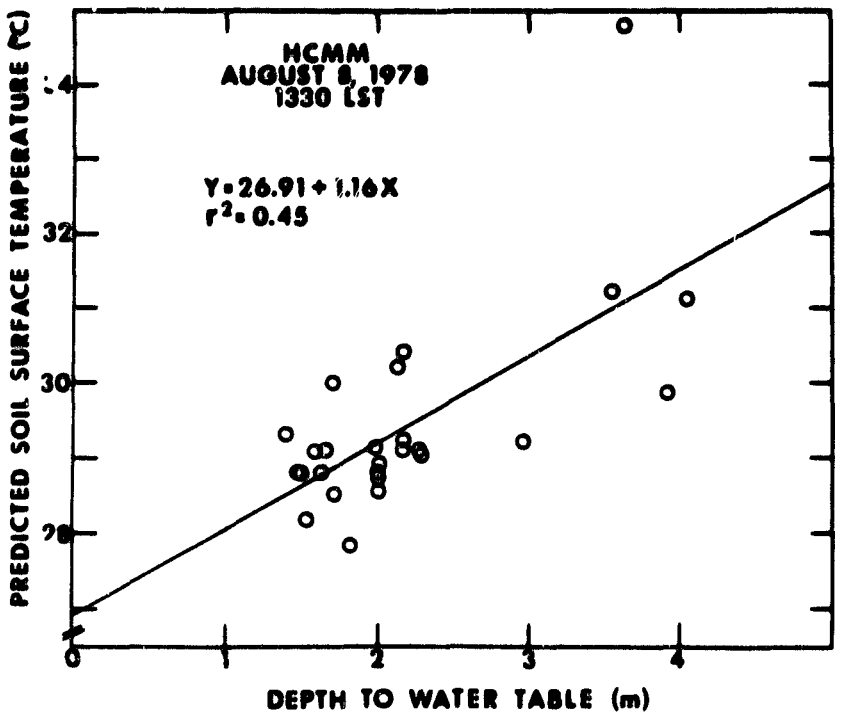

Figure 4. Relationship between predicted soil surface temperature and water table depth on August 8, 1978.

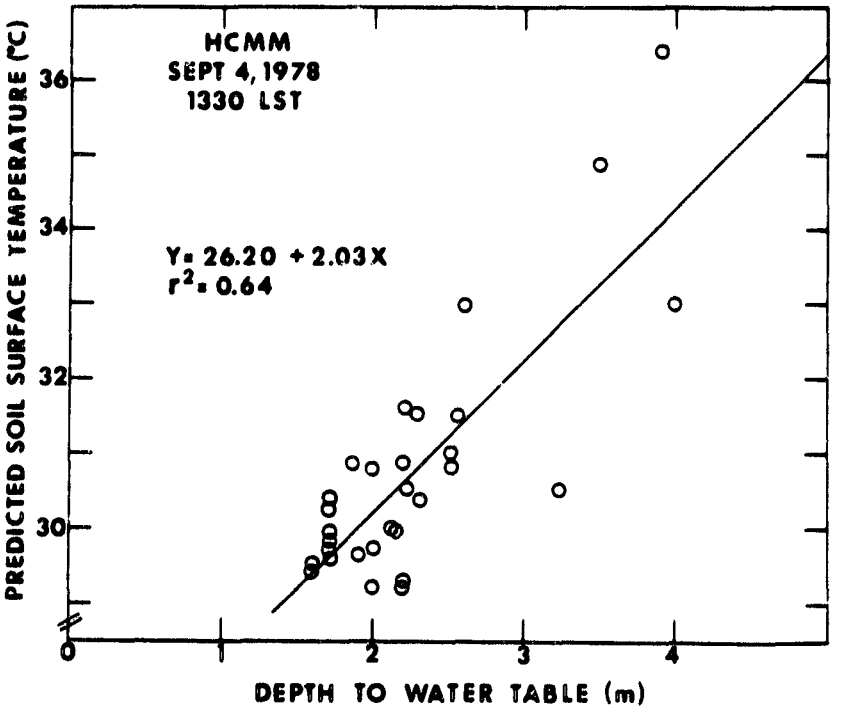

Figure 5. Relationship between predicted soil surface temperature and water table depth on September 4, 1978.

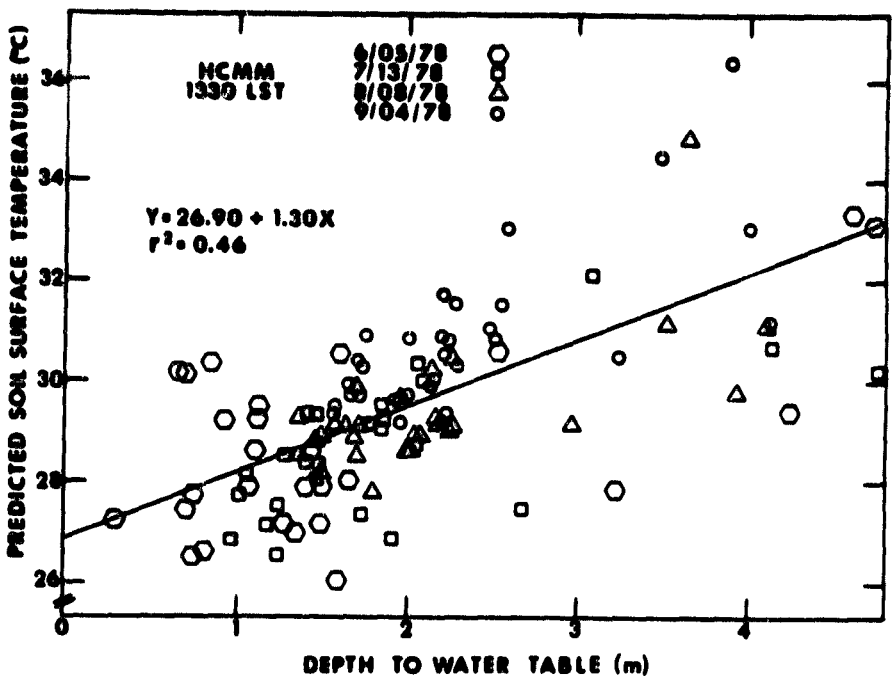

Figure 6. Relationship between predicted soil surface temperature and water table depth when data from the four dates were pooled.

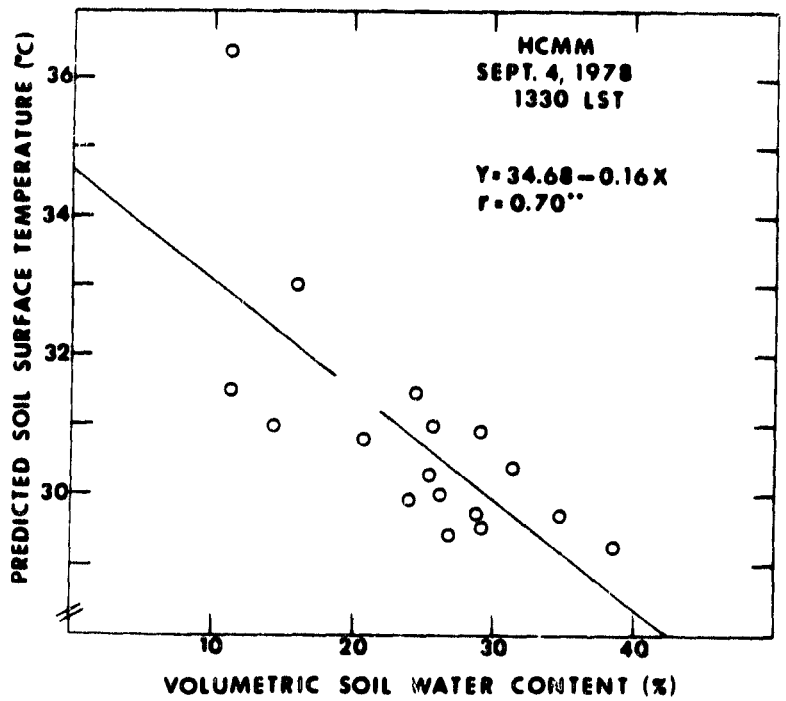

Figure 7. Relationship between predicted soil surface temperature and volumetric soil water content in the 0 to 4-cm layer.

REFERENCES

Cartwright, K. 1968a. Temperature prospecting for shallow glacial and alluvial aquifers in Illinois, Ill. State Geol. Surv. Circ. 433.

_____. 1968b. Thermal prospecting for groundwater, Water Resour. Res. 4:395-401.

_____. 1970. Groundwater discharge in the Illinois basin as suggested by temperature anomalies. Water Resour. Res. 6:912-918.

_____. 1974. Tracing shallow groundwater systems by soil temperatures. Water Resour. Res. 10:847-855.

Chase, M.E. 1969. Airborne remote sensing for groundwater studies in prairie environment. Can. J. Earth Sci. 6:737-741.

Ellis, M.E., D.G. Adolphson, and R.E. West. 1969. Hydrology of a part of the Big Sioux Drainage Basin, eastern South Dakota. USGS Hydrology Investigation Atlas 311.

Heilman, J.L., and D.G. Moore. 1980. Thermography for estimating near-surface soil moisture under developing crop canopies. J. Appl. Meteor. 19:324-328.

Myers, V.I., and D.G. Moore. 1972. Remote sensing for defining aquifers in glacial drift. Proc. of Tenth International Symp. on Remote Sens. Environ., University of Michigan, Ann Arbor, pp. 985-994.

CHAPTER IV: USE OF HEAT CAPACITY MAPPING MISSION DATA IN SOIL GEOGRAPHY STUDIES

(Abstract presented as poster paper at American Society of Agronomy. Westin, F.C., J.L. Heilman, and D.G. Moore. 1980. Use of Heat Capacity Mapping Mission (HCMM) Satellite Data in Soil Association Studies. Agronomy Abstracts, Nov. 30-Dec. 5, 1980, Detroit, Michigan, p. 189).

USE OF HEAT CAPACITY MAPPING MISSION (HCMM) DATA IN SOIL GEOGRAPHY STUDIES

INTRODUCTION

Producing enough food is an increasingly serious problem in the world. Production of food, directly or indirectly depends partly on soil. Although inventory of soil resources is well along in some countries it lags in others.

The Heat Capacity Mapping Mission (HCMM) satellite is a new tool that may be used in reconnaissance soil inventories. HCMM was launched in April 1978, and collects data in the visible and near infrared (.5-1.1 μm) and thermal infrared (10.5-12.5 μm) regions on the spectrum at a spatial resolution of 0.5 x 0.5 km. At mid-latitudes the satellite collects data at approximately 0230 and 1330 local standard time with a repeat coverage of five days. The two channels on the HCMM allow both reflectance and thermal properties to be used in soil studies. The objective of this study was to compare land characteristics such as elevation, soil texture, and slope aspect of known areas on HCMM imagery.

BRIEF LITERATURE REVIEW

Lattman (1963) found valley side springs showed up more clearly on night time aerial TIR images than on conventional aerial photography. This was thought to be due to differences in the night time temperatures of the ground and the warmer ground water coming from the springs.

Cantrell (1964) working with surface water found that as stream water begins cooling the thermal energy given off seems to warm the

vegetation and air thus forming a heat sink. The heat sink superimposes the drainage net on the imagery.

Sabins (1969) used IR imagery for structural mapping in Southern California. He found that flooded fields in the Imperial Valley appeared warm on the imagery. Damp ground gave a cold signature.

Cannon (1973) found that predawn IR Imagery provided a detailed drainage map and was a good way to inventory surface water distribution.

Offield (1975) mapped structure of the front range and adjacent plains of Colorado on IR images derived from a scanner on a RB 57 aircraft.

Schnieder et al (1979) used enhanced night time thermal imagery and digital data from a NOAA polar orbiting satellite to map drainage patterns and landforms in North and South Dakota. The Missouri and Prairie Coteaus, glacial moraines and partial drainage boundaries of major rivers were discerned. Analysis of satellite digital thermal data for western tributaries of the Missouri River showed north-facing slopes to be warmer than south-facing slopes by an average of 1.5^{o}C.

THE STUDY AREA

HCMM imagery of South Dakota was examined for a number of dates. Visible and thermal IR images (day and night) were used. Figure 1 shows a night IR mosaic from August for an area in east-central South Dakota. The same scene appears in both panels. The annotation in the lower panel indicates elevation, soil texture and slope aspect differences. The upper right area labeled "warm-lower elev." is the east facing slope of the Prairie Coteau and the lower lying Minnesota-Red River Valley.

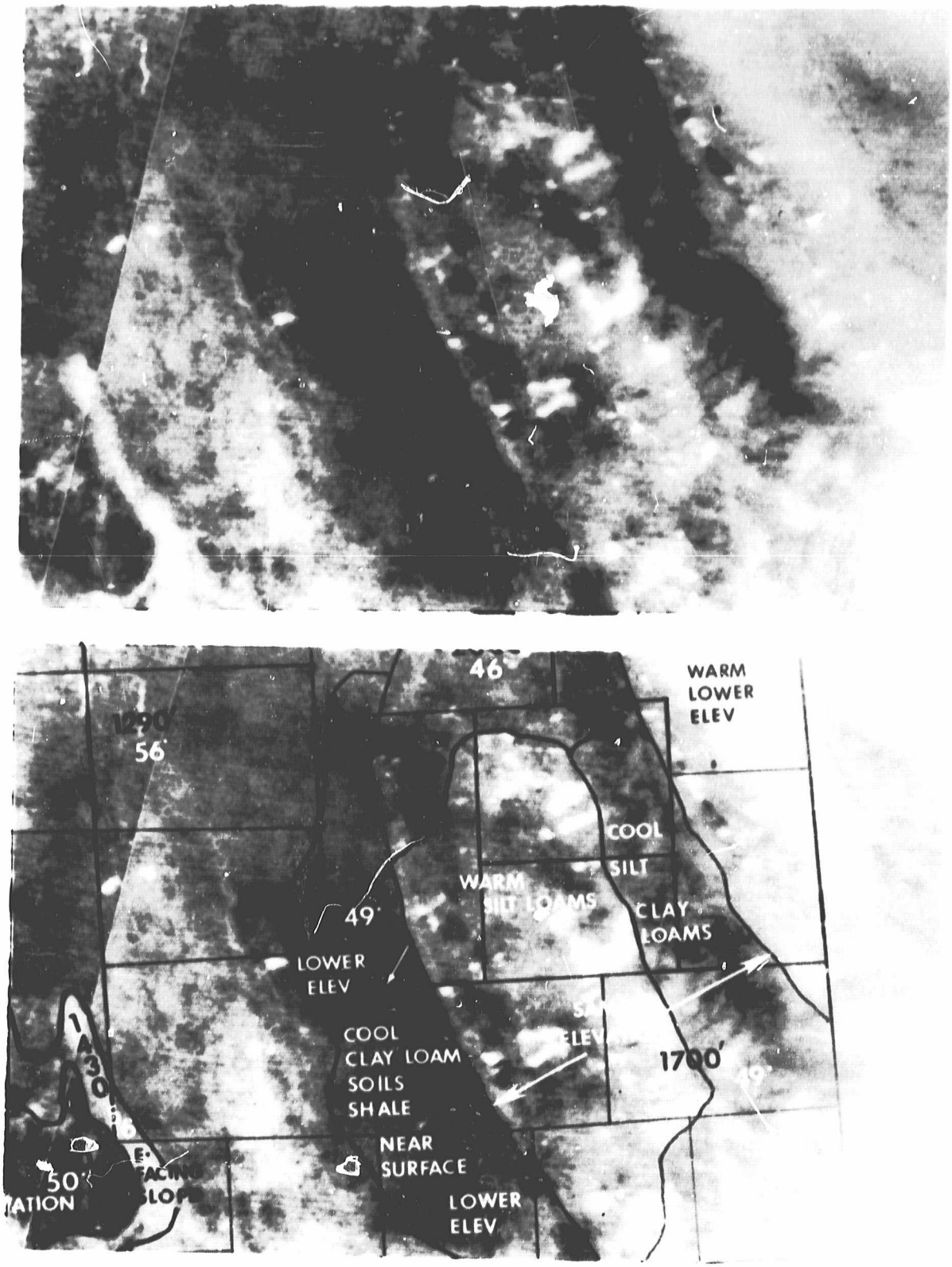

Figure 1. Predawn thermal infrared HCMM image (dark is cool) for an area in east-central South Dakota.

The Prairie Coteau lying west of this separates into two areas - the eastern cooler area of finer textured silty clay loam soils (Kranzburg series) and the warmer silt loam soils (Poinsett series). These two areas have about the same elevation (1700 ft.) but the temperature at the time the image was recorded was 49°F for the cooler Kranzburg series and 52°F for the warmer Poinsett series. West of the Prairie Coteau the elevation is about 1280 ft. and the temperature is 49°F. This cool area has more dense clay loam soil having a high component of shale and has shale bedrock nearer the surface than the rest of the James Valley to the west. Temperature in the warmer part of the James Valley lowland (elevation about 1290') was about 56°F. In the lower left of the scene the warmer northeast and east facing coteau escarpment is seen. West of the escarpment is the higher lying and cooler Missouri coteau.

Figure 2 shows the portion of the mosaic west of Figure 1. The warmer Missouri escarpment is clearly delineated as are the cooler Missouri coteau and the somewhat warmer James River Lowland.

Figure 3 coverage lies west of the area shown on Figure 2 and encompasses the Black Hills on the extreme west and the plains east of the Black Hills. The Black Hills appear cooler on the image while the north-facing slopes of the east-flowing streams and rivers are warmer. This verifies the results found by Schneider et al that the north-facing slopes are warmer than crest positions or south facing slopes.

DISCUSSION

The 3 figures show landscapes from night IR taken in August. The results show that elevated areas, finer textured soils, and crest or

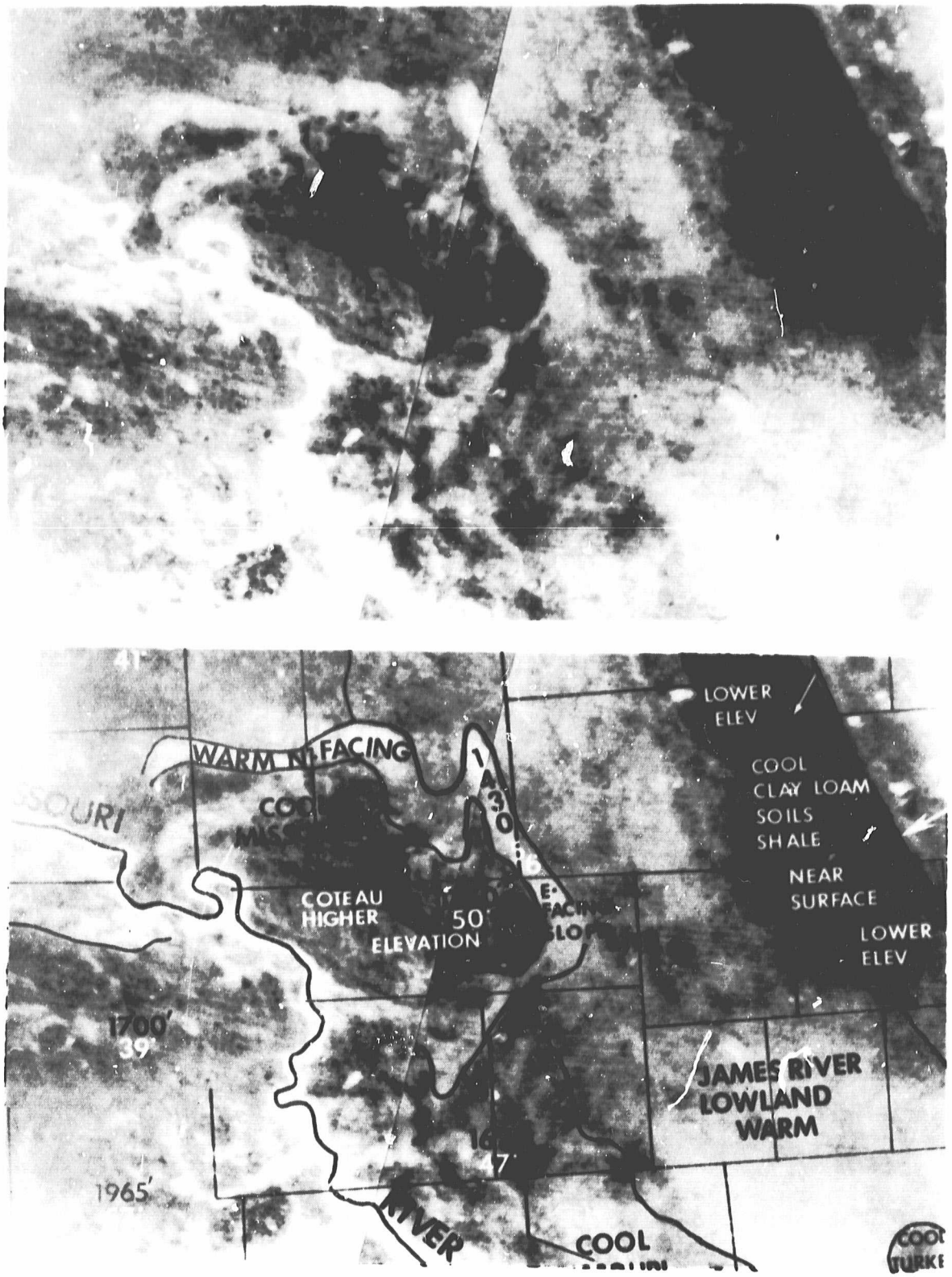

Figure 2. Enlarged area from Figure 1.

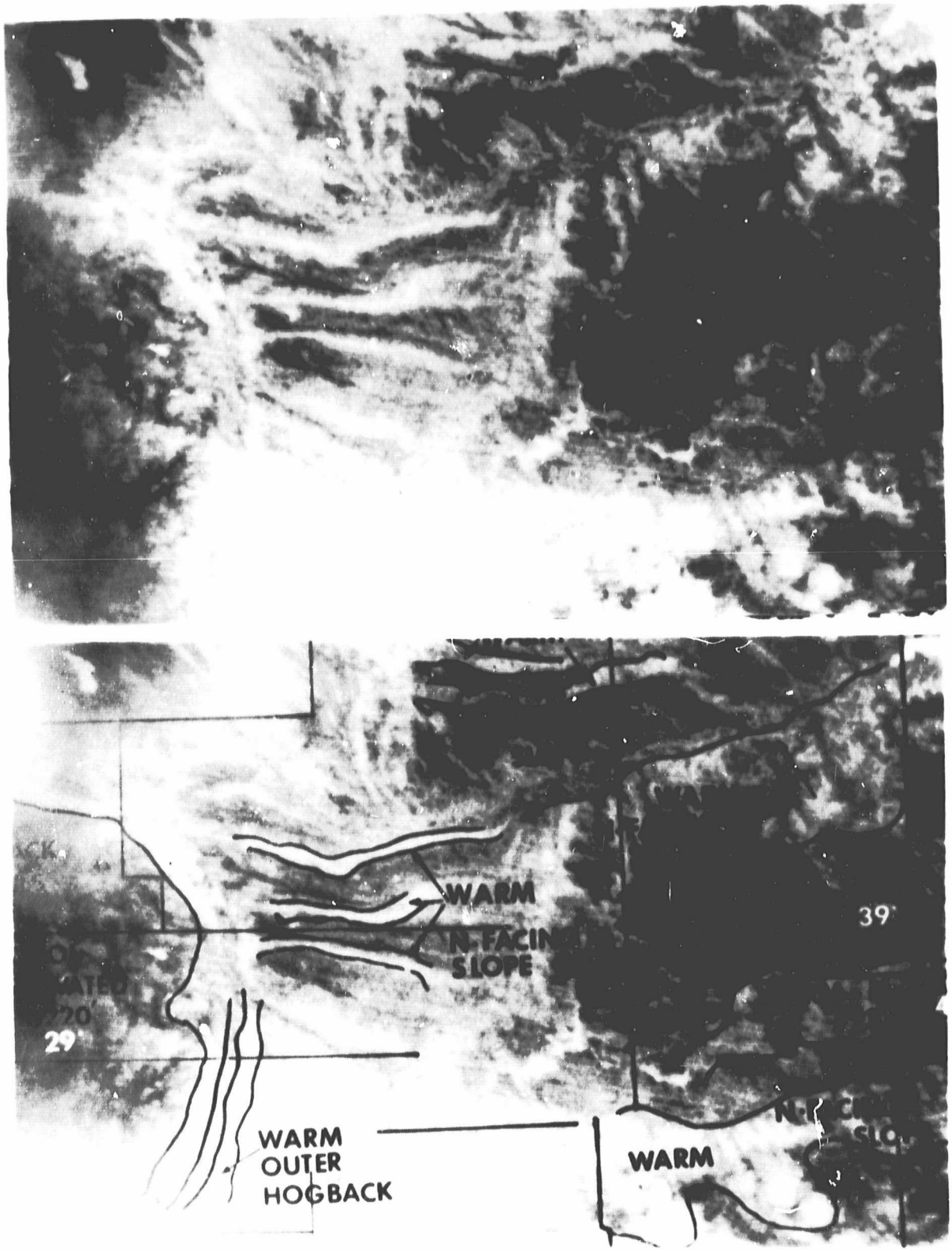

Figure 3. Predawn HCMM thermal infrared image of area including the Black Hills of South Dakota (dark is cool).

south-facing slopes are cooler than lower lying areas, coarser textured soils, and north-facing slopes. Scenes examined for June 21, 1978, and May 14, 1978, show the same relationships.

Perhaps the most significant relationship for soil geography is the warmer temperatures that exist on north-facing slopes. Logically the opposite situation would be expected since these slopes escape the direct rays of the sun. It appears that the lack of direct sunlight results in cooler temperatures during the day which in turn means less evapotranspiration. Thus, more moisture is available which holds heat better than the drier crest and south-facing slopes.

No difference in soil mapping units in soil survey operations is recognized on north-facing slopes from other aspect sites. One reason is that prior to HCMM there was no means to measure this heat difference. Yet the heat difference must be a significant factor in vegetative growth. Since most of western South Dakota is rangeland the difference in grass production and stocking rate probably is the principal kind of land use affected.

Elevation differences of as much as 1000 feet occur between the northern part of the Prairie Coteau and the Red River-Minnesota River Lowland. Elevation differences are somewhat lower than this (about 600-700 feet) between the northern part of the Prairie Coteau and the James River Lowland. Separate soil series have been mapped on the northern Prairie Coteau and the lowlands on either side due to soil parent material differences (texture and mineralogy differences). Although it was realized that temperature differences also occur

among these areas there has been no method for showing this spatially until the introduction of thermal imagery.

Soil texture differences exist between the cooler eastern side of the Prairie Coteau and the warmer western side. The eastern area is covered by older glacial materials and has a mature landscape where streams drain off excess water. These are the Kranzburg soils. The western area is characterized by younger glacial deposits in an irregular immature landscape. Here precipitation tends to remain in the area since few streams exist and water drains to a nearby marsh or lake. This is the Poinsett soil area. The HCMM image clearly shows the high concentration of surface water present in the western Prairie Coteau area. In fact the warmer temperatures of this area of coarser textured soils may be due in part to the significant percentage of surface water holding heat through the night over the entire area.

REFERENCES

Cannon, P.L., (1973), The application of radar and infrared imagery to quantitative geomorphic investigation. Proceedings of the Remote Sensing of Earth Resources Second Annual Conference, Tullahoma, Tennessee, pp. 503-527, The Univ. of Tennessee Space Inst., Tullahoma

Cantrell, J.L., (1964), Infrared geology, Photogram. Eng. 30:916-922.

Lattman, L.H., (1963), Geologic interpretation of airborne infrared imagery, Photogram. Eng. 29:81-87.

Offield, T.R., (1975), Thermal images as a basis for structure mapping front range and adjacent plains in Colorado. Geol. Soc. Am. Bull. 86:495-502.

Sabins, F., (1969), Thermal infrared imagery and its application to structural mapping in Southern California, Geol. Soc. Amer. Bull., 80:397-404.

Schneider, S.R., D.F. McGinnis, Jr., and J.A. Pritchard. 1979. Use of Satellite Infrared Data for Geomorphology Studies, Remote Sensing of Environment, Elsevier, North-Holland.

CHAPTER V: MODEL DEVELOPMENT FOR MONITORING WATER TABLES AND NEAR-SURFACE SOIL MOISTURE BY THERMOGRAPHY

Tunheim, J.A., G.A. Beutler, S.D. Ness, and D.G. Moore (not submitted to date as journal publication).

Appendix A: HPL PROGRAM FOR FINITE-DIFFERENCE HEAT FLOW SIMULATION MODEL.

MODEL DEVELOPMENT FOR MONITORING WATER TABLES AND NEAR-SURFACE SOIL MOISTURE BY THERMOGRAPHY[1/]

Co-Authors

J.A. Tunheim, G.A. Beutler and S.D. Ness
Physics Department
South Dakota State University
Brookings, South Dakota 57007

and

D.G. Moore
Remote Sensing Institute
South Dakota State University
Brookings, South Dakota 57007

February 1981

[1/] Investigation was supported by NASA under contract NAS5-24206.

ABSTRACT

Experimental and theoretical investigations were carried out relating to the detection and mapping of near-surface groundwater by the use of remote-sensed thermal emittance data (thermography). Soil temperature profiles, thermal emittance, soil moisture, depth to groundwater table, and other pertinent data were collected for test plots under fallow and crop cover conditions.

Data were collected simultaneously for two plots having similar surface conditions except that one of the plots was irrigated to create a difference in soil moisture profile. Calculations of surface temperature differences as a function of time for these soil moisture conditions were made utilizing a finite-difference model. The functional form of the theoretical temperature difference with time was shown to be very close to the experimental apparent temperature difference for both crop cover and bare soil conditions. This result strongly suggests that a technique can be developed by which the effects of near-surface soil moisture can be separated from the total thermal emittance data by subtracting the data component having this functional form from total thermal emittance. This component could then be used to calculate soil moisture differences for a group of chosen sites. If a soil moisture profile is measured at one site, the soil moisture profile could be calculated for other sites.

A series of model calculations were carried out to simulate the effect of a near-surface water table at one site and a similar site without such a water table. These calculations show the effect of a water table is to give rise to a temperature difference at the surface which is nearly constant through time over a current cycle. The presence of a water table thus may be detected from a component of thermal emittance difference which remains constant during the diurnal cycle when compared to a reference site.

The model was tested utilizing widely spaced sites resolved by HCMM. Theoretical surface temperature differences calculated using the model agreed well with apparent temperature differences measured by HCMM.

INTRODUCTION

Recent launchings of satellites with thermal infrared imaging sensors together with those planned in the near future hold great promise for application of thermal emittance data as a tool for resource management and development. These earth resources satellites allow time-sequential monitoring of land surface emittance over large areas of the earth at relatively low cost. They allow data to be readily available on a routine basis for use by the resource specialist in making management decisions.

The potential use of thermography for monitoring groundwater uses remote sensing measurements of thermal emittance to estimate surface temperature. Any factor which causes a variation in surface temperature may thus be measured by thermography. Near-surface groundwater is such a factor. Its presence causes large changes in the specific heat and thermal conductivity of the soil. Phase transformations of water during evaporation or freezing also have large thermal effects on the energy budget of land surface and thus affects the land surface temperature.

Complications with this method arise because soil temperature and surface emittance depend on a multitude of physical factors. Plant growth, aspect of slope, water table, wind velocity and other variables alter soil temperatures and thermal emittance in addition to variations associated with differing water table depths. Thus isolation of emittance variations caused by the presence of soil moisture alone is very difficult. Therefore, models describing emittance variations associated with various physical features must be developed to isolate their effects and to understand their interdependence. This may allow one to compensate for their effect during data analysis or to schedule the collection of data when their effect is small.

Another complication arises when the thermal infrared (TIR) image is obtained from satellite-borne sensors. The image includes components of radiation

emitted and reflected by the surface modified by absorption and emission from the intervening atmosphere. To determine exact values of surface temperature, corrections in the measured signal must be made which depend very heavily on atmospheric conditions and thus change with time. Corrections must also be made for surface emissivity and reflection which also change with surface conditions. Thus considerable difficulty is involved in converting a satellite image into a surface temperature map. Temperature differences between two points on the earth may be much easier to obtain with reasonable accuracy from TIR satellite data than to obtain exact temperatures. For example, absorption by the atmosphere will decrease the apparent temperature of two points but the apparent temperature difference between the two points will remain nearly constant if the absorption is similar over both points. Also emissivity and reflectivity differences can also be minimized by making the comparisons between points which have the same plant cover such as two wheat fields.

The emphasis of the effort was on relating these surface temperature differences to the variation in groundwater presence. Particular attention was placed on the use of the variations in temperature differences during the diurnal cycle to separate effects of groundwater tables in the top 50 cm of soil from that at larger depths. A technique of this type would be particularly applicable to satellites such as HCMM which allow more than one apparent temperature measurement during a single diurnal cycle.

The technique envisioned for mapping groundwater over large areas using data collected by a satellite such as HCMM would be as follows:

1. A reference site would be selected where groundwater would be monitored (water table and near-surface soil moisture) on a continuing basis.
2. The proposed model would be used to calculate the difference in near-surface soil moisture and water table depths between this site and a

second from the difference in apparent temperatures acquired by remote sensors during a diurnal cycle.

3. This procedure can then be repeated using any group of sites and thus near-surface soil moisture and water table maps may be constructed.

The general objective of this phase of the project was to develop and test a model which could be used as described in step 2 of the above procedure.

BACKGROUND LITERATURE

The study was to develop a model useful for interpreting remote sensing data for mapping of near-surface soil moisture and measurement of water table depth. TIR images have been used to locate springs and wells (Myers and Moore, 1972) by the use of predawn images. This together with a former study by Myers and Heilman (1969) showed that predawn images exhibited a higher surface temperature for bare soil with higher moisture content in the top 50 cm. Myers and Moore (1972) evaluated the use of airborne thermography for mapping shallow aquifers using emittance patterns of predawn thermography. They obtained statistically significant results for predicting the thickness of the saturated sands and gravels for an August (maximum annual downward temperature gradient) predawn flight over shallow aquifers in eastern South Dakota. In a further study, Moore and Myers (1972) illustrated the thermal response to climatic variables for diurnal and seasonal thermography. Land use, soil moisture, and other sources of thermal differences were easily observed for daytime thermography with their effects diminishing for predawn thermography. They concluded predawn August data were the most useful for identifying shallow aquifers in South Dakota.

Several investigators have studied the relationship between thermal emittance measured from aircraft altitudes and soil temperatures. Schmugge (1978) and Reginato (1976) have shown agreement between such TIR temperatures and those measured by thermocouples in contact with the soils. A study by Tunheim (1977) found a positive correlation between aircraft TIR imagery and soil temperature fields caused by near-surface water tables associated with saline seeps. Results of this project showed the need for modifying the existing model to include the effects of near-surface soil moisture.

The first evaluation of satellite thermography as an indicator of soil moisture was performed by Moore, et al (1975). Analysis of SKYLAB data showed

a positive correlation between soil moisture and thermal emittance. It was concluded that thermal data from satellite altitudes had good potential for use in monitoring soil moisture and for irrigation scheduling.

Quantitative estimates of soil moisture using thermal emittance data, however, require a model relating the effects of subsurface soil moisture on the surface temperature. No such model has yet been developed, although several similar types of models exist. A model proposed by Kahle, et al (1975) relates the change in land surface temperature during the diurnal cycle to the thermal inertia of subsurface geological materials. This model, however, does not allow for effects of groundwater, soil moisture , evapotranspiration, or crop cover.

Two other models have been developed by Meyer (1972) for relating surface thermal emittance to the presence of shallow aquifers. These models use the assumption that a shallow aquifer would cause the soil temperature at a 50-cm depth to vary 1°C to 3°C from that of a non-aquifer region. The ability of this subsurface thermal anomaly to produce a corresponding surface thermal anomaly was investigated by use of these models. The first model simulated the development of a surface thermal anomaly during a single night and the second simulated the behavior of the thermal anomaly during several successive days.

Each model considered heat transfer in two identical soil layers of 50-cm thickness. Since daily variations in the temperature are small at 50 cm (Cartwright, 1968; Carson, 1961) the lower boundary temperature of each soil layer was held constant. The subsurface thermal anomaly was presented by letting these fixed temperatures differ by an amount ΔT.

The first model assumed a constant heat flux due to radiation. Using a finite integral transform, the heat transfer problem was analytically solved. Results predicted that a surface temperature difference ranging from 20% to 40% of that assumed at a 50-cm depth would develop in 9 hours. The rate of development

depended only on the thermal diffusivity of the 50-cm soil profile. Values of diffusivity for the calculations were chosen according to Sutton (1953). A result of this calculation was the prediction that the development of a surface thermal anomaly does not depend on the magnitude of the heat flux radiated from the surface.

The second model assumed a surface heat flux approximated by a rectified sine wave and a terrestrial radiation term as suggested by Smith (1966). No analytic solution was possible in this case and thus a finite-difference technique was used in a numerical solution by computer. Calculated temperature profiles showed good qualitative agreement with data taken by Carson (1961).

One significant result was that a maximum value for the thermal anomaly would occur at 0700 hours. This result has recently received support experimentally for the case of ground water associated with saline seeps Aaron, et al (1976).

The finite-difference model by Meyer is the one which was modified and applied to this project.

THEORETICAL MODEL

The finite difference heat flow model developed by Meyer (1972) uses homogeneous soil profiles, each 50 cm in thickness. The 50-cm depth was chosen since daily variations in soil temperature are small at this depth (Cartwright, 1968; Carson, 1961). The 50-cm soil profile is divided into 50 one-cm layers with 50 equally spaced reference nodes as shown in Figure 1. The m reference points are usually referred to as nodal points. Notice that nodal point 1 coincides with the upper surface of the slab at x = 0. The point m coincides with the other boundary at x = 50 cm. The heat flux into the surface x = 0 has been denoted q_s while the heat flux out of the lower surface at x = L is denoted as q_L.

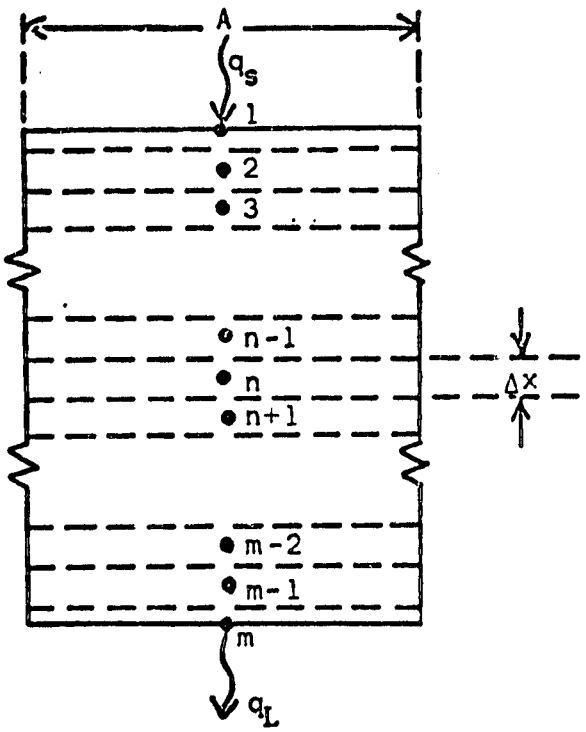

Figure 1. Assignment of Nodal Points and Heat Flux Terms for the Finite Difference Model.

A rectified sine wave is used to approximate heat flux q_s (Smith, 1969). Since it is difficult to measure, it was treated as a parameter composed of a sinusoidal solar term and a blackbody radiation term. Its functional form was taken as:

$$q_s = M \sin \frac{\pi t}{L} - R \tag{1}$$

where M, the amplitude of the solar term, is the maximum solar radiation during the daylight hours. The variable t is the time of day measured from sunrise and L is the number of hours of daylight. The second term R is the terrestrial radiation term as suggested by Smith (1969). The radiation term results in a negative surface heat flux during the night as has been observed experimentally (Lettau and Davidson, 1957). The terrestrial radiation equation used was,

$$R = \sigma[T^4 - (T')^4], \tag{2}$$

where R is the net outgoing radiation, σ is the Stefan-Boltzmann constant, T is the surface temperature in degrees Kelvin, and T' is the effective atmospheric temperature in degrees Kelvin (Fleagle, 1950).

Consider a volume of material surrounding node n (n = 2, 3, $\cdots$, m-1) as shown in Figure 2. The volume of the material surrounding node n is $A\Delta x$ where A is a unit surface area and Δx is the distance between nodal points. The amount of heat transferred from node n-1 to node n is denoted by $q_{n-1,n}$ and the amount of heat transferred from node n to node n+1 is denoted by $q_{n,n+1}$. The heat stored within the volume is given by $\dot{E}_{sn}$.

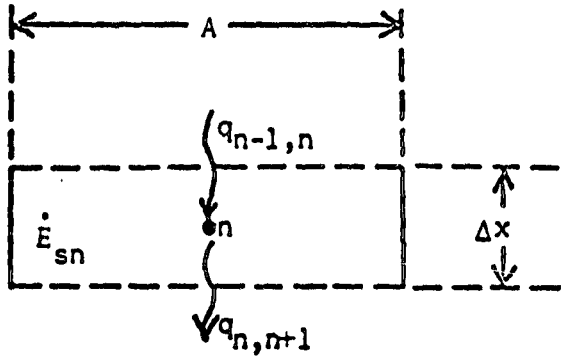

Figure 2. Energy Balance for Node n.

For one dimensional heat transfer, the law of conservation of energy applied to node n results in the equation

$$q_{n-1,n} = q_{n,n+1} + E_{sn} \tag{3}$$

The rate at which heat is transferred between nodal points is written in finite difference form as

$$q_{n-1,n} = - kA \frac{T_n - T_{n-1}}{\Delta x} \tag{4}$$

$$q_{n,n+1} = - kA \frac{T_{n+1} - T_n}{\Delta x} \tag{5}$$

where T_{n-1} is the temperature of node n-1, T_n is the temperature of node n, T_{n+1}, is the temperature of node n+1, and k is the thermal conductivity of the material between the nodal points. If the conductivity of the volume element surrounding each nodal point is different, the conductivity between nodal points may be written as the average of the volume elements. Thus for equation (5)

$$k = \frac{k_{n-1} + k_n}{2} \tag{6}$$

Equation (4) may then be written as

$$q_{n-1,n} = -\left(\frac{k_{n-1} + k_n}{2} \right) A \frac{T_n - T_{n-1}}{\Delta x} \tag{7}$$

Similarly, equation (5) becomes

$$q_{n,n+1} = - \left(\frac{k_n + k_{n+1}}{2} \right) A \frac{T_{n+1} - T_n}{\Delta x} . \tag{8}$$

The energy storage term expresses the rate at which the temperature of the volume changes. This term may be written in finite difference form as

$$\dot{E}_{sn} = (\rho c)_n A \Delta x \frac{T_n' - T_n}{\Delta t} \tag{9}$$

where Δt is the time increment, T_n is the temperature of node n at time t and T_n' is the temperature of node n at time $t+\Delta t$.

Substituting equations (7), (8), and (9) into equation (3) and rearranging terms yields

$$\frac{T_n'-T_n}{\Delta t} = \frac{1}{2(\rho c)_n(\Delta x)^2}\left[(k_{n-1} + k_n)T_{n-1} - (k_{n-1} + 2\,k_n + k_{n+1})\,T_n \right. \tag{10}$$

$$\left. + (k_n + k_{n+1})\,T_{n+1} \right] .$$

Solving for the temperature at time t+Δt results in the equation

$$T_n' = \frac{(k_{n-1} + k_n)\Delta t}{2(\rho c)_n(\Delta x)^2}\,T_{n-1} + \left[1 - \frac{(k_{n-1} + 2k_n + k_{n+1})\Delta t}{2(\rho c)_n(\Delta x)^2} \right] T_n$$

$$+ \frac{(k_n + k_{n+1})\Delta t}{2(\rho c)_n(\Delta x)^2}\,T_{n+1} . \tag{11}$$

Now consider the transfer of heat at the surface x = 0. Figure 3 shows the volume element for node 1.

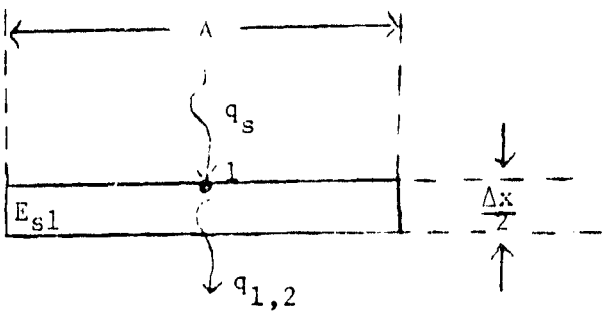

Figure 3. Energy Balance for Node 1.

The energy balance can be written as

$$q_s = q_{1,2} + \dot{E}_{s1}. \tag{12}$$

The rate of heat transfer from node 1 to node 2 is

$$q_{1,2} = -\left(\frac{k_1 + k_2}{2} \right) A\,\frac{T_2 - T_1}{\Delta x} . \tag{13}$$

Since node 1 is at the surface, the volume of material surrounding node 1 is $\frac{\Delta x}{2}$ A. The energy storage term is then

$$\dot{E}_{s1} = (\rho c)_1 A \frac{\Delta x}{2} \frac{T_1' - T_1}{\Delta t} . \tag{14}$$

Substituting equations (12) and (13) into equation (14) and rearranging yields

$$\frac{T_1' - T_1}{\Delta t} = \frac{2q_s}{A(\rho c)_1 \Delta x} + \frac{k_1 + k_2}{(\rho c)_1 (\Delta x)^2} [T_2 - T_1]. \tag{15}$$

Solving for the new temperature T_1' gives

$$T_1' = \frac{2q_s \Delta t}{A(\rho c)_1 \Delta x} + [1 - \frac{(k_1+k_2)\Delta t}{(\rho c)_1 (\Delta x^2)}] T_1 + \frac{(k_1+k_2)\Delta t}{(\rho c)_1 (\Delta x)^2} T_2. \tag{16}$$

Finally, consider the node at the lower boundary x = L. Figure 4 shows the volume element for node m.

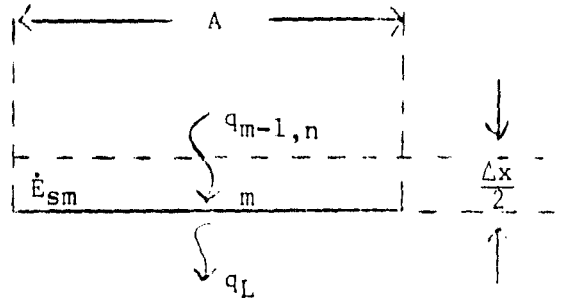

Figure 4. Energy Balance for Node m.

The energy balance equation for node m is

$$q_{m-1,m} = q_L + \dot{E}_{sm}. \tag{17}$$

The rate of heat transfer from node m-1 to node m is

$$q_{m-1,m} = - (\frac{k_{m-1} + k_m}{2}) A \frac{T_m - T_{m-1}}{\Delta x} . \tag{18}$$

Again since the volume element surrounding node m is only $\frac{\Delta x}{2}$ A, the energy storage term can be written as

$$\dot{E}_{sm} = (\rho c)_m A \frac{\Delta x}{2} \frac{T_m' - T_m}{\Delta t} . \tag{19}$$

Substituting equations (17) and (18) into equation (19) and rearranging results in the equation

$$\frac{T_m' - T_m}{\Delta t} = \frac{k_{m-1} + k_m}{(\rho c)_m (\Delta x)^2} T_{m-1} - T_m - \frac{2 q_L}{A(\rho c)_m \Delta x} . \tag{20}$$

Solving for the new temperature T_m' gives

$$T_m' = \frac{(k_{m-1} + k_m)\Delta t}{(\rho c)_m (\Delta x)^2} T_{m-1} + \left[1 - \frac{(k_{m-1} + k_m)\Delta t}{(\rho c)_m (\Delta x)^2}\right] T_m - \frac{2 q_L \Delta t}{(\rho c)_m A \Delta x} . \tag{21}$$

The finite difference equations have now been derived. These are equations (11), (16), and (21). To solve a heat transfer problem, the initial temperature of each of the m nodal points must be specified. This is identical to the specification of an initial condition for an analytically solved problem. To calculate the new temperature at time Δt, the heat flux terms q_s and q_L must be specified. Equations (16) and (21) can be used to determine the new boundary temperatures. The new temperature of each of the interior nodal points can be determined by solving equations (11) for each node. The resultant temperatures obtained for the m nodal points can be used to calculate the temperature at time $2\Delta t$. The interation process is continued to obtain the temperature at any desired future time.

Choice of values for Δx and Δt depends on the thermal properties of the soil considered and the thickness of the soil layer. For the 50-cm layer considered and the thermal properties of soil used, the values Δt = 60 seconds and Δx = 1 cm were found to be sufficient.

The model was modified during this study by considering two soil profiles having different soil moistures but which were identical in other respects. When the percent soil moisture (θv_w) and percent soil solids (θv_x) are known, the percent air (aeration porosity Ea) can be found. With these values, the heat capacity and conductivity can be calculated in the following manner.

$$C = \theta v_w C_w + \theta v_s C_s + E_a C_a, \tag{22}$$

where C_w, C_s and C_a are the heat capacities of water, soil and air, respectively.

The values used for heat capacities are:

$C_w = 1.00$ cal/cm^3/°C

$C_s = 0.48$ cal/cm^3/°C

$C_a = 0.00030$ cal/cm^3/°C

Since C_a is a small part of the heat capacity, it is neglected in model calculations. The original model was only applicable to a homogeneous soil layer of 50-cm, thus it was modified so each 1-cm soil layer could have a different moisture value. If the moisture of the soil profile varies with depth, variations in heat capacities and thermal conductivities occur. To adapt to these non-homogeneous conditions the model was modified to accept experimental soil moisture values at depths of 1, 8, 25, and 42 cm. Values are then calculated by the model by interpolation and extrapolation over the rest of the 50-cm profile. Thermal conductivity for each soil volume is calculated by the method developed by DeVries (1963). This method generates an apparent thermal conductivity which approximates heat transfer due to mass movement of water, phase changes of water, convection, and conduction.

This equation is given by:

$$\lambda = \frac{\Sigma \kappa_i \; x_i \; \lambda_i}{\Sigma \kappa \; x_i}, \tag{23}$$

where λ is the apparent thermal conductivity of a granular material; λ_i is the thermal conductivity of the soil's individual components; x_i is the volume fraction occupied by each soil fraction; and κ_i is the ratio of the average temperature gradient in the granules across the medium. The value of κ can be calculated from the following question:

$$\kappa_i = 1/3\Sigma_i \left[1 + \left(\frac{\lambda_i}{\lambda_o} - 1\right)g_a\right]^{-1}. \tag{24}$$

The g_a value is found using an unsaturated soil using water as a continuous medium:

$$g_a = 0.333 - \frac{E_a}{\Sigma}(0.333\text{-}0.035) \tag{25}$$

where Σ is the soil porosity.

The conductivities of the various soil constituents, λ, are given these values:

λ_s = conductivity of soil = 0.00525 cal/cm sec °C

λ_w = conductivity of water = 0.00142 cal/cm sec °C

λ_a = conductivity of air = 0.0000615 + 0.00196 x_w cal/cm sec °C

The finite-difference model (Figure 5) has the following inputs: (1) soil heat flux, (2) soil moisture profile, (3) dry soil conductivity, (4) physical properties of the soil which include (a) bulk density, ρ, (b) amount of soil by volume, (5) initial temperature profile and (6) effective air temperature.

The effect of water table is entered into the model as a difference in soil temperature at the 50-cm depth. For example, a water table present at one site causes its soil temperature at a 50-cm depth to be cooler by a constant amount in summer than an identical site with no near-surface water.

Outputs from the model calculations are soil temperature profiles for the two sites and a surface temperature difference as a function of time.

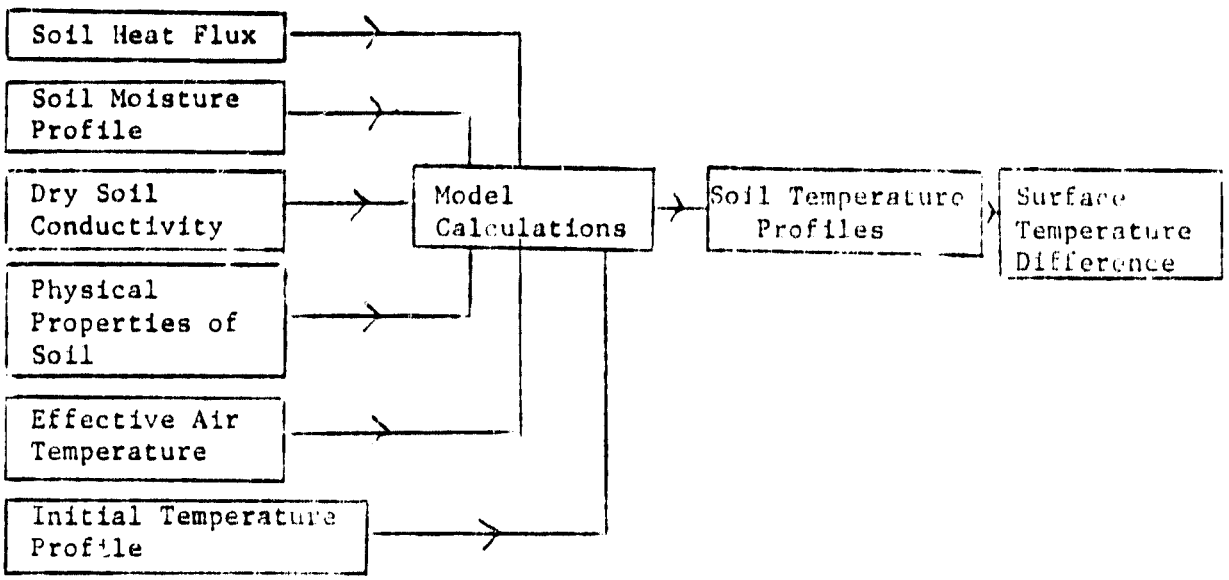

Figure 5. Schematic representation of the finite-difference model in its present format.

DATA COLLECTION

Data used in this phase of the project were of two types. The first type consisted of intensive data collected on small soil plots over several diurnal cycles. The second was a series of data collections on a group of sites which were separated so as to allow resolution by HCMM sensors. Only the first type of data collection is described here.

Sites chosen for this study were located at the South Dakota State University Agricultural Engineering Farm, which is near Brookings, South Dakota. Since soils vary considerably in this area, soil texture by hydrometer method, bulk density and porosity were analyzed throughout the profile depth of 50 cm. Results are shown in Table 1 and in Figures 6, 7, and 8. The percent of volume occupied by soil particles for a dry soil condition is shown in Figure 6. Since the percent soil particles increases with depth, the porosity decreases with depth. Figure 7 shows the variation in soil components with depth. The bulk density increases with depth as shown in Figure 8.

Table 1. Physical Properties of Soil Used.

Sample Depth	Particle Size			Porosity (Ea)	Bulk Density
	Sand	Silt	Clay		
(cm)	(%)	(%)	(%)		(g/cm^3)
0.0 - 7.6	27.7	61.5	10.9	.49	1.36
15.2 - 22.9	25.0	65.5	9.5	.4.	1.40
30.5 - 38.1	18.6	74.3	7.1	.41	1.47
45.7 - 53.3	15.6	78.4	6.0	.39	1.61

Each data collection site was divided into two plots, each approximately $10m^2$. To prevent water movement from one plot to the other a trench was excavated to a depth of 100 cm and a plastic barrier buried. This barrier allowed one plot to remain dry while the other was irrigated to whatever soil moisture desired.

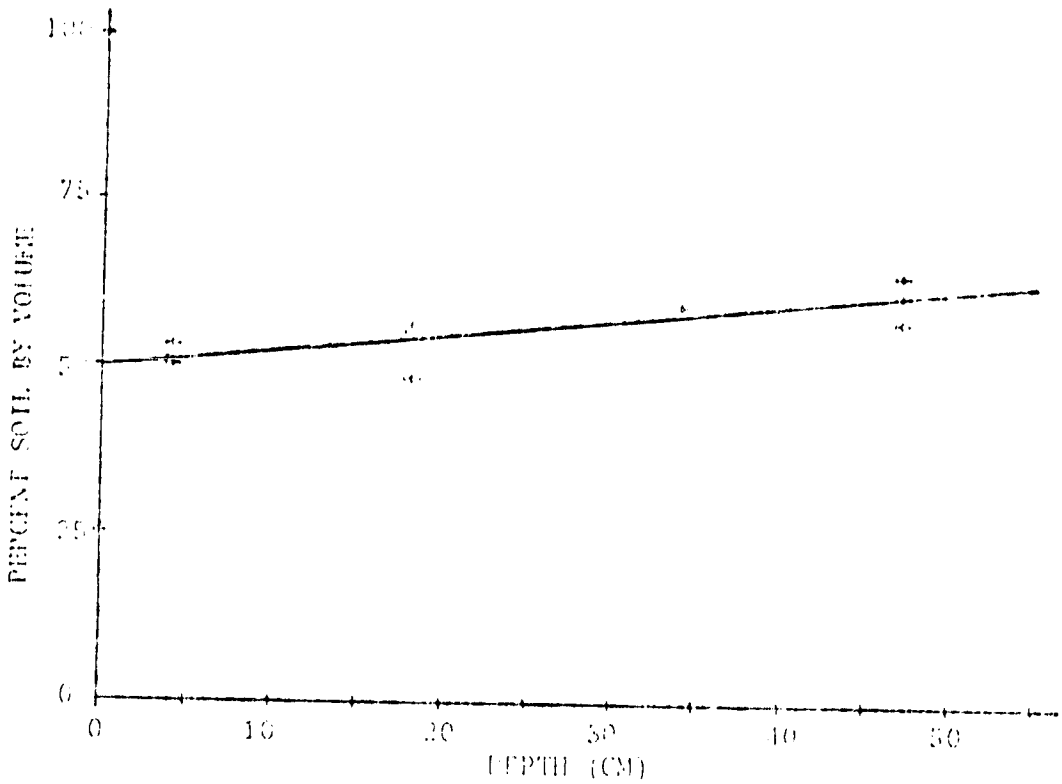

Figure 6. Percent soil solid by volume of soil profile as a function of depth.

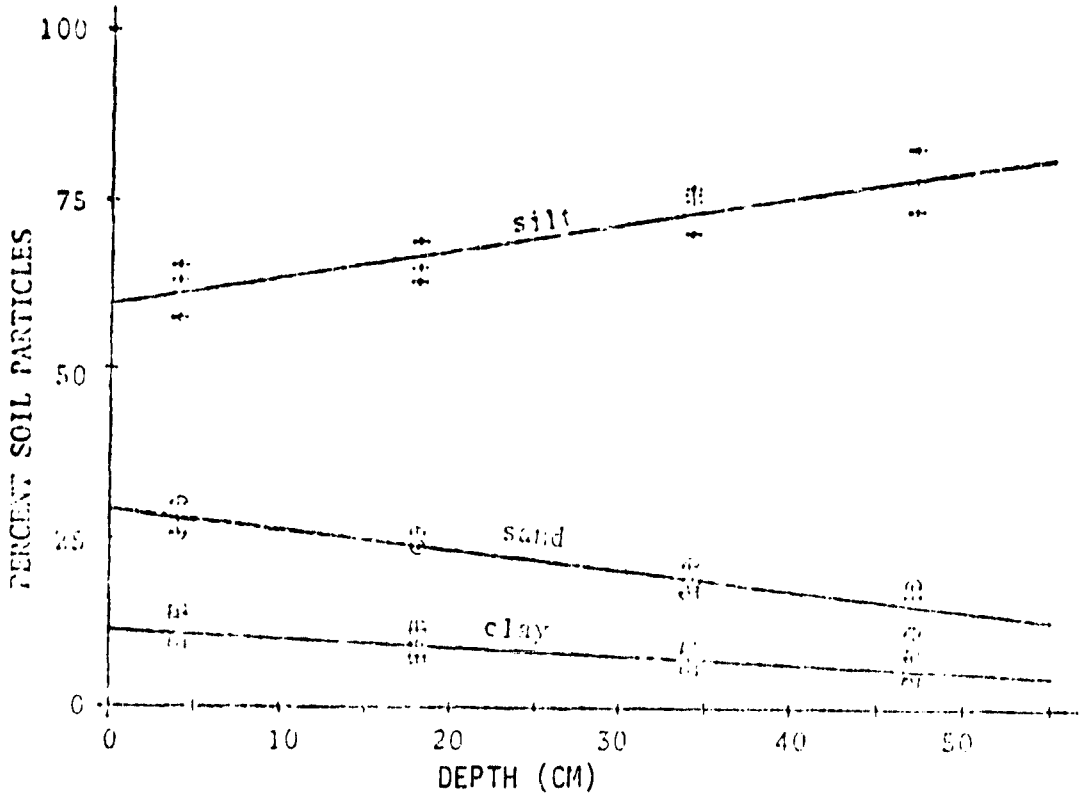

Figure 7. Percent of the soil particles composed of sand, silt and clay as a function of depth.

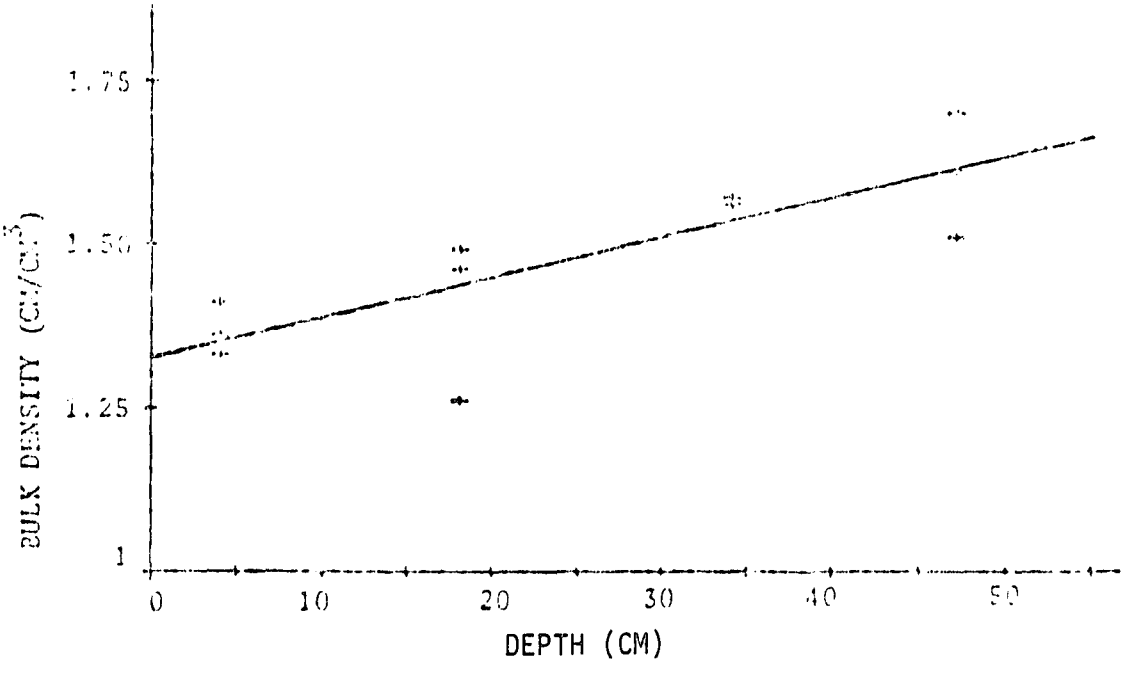

Figure 8. Bulk density of soil profile as a function of depth.

To measure soil temperatures, thermocouples were implanted in each plot at depths of 1, 5, 10, 25, 50, and 100 cm. Thermal emittance (apparent surface temperature) was measured utilizing a Barnes PRT-5 mounted on an appartus as shown in Figure 9 which scanned each plot every 15 minutes during data collection. Soil and air temperatures together with relative humidity were collected every hour while solar radiation and net radiation data were collected every fifteen minutes.

Soil moisture data were acquired by the gravimetric method with collection of soil samples an hour before solar noon (Jackson et al., 1976) to best represent the average moisture content. The gravimetric method of soil moisture gives a value of soil moisture by weight, θ_m,

$$\theta_m = \frac{\text{mass water}}{\text{mass dry soil}} \tag{26}$$

In the model soil moisture by volume is required. Thus θ_m is multiplied by bulk density to give the model input or,

$$\theta_v = \rho\theta_m \tag{27}$$

where θ_v is volumetric soil moisture.

Data were collected for several diurnal cycles for both barley and rye crop covers together with bare soil conditions after these canopies were removed. Figure 10 shows the barley crop canopy for which detailed data are used in this report. Data for the rye crop were qualitatively similar and will not be shown in detail.

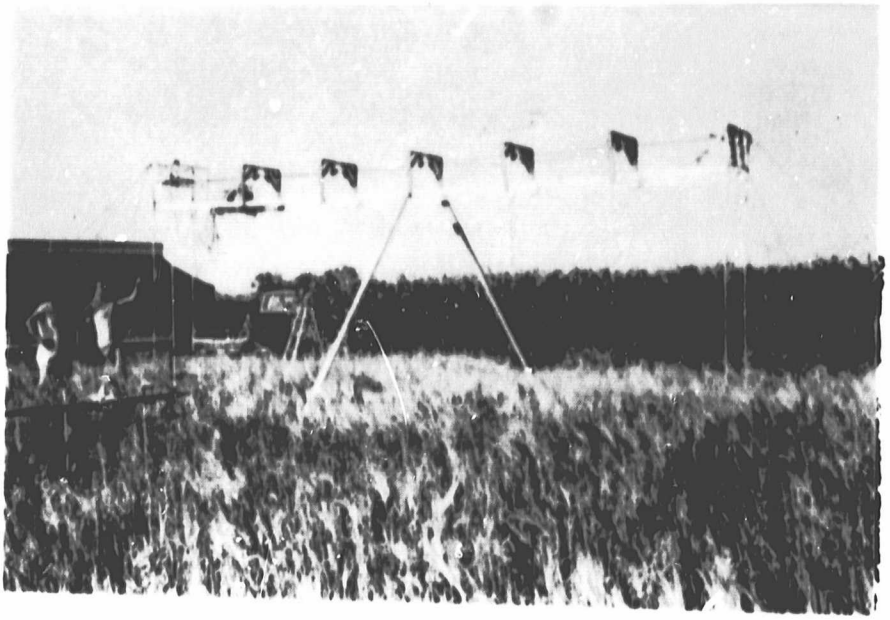

Figure 9. Photograph showing the scanning apparatus used to move the Barnes PRT-5 across the experimental plots.

Figure 10. Barley crop canopy present during the data collection on August 5 and 6, 1978.

RESULTS

Data were collected for bare surface conditions for a 52-hour period starting at 1000 hours, August 7, 1978. Two adjacent plots were prepared as previously described so that one plot would have a higher soil moisture profile than the other. Gravimetric soil moisture measurements for these plots were made as a function of depth. A smoothing of the curve of field measurements was conducted using a cubic spline as described by Kimball (1976).

Apparent surface temperatures of these plots are shown in Figures 11 and 12 for the 52-hour period. The measurements were made utilizing the Barnes-PRT 5 mounted on the scanning apparatus shown in Figure 9. The points shown are the field values while the continuous curve resulted from smoothing data by use of a cubic spline. Note the amplitude of the temperature variation during the diurnal cycle is less for the higher moisture plot. This is consistent with the results reported previously by Idso et al (1975).

The apparent surface temperature difference between the two plots is shown as a function of time in Figure 13. Values for this plot are temperature differences calculated from the values of the cubic spline curves of Figures 11 and 12. A surprising feature is its close similarity in functional form to the individual apparent temperature curves from which it was derived. This similarity is particularly significant since the diurnal amplitude of the surface temperature has previously been related to near-surface soil moisture (Idso et. al. 1975: Idso and Ehler, 1976; Schmugge et. al., 1978). Since the temperature difference curve shows the same functional form as curves of surface temperatures, the amplitude of the temperature difference should also be related to soil moisture differences. This type of technique for remotely measuring soil moistures would have the advantage of bypassing the calibration problems inherent in thermal emittance measurements.

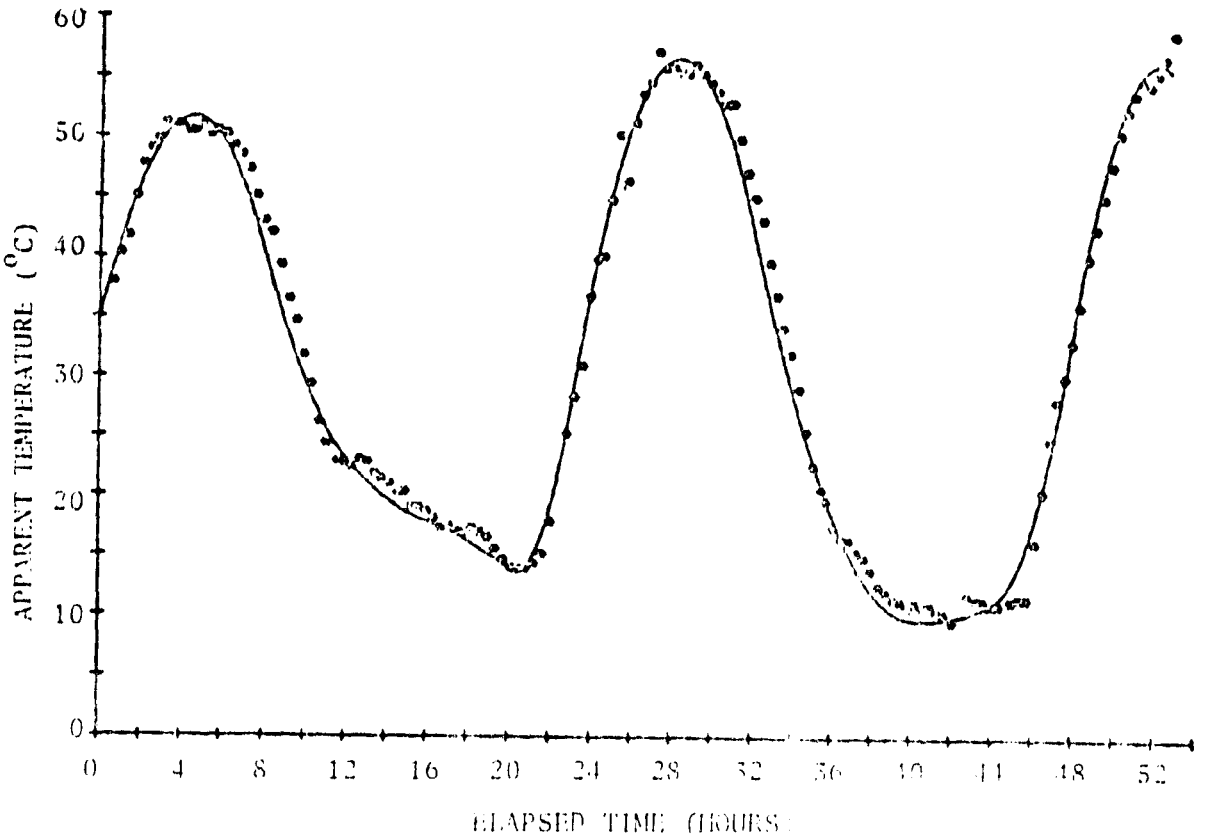

Figure 11. Apparent temperature for bare soil surface of the dryland plot soil profile beginning 1000 hours, August 7, 1978 and continuing for 52 hours thereafter.

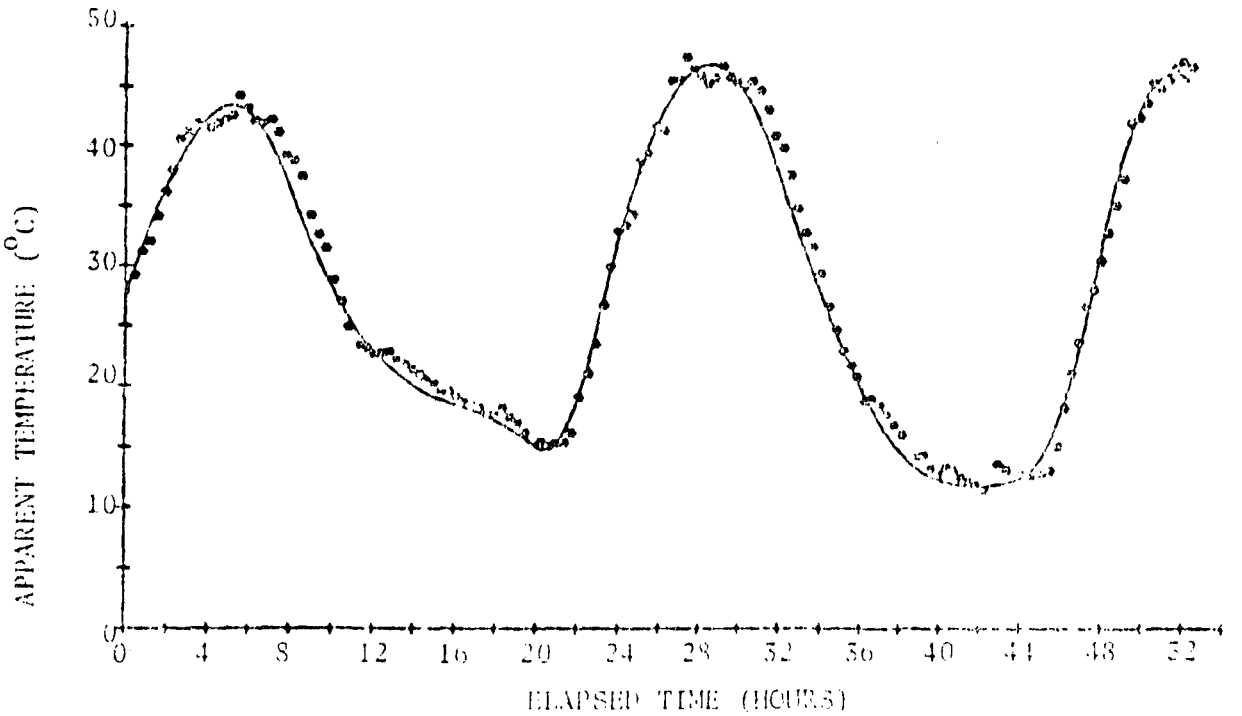

Figure 12. Apparent temperature for bare soil surface of the irrigated soil profile beginning 1000 hours, August 7, 1978 and continuing for 52 hours thereafter.

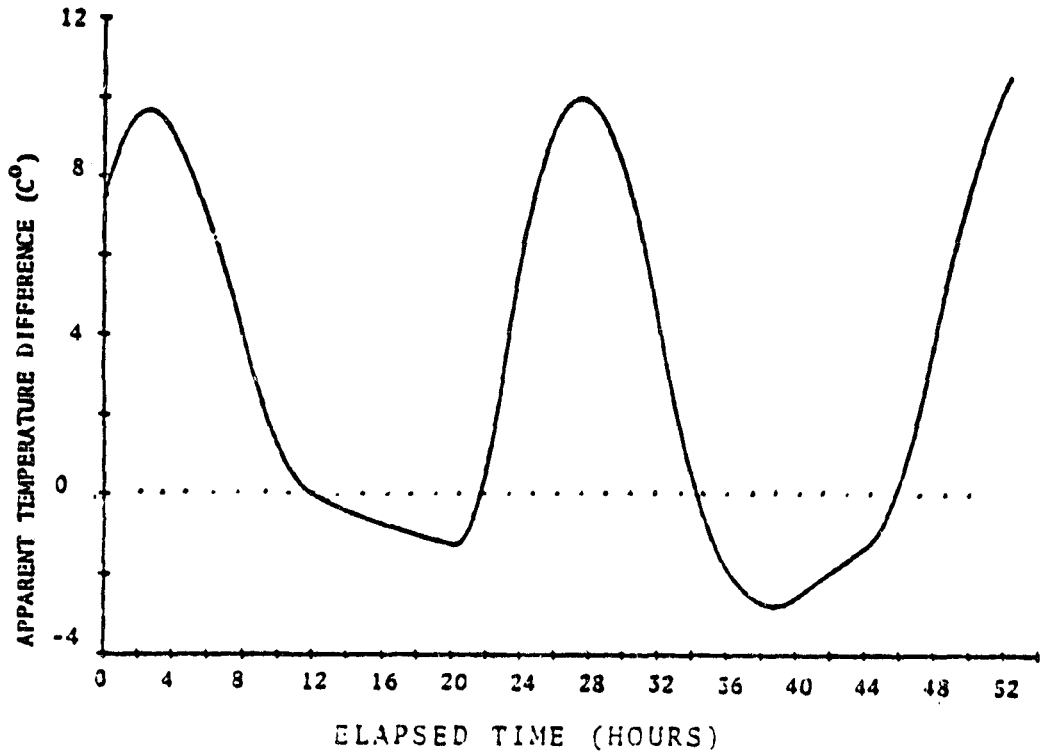

Figure 13. Apparent temperature difference between the dry and irrigated plots for bare soil. Data is shown for a 52-hour period starting at 1000 hours, August 7, 1978.

Results of theoretical model calculations for August 8, 1978, are shown in Figure 14. Inputs to the calculation are the bulk densities of the soil, the measured net radiation, and percent soil moisture by volume (See Appendix A). Comparing Figure 14 with the experimental plot of Figure 13 shows the functional dependence of the theoretical curve to agree very well with the experimental curve, particularly during the daylight hours. The magnitude of the calculated daylight temperature difference is smaller with a maximum calculated temperature difference of about 7° C compared to a measured difference of about 10° C. A possible explanation of this difference is the additional cooling of the irrigated plot due to water evaporation from the surface. Increasing the amplitude for net radiation allows the model to simulate the daytime surface temperature differences very accurately. However, the calculated soil temperature profiles become much warmer than those measured.

Experimental soil temperatures are compared in Figures 15-18 with theoretical temperature profiles calculated by the model using measured inputs. The functional form of the calculated temperature profiles are very similar to the measured profiles. The theoretical values, however, tend to be warmer during the day and cooler during the night. This result also implies that evaporation from the surface cannot be ignored in model calculations and must be accounted for with a parameter which effectively reduces the net radiation term to obtain the soil heat flux.

Data were collected for the barley canopy shown in Figure 10 for these same two plots prior to the bare soil data previously discussed. These plots were prepared in the same general manner as the bare plots and the same types of data were collected. Figures 19 and 20 show the apparent surface temperatures of the two plots for a 32-hour period beginning at 1100 hours, August 5, 1978. Figure 21 shows the apparent surface temperature difference obtained by subcontracting corresponding apparent temperatures from the cubic spline graphs of Figures 19 and 20.

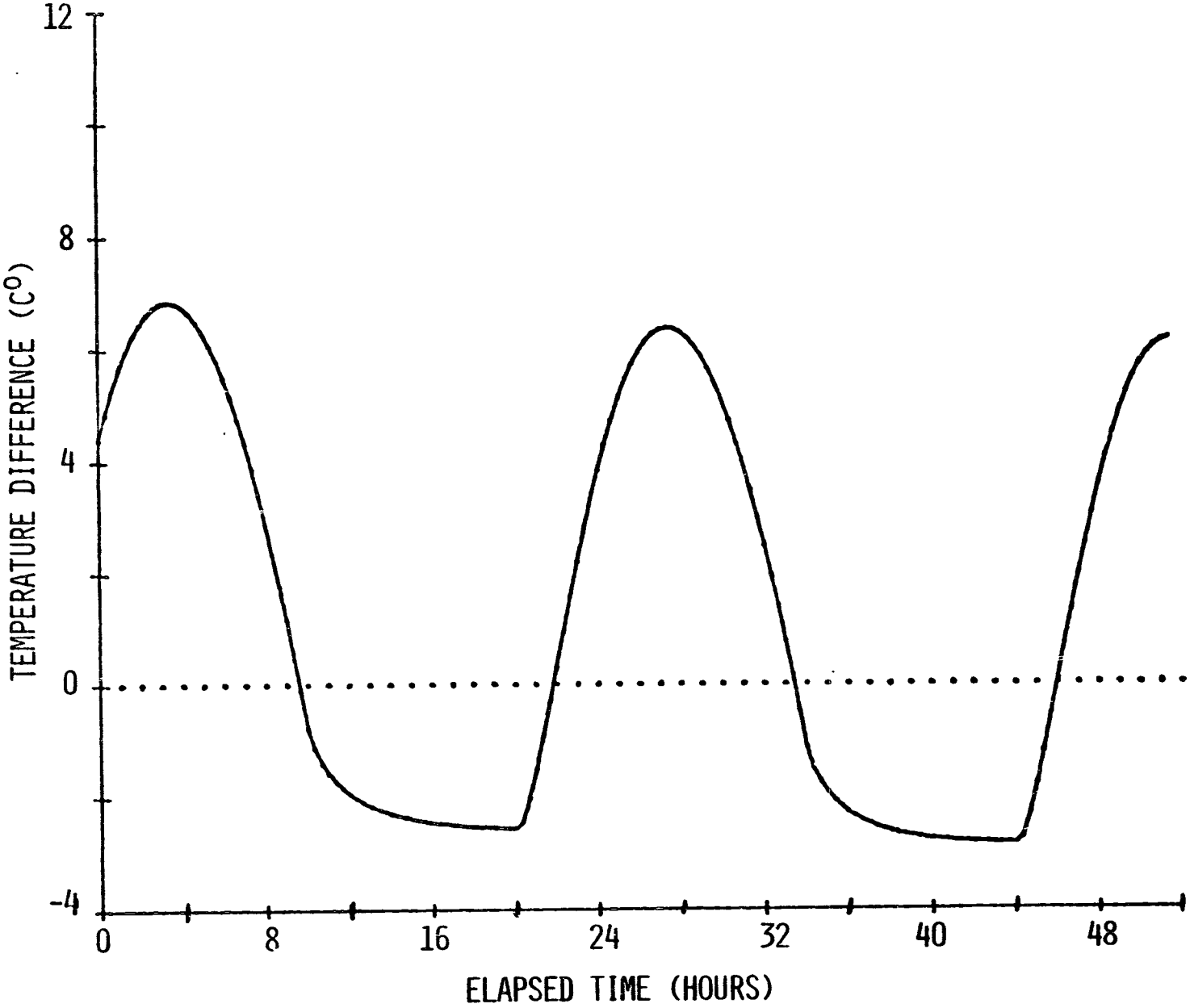

Figure 14. Theoretical model calculation of surface temperature difference between the dry and irrigated plots for a 52-hour period starting at 1000 hours, August 7, 1978.

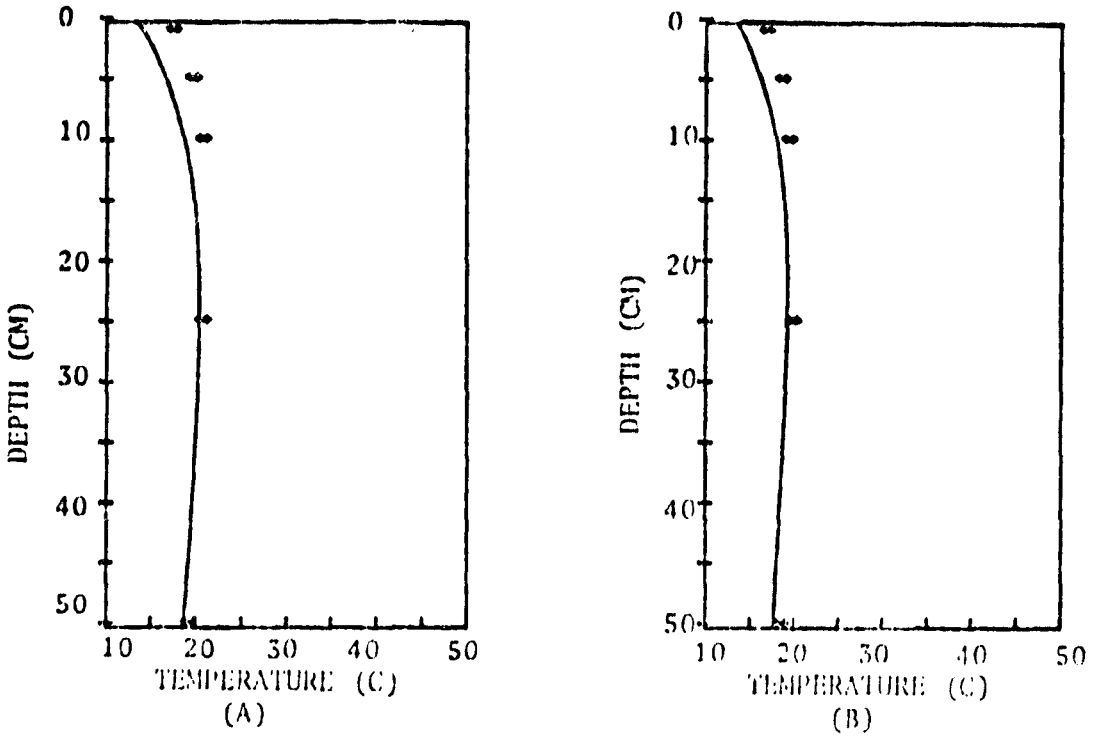

Figure 15. Soil temperature profiles calculated by the theoretical model for the dry plot (A) and the irrigated plot (B) for August 7, 1978 at 0400 hours. Experimental temperatures are represented by (++).

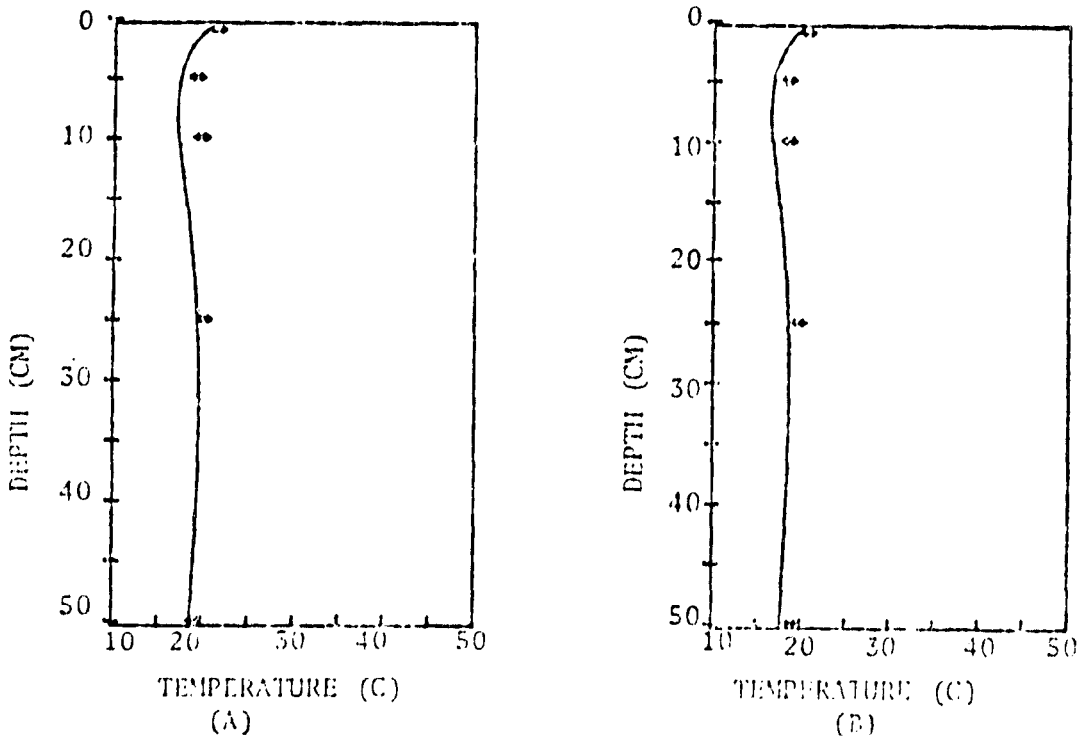

Figure 16. Soil temperature profiles calculated by the theoretical model for che dry plot (A) and the irrigated plot (B) for August 7, 1978 at 0800 hours. Experimental temperatures are represented by (++).

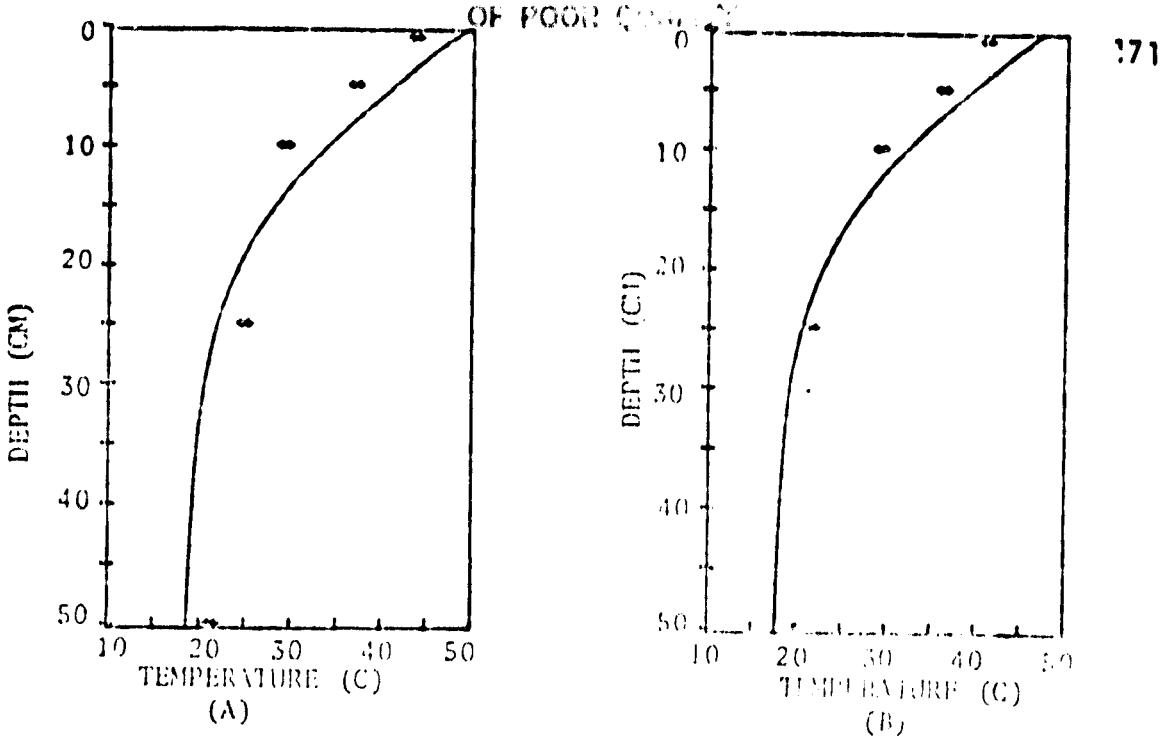

Figure 17. Soil temperature profiles calculated by the theoretical model for the dry plot (A) and the irrigated plot (B) for August 7, 1978 at 1600 hours. Experimental temperatures are represented by (++).

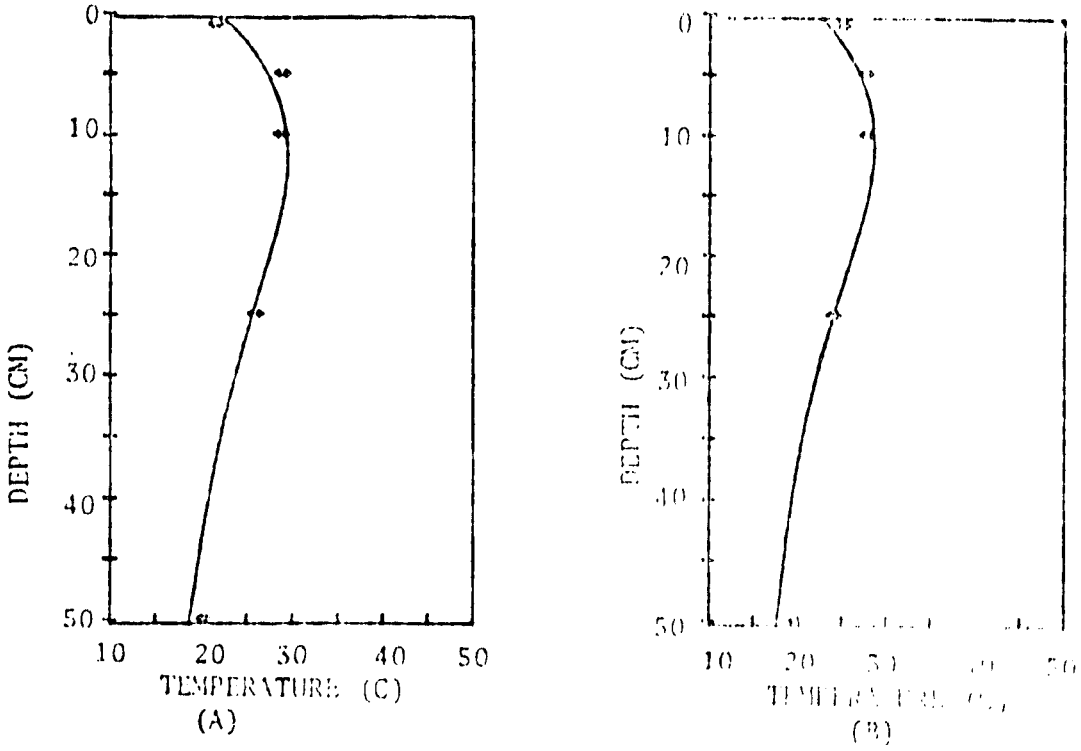

Figure 18. Soil temperature profiles calculated by the theoretical model for the dry plot (A) and the irrigated plot (B) for August 7, 1978 at 2200 hours. Experimental temperatures are represented by (++).

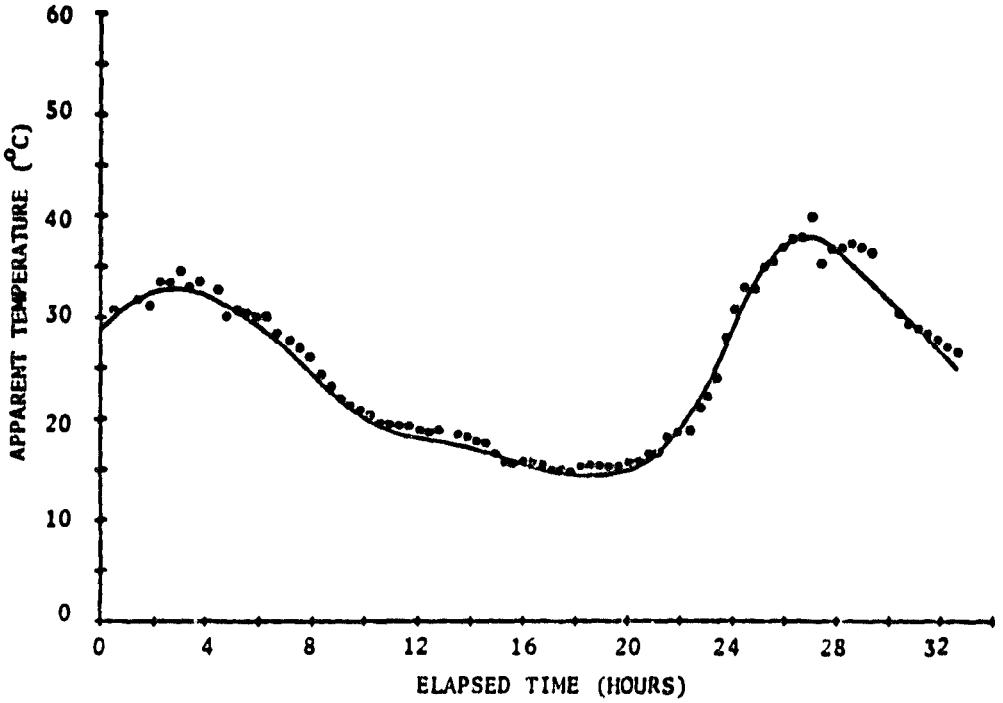

Figure 19. Apparent temperature measured over the barley canopy of the dryland plot. Data collection begins at 1100 hours, August 5, 1978 and continues for 32 hours thereafter.

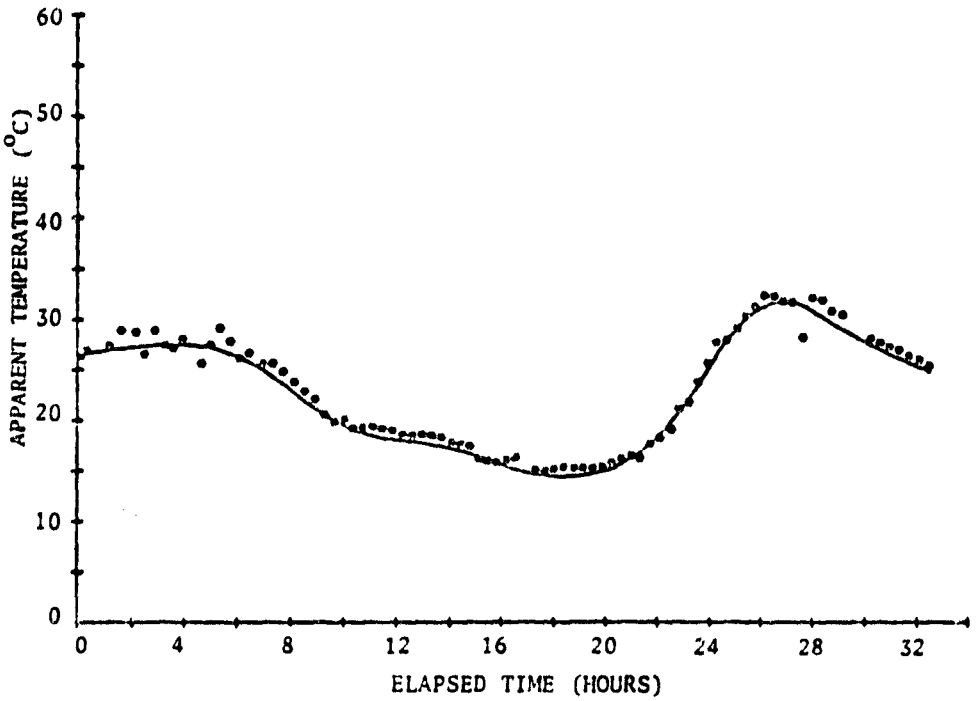

Figure 20. Apparent temperature measured over the barley canopy of the irrigated plot. Data collection begins at 1100 hours, August 5, 1978, and continues for 32 hours thereafter.

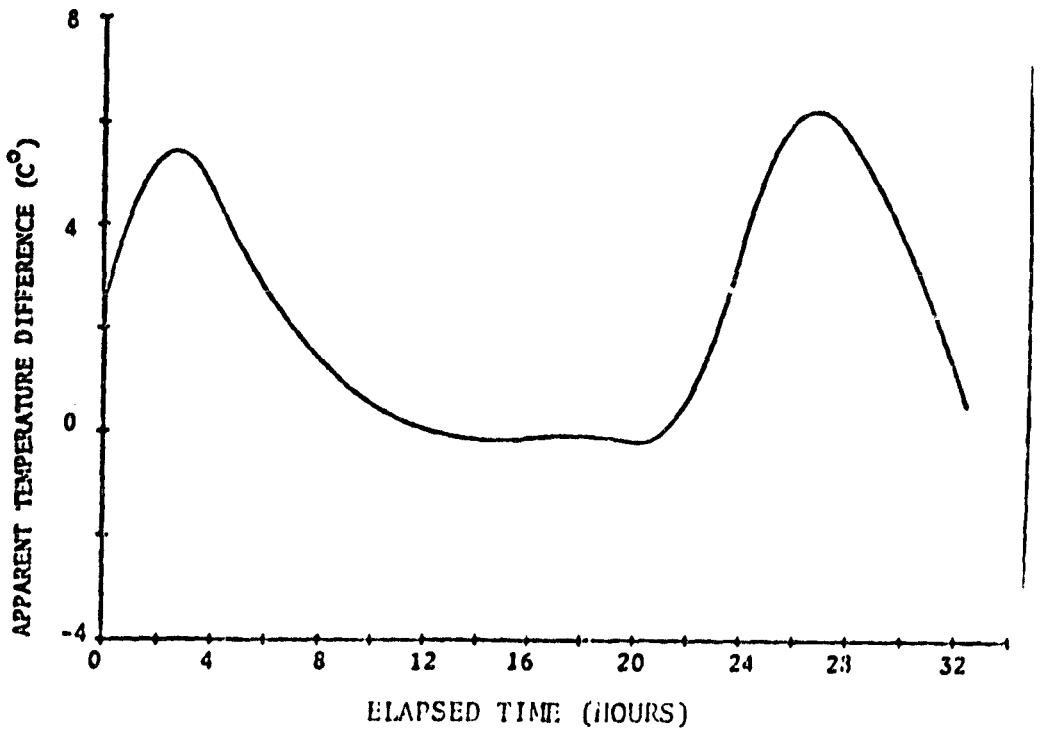

Figure 21. Apparent temperature difference between the dry and the irrigated plots with a crop canopy. Data is shown for a 32-hour period starting at 1100 hours August 5, 1978.

Comparison of Figures 19 and 20 with Figures 11 and 12 shows a drastic effect of the plant canopy on apparent surface temperatures. Both the functional dependence and the actual apparent temperature values are quite different for the barley canopy. However, the functional dependence for the apparent temperature differences as shown in Figures 13 and 21 are considerably more alike in functional form than the apparent surface temperatures. During the daylight hours the barley plots exhibit approximately one half the temperature difference of the bare plots but the only difference in functional form is a slightly slower rate of decrease in temperature difference late in the afternoon. The crop canopy, however, essentially eliminates the observed temperature difference for the nighttime hours. These results suggest that apparent temperature differences during the middle of the day may be the most likely indicator of soil moisture differences in the case of a thick plant canopy.

A theoretical calculation of the surface temperature difference for the barley plots is shown in Figure 22 for August 5, 1978. Again the calculated temperature difference is smaller than the measured apparent temperature difference; but the ratio of the two is approximately the same as for the wet/dry bare soil discussed previously. Since no apparent temperature difference is observed for the barley canopy during the night, the model obviously is not valid in its present form for that time period.

Several calculations were carried out to determine the dependence of the surface temperature difference on surface soil heat flux. In these calculations two plots were considered with soil properties identical to the experimental plots used for this study. Soil moisture by volume was assumed to be 10% in one plot and 20% in the second. Soil heat flux values were chosen to span a range which would include most experimental situations for a clear day. The maximum temperature difference predicted during the day was plotted as a function of the maximum soil heat flux. Results shown in Figure 23 display the resulting relationship. If

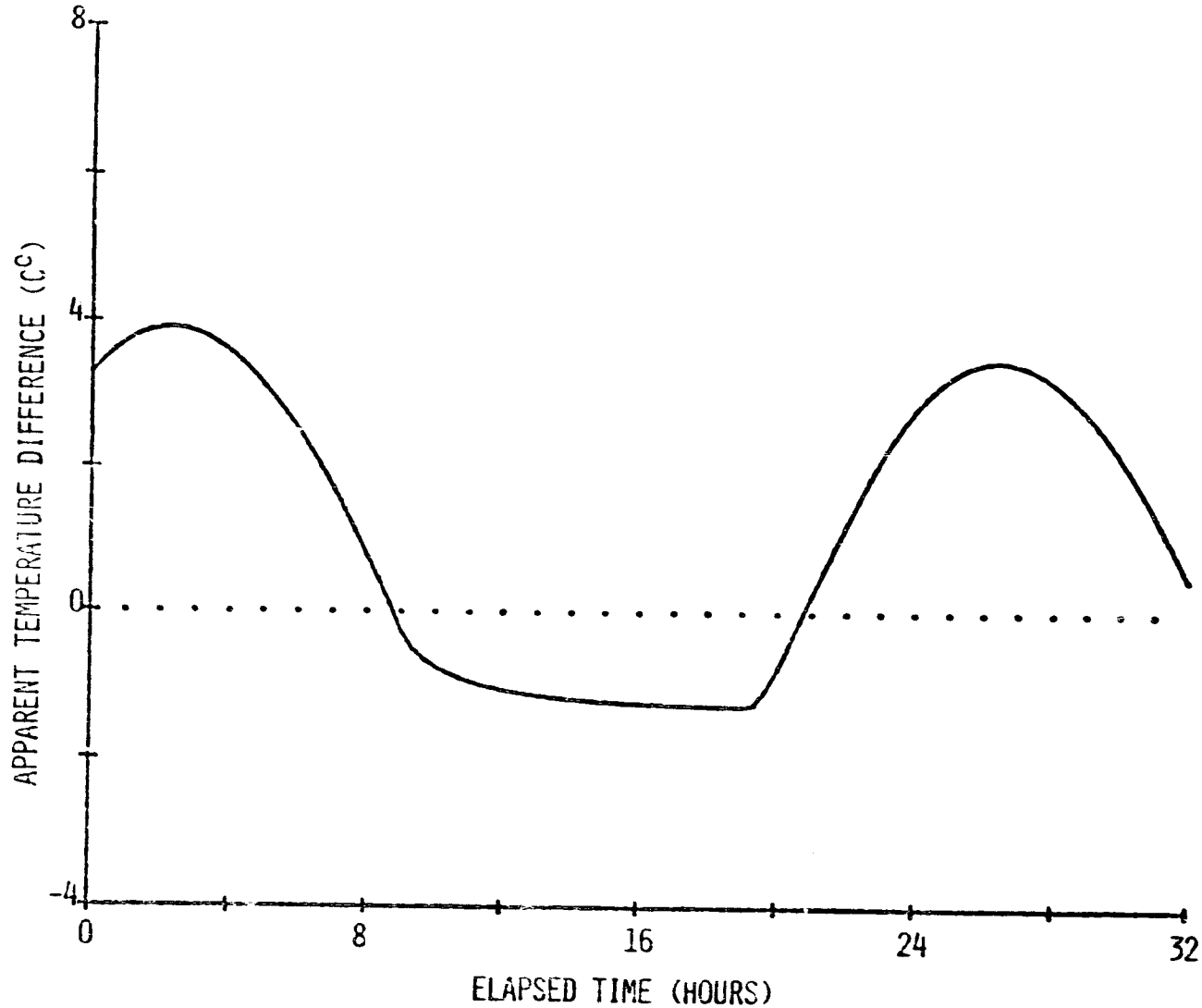

Figure 22. Theoretical model calculation of surface temperature difference between the dry and irrigated plots for a 32-hour period starting at 1100 hours August 5, 1978.

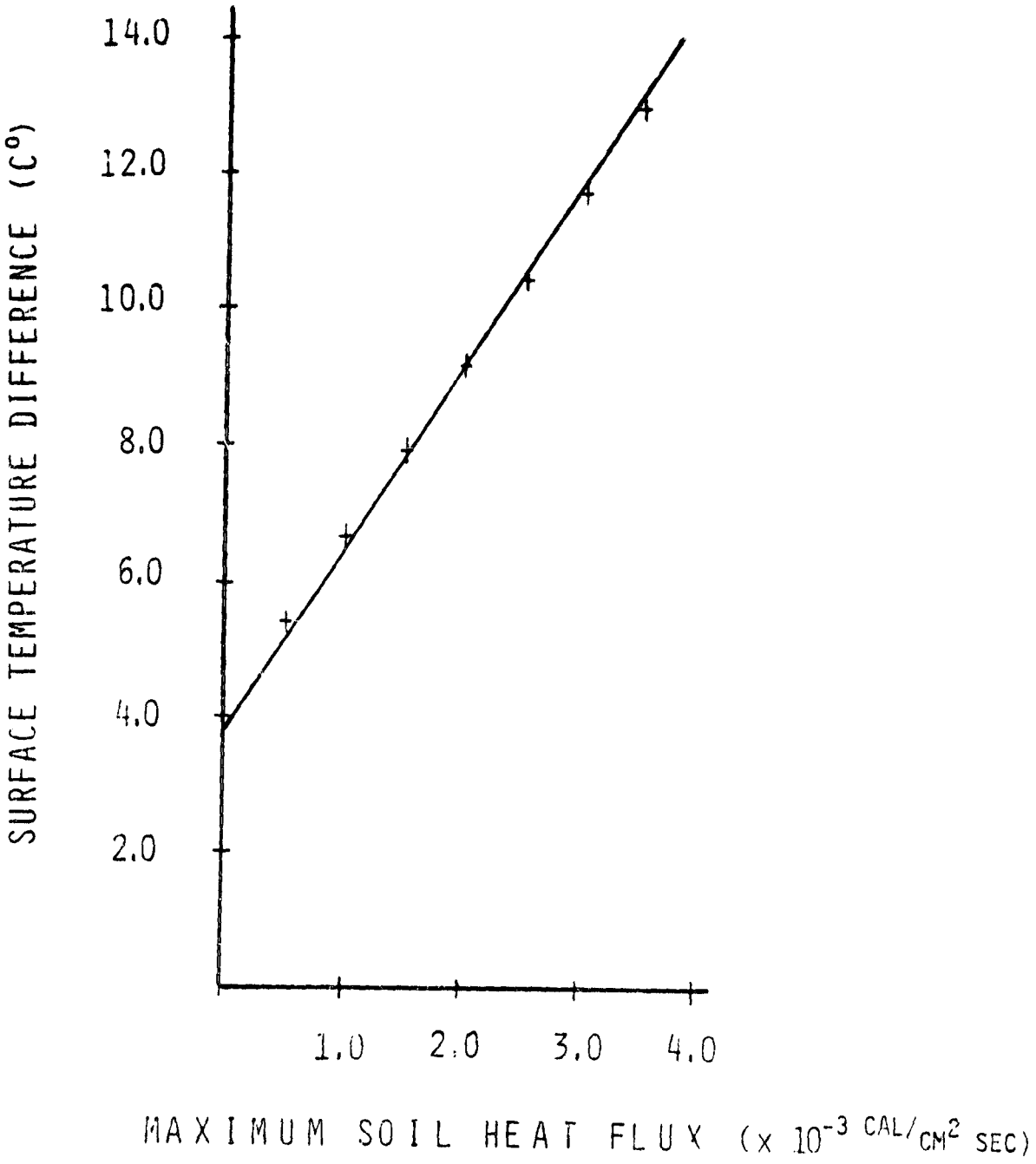

Figure 23. Calculated surface temperature difference between two plots as a function of soil heat flux amplitude. One plot is considered to have a constant soil moisture profile of 10% by volume while the other has a constant profile of 20%.

further theoretical and experimental results show this relationship to be valid, differences in daily solar radiation which exist during the satellite overpass could be easily accounted for during analysis of data.

Calculations were also carried cut to determine the relationship which would be expected to exist between moisture difference and maximum temperature difference observed during the day. Values for soil heat flux and physical properties of the soil were again chosen to correspond to the experimental plots of this study. The reference plot was chosen to have a soil moisture of 10% by volume and the soil moisture of the other was varied to a maximum of 21%. Results shown in Figure 24 display an approximately parabolic relationship. If this proves true in further theoretical and experimental investigations, the development of a paractical technique for utilizing apparent surface temperature differences to measure soil moisture will be greatly simplified.

A series of calculations were carried out to determine the feasibility of using dirunal surface temperature fluctuations (thermal inertia) as a measure of presence of water tables below the 50-cm profile. Two identical soil profiles were considered with the temperature at a 50-cm depth for one of these profiles cooler by an amount ΔT due to the presence of groundwater. Both profiles in these calculations were assumed to have the same soil heat flux at the surface.

The amplitudes of the surface temperature variations for a diurnal cycle were the same for both profiles. The surface temperature of the profile with the cooler 50-cm temperature, however, remained cooler throughout the diurnal cycle by a constant amount. This constant surface temperature difference varied between 20% and 50% of the 50-cm difference of ΔT depending on soil parameters.

These calculations suggest the variation in surface temperature differences during a diurnal cycle does not depend on the temperature at a 50-cm depth, but rather on soil parameters within the 50-cm profile and the soil heat flux. Thus thermal inertia would seem an unlikely candidate for determining presence of

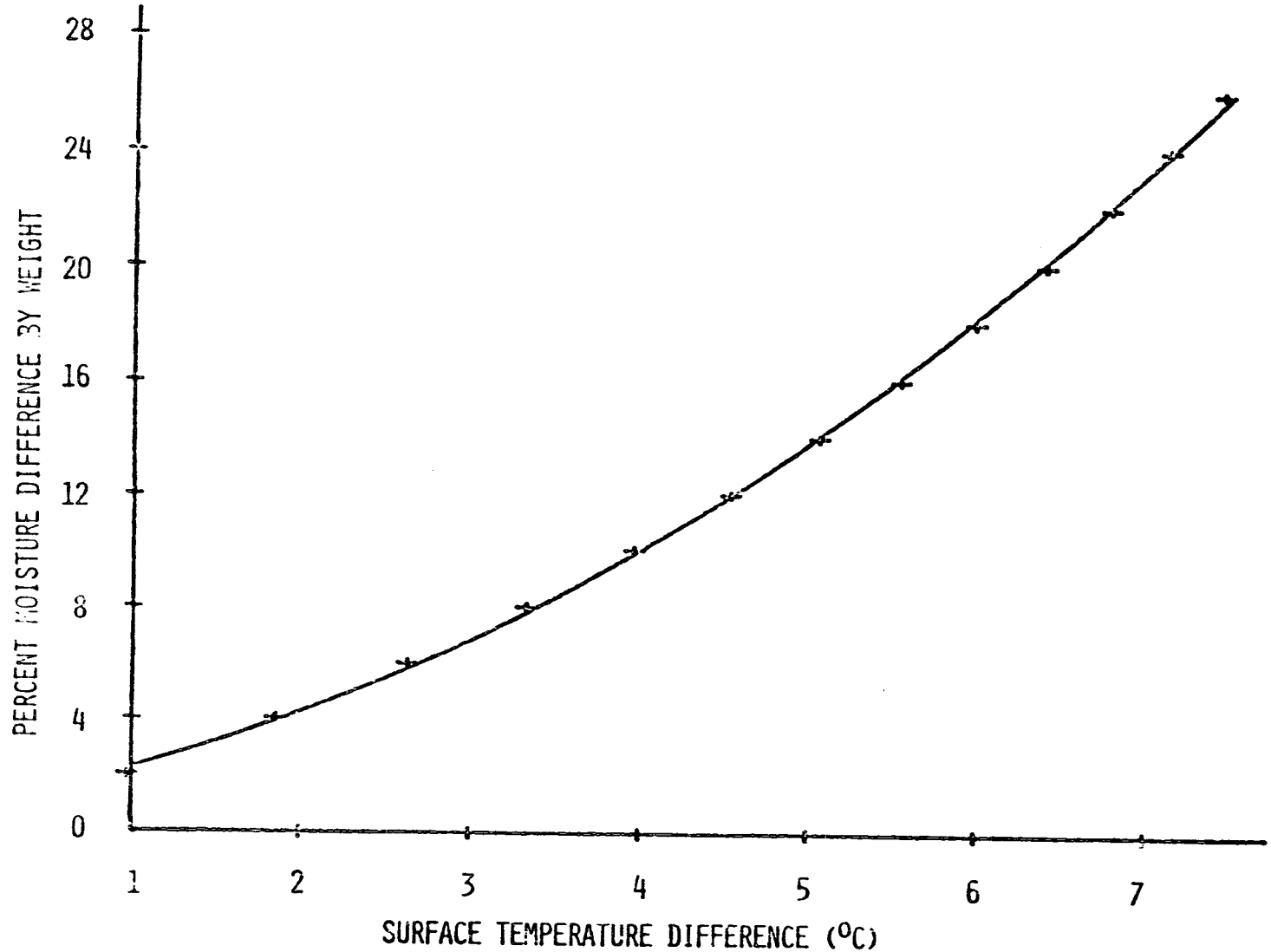

Figure 24. Calculated surface temperature difference between two soil plots as a function of moisture difference. One plot is considered to have a fixed soil moisture profile of 10% by volume while the other is varied from that value.

TABLE II

COMPARISON OF MODEL CALCULATIONS WITH HCMM APPARENT TEMPERATURE OBSERVATIONS

Site Numbers	Date	Crop Type	% Crop Cover	Max. Soil Heat Flux Dif. (cal/cm^2/sec.) (x 10-4) |A-B|	Percent Difference of Soil Moisture in 50-cm Profile |A-B|	Measured Temp. Dif. at 50 cm (^{o}K) |A-B|	Apparent Surface Temp. Difference Est. w/HCMM |A-B|	Model Predicted Surface Temp. Div. (^{o}K) |A-B|
A. BG-75-D B. GSBR-75-G	4 Sept.	Pasture Corn	50% 95%	-4.0	17.5%	3.5	2.0	2.33
A BR-75-E B. 110-51-16	4 Sept.	Stubble Stubble	50% 30%	-1.5	11.0%	2.4	2.4	2.39
A. GSBR-75-H B. GSBR-75-G	4 Sept.	Corn Pasture	95% 95%	0	16.0%	4.4	1.2	1.18
A. BD-75-K B. #4	4 Sept.	Pasture Pasture	70% 80%	-3.0	11.0%	1.3	1.2	1.29
A. 110-51-02 B. 111-50-10	8 Aug.	Alfalfa Corn	75% 70%	+2.0	2.0%	-1.4	1.0	0.95
A. 111-50-10 B. BR-75-IGS	8 Aug.	Corn Oats	70% 90%	-7.5	8.0%	2.8	0.6	0.71
A. BD-75-K B. BD-75-L	4 Sept.	Pasture Pasture	70% 90%	-4.5	7.0%	3.5	1.0	1.13
A. BG-75-D B. 110-51-11	4 Sept.	Pasture Corn	50% 95%	-3.0	8.5%	3.3	0.8	0.76
A. 111-51-02 B. BR-76-E	4 Sept.	Alfalfa Pasture	75% 50%	+0.5	3.5%	-3.9	0.4	0.51
A. BD-75-L B. #4	4 Sept.	Pasture Pasture	30% 80%	-4.7	8.0%	-1.4	0.8	0.89
A. BD-75-M B. 110-51-16	4 Sept.	Stubble Stubble	30% 30%	0	12.0%	1.1	1.6	1.58
A. BR-75-E B. BR-75-F	4 Sept.	Stubble Stubble	20% 50%	-0.9	2%	-1.4	0.4	0.47
A. 110-51-11 B. 111-50-10	8 Aug.	Corn Corn	85% 70%	-1.0	1.0%	-1.0	-0.2	-0.25
A. 111-50-10 B. 110-51-11	4 Sept.	Corn Corn	90% 95%	-5.5	3.5%	3.9	-0.8	-0.20
A. 110-50-18 B. 110-51-02	4 Sept.	Soybean Alfalfa	90% 75%	-5.5	3.0%	0.8	-1.6	-0.92

subsurface water tables unless the presence of these water tables affect the soil moisture in the 50-cm profile. However, the presence of such a subsurface water table will give rise to a constant temperature difference at the surface. In order to separate this factor from other factors which would give rise to time dependent temperature differences one will need a minimum of two observations of apparent surface temperature differences during a diurnal cycle which a satellite such as HCMM makes available. Also data from several successive days would be helpful in removing other factors from the data.

Calculations were made for the series of sites where ground truth was collected at the time of HCMM overpass. For these calculations average soil parameters for the area were used as model inputs together with experimentally measured soil moistures and 50-cm soil temperatures. Soil heat flux was adjusted in the model so that soil temperatures calculated agreed approximately with experimental values. This value was then used for all calculations for the respective site. To account for differences in crop cover, the value of soil heat flux was adjusted for one of the two sites.

Results of the calculations are shown in Table II. Calculated surface temperature differences agree well with the apparent surface temperature differences from HCMM. To use the model as a method of estimating near-surface soil moisture and depth to water tables, the differences in surface soil heat flux was used as a parameter in these calculations.

Therefore, differences in soil heat flux must be measured, predicted by a model, or empirically estimated using readily available data. Since percent cover, differences, temperature difference at 50-cm, and apparent surface temperature difference data were available for this investigation, a step-wise multiple regression (28) was conducted to determine their use in predicting surface heat flux differences using data presented in Table II.

$$y = (7.64\ x_1 + 1.56\ x_2 - 1.0\ x_3 - 5.2)\ (10^3) \quad (28)$$

where y is soil heat flux difference, x is percent difference of canopy cover, x_2 is percent soil moisture difference, and x_3 is 50-cm soil temperature difference. The resulting equation when entering variables significant at the 0.05 level follows with a multiple step-wise correlation coefficient as 0.835 = R. Therefore, up to 70% of the variation could be accounted for using measurements or model predication which could be available during model implementation. Percent cover could be estimated with Landsat, apparent surface temperature difference between two sites estimated with HCMM or other satellites, and the 50-cm temperature difference estimated with a model prediction. Soil moisture and heat flux differences may possibly be separated by use of multiple data collections of surface apparent temperature differences during the diurnal cycle. The technique shows promise and should be explored further.

PROJECT CONCLUSIONS

Conclusions of this study are:

1. Soils with different soil moisture profiles differ in surface temperature in a well-defined functional manner during the diurnal cycle. This functional dependence is similar to the diurnal surface temperature variations for each plot.
2. A thick crop canopy destroys the water-related apparent surface temperature difference during the nighttime hours.
3. The functional form of the apparent surface temperature difference measured in the field diurnally which was associated with a soil moisture difference is changed less by the presence of a crop canopy than the functional form of the individual surface temperatures.
4. The theoretical model used in this study predicts a functional form for the apparent surface temperature difference very similar to that observed for the daylight hours. However, the magnitudes of the theoretical temperature differences are smaller than the experimental values for both a bare soil and a crop canopy. The ratio of calculated temperature difference to that measured is approximately the same in both cases. Multiple pass satellite data would serve a better purpose if acquired solely during daylight hours rather than in an orbit similar to HCMM where a night pass is included.
5. Since the observed nighttime surface temperature differences vary considerably in functional form for the bare soil situation and are zero for dense crop canopies during the night, nighttime emittance data do not seem promising for use in measuring soil moisture.
6. Model calculations predict a linear relationship between soil heat flux and the surface temperature difference arising from soil moisture variations.
7. Model calculations predict a relationship between surface temperature difference and soil moisture difference. Only limited field studies were

conducted during this effort and further field verification should be pursued.

8. Model calculations indicate that day-minus night apparent temperatures are not useful in predicting depth to the water table. However, either day or night temperature differences between two sites are related to differences in water table depths. Field data showed that where dense crop canopies were present, the night data differences are not observed.
9. Model calculations of surface temperature differences agree well with observed apparent temperature differences from HCMM when soil heat flux is used as a parameter.
10. Initial observations are that a significant portion of the variance of soil heat flux can be accounted for with remote sensing observations and model estimates. Further investigation into the approach is warranted.
11. The overall results of this study reveal promise for the development of a method to monitor soil moisture by satellite. Using points on the curve comparing apparent surface temperature differences, one could calculate soil moisture differences for a group of chosen sites. If soil moisture is then measured at one site, soil moisture may be calculated for the other site.

LITERATURE CITED

Aaron, D.B., J.A. Tunheim, and D.G. Moore. 1976. Soil temperature fields associated with saline seeps. Proceedings of South Dakota Academy of Science, Vol. 55, p. 25-36.

Carson, J.E. 1961. Soil temperature and weather conditions. AEC research and development report ANL-64-70, Argonne, Illinois, pp. 244.

Cartwright, K. 1968. Thermal prospecting for groundwater. Water Resources Res. 4:395-401.

Fleagle, R.G. 1950. Radiation theory of local temperature differences. Journal of Meteorology 7:114-119.

Idso, S.B., and W.L. Ehrler. 1976. Estimating soil moisture in the root zone of crops: A technique adaptable to remote sensing. Science 189:991-992.

Idso, S.B., T.J. Schmugge, R.D. Jackson, and R.J. Reginato. 1975. The utility of surface temperature measurements for the remote sensing of surface soil status. Journal of Geophysical Research 80:3044-3049.

Jackson, R.D., R.J. Reginato, and S.B. Idso. 1976. Timing of ground truth acquisition during remote assessment of soil-water content. Remote Sensing of Environment 4:249-255.

Kahle, A.B., A.R. Gillispie, A.F.H. Goetz and J.D. Addington. 1975. Thermal inertia mapping. Proceedings, 10th International Symposium on Remote Sensing of the Environment, Ann Arbor, Michigan 985, 994.

Kimball, B.A. 1976. Smoothing data with cubic splines. Agronomy Journal 68:126-129.

Lettau, H.H., and B. Davidson, Ed. 1957. Exploring the atmosphere's first mile. Vol. 2, Pergamon Press, London.

Meyer, C.R. 1972. Simulation of a surface thermal anomaly. South Dakota State University, M.S. Thesis (Unpublished).

Moore, D.G., M.L. Horton, M.J. Russell and V.I. Myers. 1975. Evaluation of thermal X/5 detector Skylab S-192 data for estimating evaporation and thermal properties of soils for irrigation management. Proceedings of the NASA Earth Resources Survey Symposium, Houston, Texas, NASA TM-X58168:2561-2585.

Moore, D.G. and V.I. Myers. 1972. Environmental factors affecting thermal groundwater mapping. Report No. RSI 72-06. Presented to U.S.G.S., Dept. of Interior. 23 pp.

Myers, V.I. and M.D. Heilman. 1969. Thermal infrared for soil temperature studies. Photogrammetric Engineering 35:1024-1032.

Myers, V.I. and D.G. Moore. 1972. Remote sensing for defining aquifers in glacial drift. Proceedings of the Eighth International Symposium of Remote Sensing of Environment, Ann Arbor, Michigan, 2-6 October 1972. p. 715-728.

Reginato, R.J., S.B. Idso, J.F. Vedder, R.D. Jackson, M.B. Blanchard and R. Goettelman. 1976. Soil water content and evaporation determined by thermal parameters obtained from ground-based and remote measurements. Journal of Geophysical research 81:1617-1620.

Schmugge, T.J., B. Blanchard, A. Anderson and J. Wang. 1978. Soil moisture sensing with aircraft observations of the diurnal range of surface temperature. Water Resources Bull., 14:169-178.

Shaw, R.J. 1956. Comparison of solar radiation. Bulletin of American Meteorology 37:205-206.

Smith, R.W. 1969. Thermal dynamics at the earth-air interface: The implications for remote sensing of the geologic environment. Report No. RSL 69-4, Stanford, California.

Sutton, O.G. 1953. Micrometeorology. McGraw-Hill Book Co., New York.

Tunheim, J.A. 1977. Application of heat-flow temperature model for remotely assessing near surface soil moisture by thermography. OWRT Completion Report, Project A-053-SDAK, Agreement No. 14-31-0001-6043.

Vries, D.A. de. 1963. In Physics of Plant Environment, Wijk, W.R. van, Ed., North-Holland Publishing Co., Amsterdam.

Appendix A

HPL PROGRAM FOR FINITE-DIFFERENCE HEAT FLOW SIMULATION MODEL

The following program listing is written in a language used by Hewlett-Packard in the 9835A mini-computer furnished by the Water Resources Institute at South Dakota State University

C[*]	Conductivity Profile A
D[*]	Conductivity Profile B
E[*]	Heat Capacity Profile A
F[*]	Heat Capacity Profile B
H[*]	Time of Day (Hour)
A[*]	Temperature of Profile A
B[*]	Temperature of Profile B
G[0]	Term used by DeVries in calculation of conductivity
G[1]	Heat capacity of water
G[2]	Heat capacity of soil
H[1]	Initial starting hour
H[2]	Ending hour
I[0:50]	Thermal inertia for site A
J[0:50]	Thermal inertia for site B
K[0]	Conductivity of air
K[1]	Conductivity of water
K[2]	Conductivity of soil
M[1]	Initial starting minute
M[2]	Minute when calculation is to end
O[*]	Soil moisture for site A

P[*]	Soil moisture for site B
Q[*]	Thermal diffusivity for site A
R[*]	Allocation to store old temperature for site A
S[*]	Allocation to store old temperature for site B
T[*]	Thermal diffusivity for site B
U[0:50]	Aeration porosity for site A
V[0:50]	Aeration porosity for site B
W[1]	Effective air temperature
W[2]	Amount of soil by volume at 1 cm depth
W[3]	Amount of soil by volume at 8 cm depth
W[4]	Amount of soil by volume at 24 cm depth
W[5]	Amount of soil by volume at 42 cm depth
X[1]	Distance between nodal points
Y[1]	Ending day
Z[I,J,K]	Real data
A	Soil heat flux for site A
B	Soil heat flux for site B
C	Time from sunrise to solar noon
D,E,F,G	Soil bulk density at 1, 8, 24 and 42 centimeters
I	Counter
J	Counter
K	Counter
L	Day Length
M	Amplitude of soil heat flux for site A
N	Number of equally spaced nodal points
P	Time between printouts
Q	Amplitude of soil heat flux for site B

R	Dummy variable
T	Time interval between calculation in seconds
X	Dummy variable
Z	Real data file

PROGRAM LISTING (HPL)

Operational Procedure

```
0: 705→r0;gto 119
*10302
```

Subroutine for Soil Heat Flux

```
1: "QHEAT":H[1]/60→r21
2: H[1]→r21→r22
3: r22-C→r23
4: (W[1]+273.16)/100→r24
5: (A[0]+273.16)/100→r25
6: (B[0]+273.16)/100→r26
7: .000136*r24^4→r27
8: -(.000136*r25^4-r27)→r11
9: -(.000136*r26^4-r27)→r12
10: if r23<=0;gto 15
11: if r23>=L;gto 15
12: rad
13: M*sin(r23*π/L)+r11→r11
14: Q*sin(r23*π/L)+r12→r12
15: r11→A;r12→B;ret
*17416
```

Subroutine for Construction of Profile Plot

```
16: "Plots":
17: deg;0→R
18: scl 0,10,0,7
19: fxd 0
20: csiz 1.25,1,1,0
21: plt .5,6.5,1;lbl "SOIL TEMP FOR SITE A"
22: plt 3.7,6.8,1;lbl "HOUR  "
23: plt 4.7,6.8,1
24: if H[1]<10;str(H[1])→E$;lbl "0";cplt -1,0;lbl E$,"00";jmp 2
25: cplt -1,0;str(H[1])→E$;lbl E$,"00"
26: plt 5.5,6.5,1;lbl "SOIL TEMP FOR SITE B"
27: plt 1,1,1
28: plt 4,1,2
29: plt 4,6,2
30: plt 1,6,2
31: plt 1,1,2
32: pen
33: csiz 1,1,1,0
34: for I=0 to -50 by -5
35: if I<-9;plt .4,6+I*.1,1;lbl I;jmp 2
36: plt .55,6+I*.1,1;lbl I
37: plt .95,6+I*.1,1;lbl "-";next I
38: csiz 1.25,1,1,90
39: plt .2,2.6,1;lbl "DEPTH (CM)"
40: csiz 1,1,1,0
41: for I=10 to 50 by 5
42: plt -.05+I*.075,.75,1;lbl I
43: plt .25+I*.075,1,1;lbl "|";next I
44: csiz 1.25,1,1,0
45: plt 2,.5,1;lbl "TEMP (C)"
46: if 0=R;ofs 5,0;10→R;gto 27
47: ofs -5,0;ret
*31254
```

Subroutine for Plot of Theoretical Profile A

```
48: "plotA":
49: plt .25+A[I]*.075,6+L[I]*.1
50: if I=50;pen
51: ret
*213
```

Subroutine for Plot of Experimental Profile A

```
52: "realA":
53: colt -.33,-.25
54: plt .25+Z[J,N[1]/2,1]*.075,6-N[J]*.1,1;lbl "*"
55: ret
*10070
```

Subroutine for Plot of Theoretical Profile B

```
56: "plotB":
57: plt 5.25+B[I]*.075,6+L[I]*.1
58: if I=50;pen
59: ret
*16074
```

Subroutine for Plot of Experimental Profile B

```
60: "realB":
61: colt -.33,-.25
62: plt 5.25+Z[J,N[1]/2,2]*.075,6-N[J]*.1,1;lbl "*"
63: ret
*10725
```

Subroutine for Construction of Temperature Difference Plots

```
64: "Diff plot":
65: deg;0→R
66: scl 0,10,0,7
67: csiz 1.25,1,1,270
68: plt 4.5,6.2,1;lbl "SURFACE TEMPERATURE DIFFERENCE"
69: plt 9.5,6,1;lbl "5 CM TEMPERATURE DIFFERENCE"
70: fxd 0
71: plt 1,1,1
72: plt 4,1,2
73: plt 4,6,2
74: plt 1,6,2
75: plt 1,1,2
76: pen
77: csiz 1,1,1,270
78: for I=0 to 24 by 4
79: if I<10;plt .7,6.2-I*.21,1;lbl I;jmp 2
80: plt .7,6.25-I*.21,1;lbl I
81: plt .9,6-I*.21,1;lbl "|";next I
82: csiz 1.25,1,1,270
83: plt .5,3.75,1;lbl "HOUR"
84: csiz 1,1,1,270
85: for I=-6 to 10 by 2
86: if I<9;plt 2.125+I*.1875,6.5,1;lbl I," -";jmp 2
87: plt 2.125+I*.1875,6.6,1;lbl I," -"
88: next I
89: csiz 1.25,1,1,0
90: plt 2.2,6.75,1;lbl "TEMP (C)"
91: line 1,2
92: for I=0 to 24;plt 2.125,6-I*.21;next I;pen
93: fxd 2
94: line
95: if R=0;ofs 5,0;1→R;gto 70
96: ofs -5,0;ret
*26454
```

Subroutine for Plot of Surface Temperature Difference

```
97: "plot3":
98: line
99: plt 2.125+U[I]*.1875,6-O[I]*.21
100: if I=72;pen
101: ret
*17461
```

Subroutine for Plot of 5 cm Temperature Difference

```
102: "plot5":
103: line
104: plt 7.125+V[I]*.1375,6-O[I]*.21
105: if I=72;pen
106: ret
*6896
```

Subroutine for Conductivities in Profile A

```
107: "CONDUC A":
108: .333-U[I]/(1-W[X])*(.333-.035)→G[0]
109: .0000615+.00195*O[I]→K[0]
110: (2/(1+(K[2]/K[1]-1)*G[0])+1/(1+(K[2]/K[1]-1)*(1-2*G[0])))/3→r1
111: (2/(1+(K[0]/K[1]-1)*G[0])+1/(1+(K[0]/K[1]-1)*(1-2*G[0])))/3→r2
112: ret
*31843
```

Subroutine for Conductivities in Profile B

```
113: "CONDUC B":
114: .333-V[I]/(1-W[X])*(.333-.035)→G[0]
115: .0000615+.00195*P[I]→K[0]
116: (2/(1+(K[3]/K[1]-1)*G[0])+1/(1+(K[3]/K[1]-1)*(1-2*G[0])))/3→r3
117: (2/(1+(K[0]/K[1]-1)*G[0])+1/(1+(K[0]/K[1]-1)*(1-2*G[0])))/3→r2
118: ret
*13617
```

Dimension Statements

```
119: dim A[0:50],B[0:50],C[0:50],D[0:50],E[0:50],F[0:50],O[0:105],P[0:50]
120: dim X[1],V[0:105],W[5],Z$[4]
121: dim N[0:4],I[0:2],K[0:3],G[0:2],L[0:50],Y[0:1],R[0:50],S[0:51],U[0:105]
122: dim Z[5,12,2],M[1],I[0:50],J[0:50],Q[0:50],T[0:50]
*10727
```

Entering of Calculation Parameters

```
123: ent X[1],T,N,P,M[1],H[1],M[2],H[2],Y[1],W[1]
124: ent "real data file",Z;ldf Z,Z[*]
*32553
```

Temperature Data Storage

```
125: 1→N[1];5→N[2];10→N[3];25→N[4];50→N[5]
126: -1→L[1]
127: for I=2 to 50;L[I-1]-1→L[I];next I
128: 0→J→M[3]→M[4]→r10
129: H[1]*60+M[1]→M[3]
130: 1→r13
*27980
```

Entering of Soil Temperature Profiles

```
131: ent A[0],A[1],A[5],A[10],A[25],A[50],B[0],B[1],B[5],B[10],B[25],B[50]
*8924
```

Interpolation of Soil Temperatures

```
132: for I=2 to 4;(A[5]-A[1])/4*(I-1)+A[1]→A[I]
133: (B[5]-B[1])/4*(I-1)+B[1]→B[I];next I
134: for I=6 to 9;(A[10]-A[5])/5*(I-5)+A[5]→A[I]
135: (B[10]-B[5])/5*(I-1)+B[5]→B[I];next I
136: for I=11 to 24;(A[25]-A[10])/15*(I-1)+A[10]→A[I]
137: (B[25]-B[10])/15*(I-10)+B[10]→B[I];next I
138: for I=26 to 49;(A[50]-A[25])/25*(I-25)+A[25]→A[I]
139: (B[50]-B[25])/25*(I-25)+B[25]→B[I];next I
*4089
```

Surface Temperature Difference

```
140: A[0]-B[0]→S[51]
*5957
```

Determination of Mode for Entering Heat Capacity and Thermal Conductivity

```
141: J+1→J;if J>1;gto 250
*25970
```

Entering of Soil Physical Properties

```
142: ent O[1],O[8],O[25],O[42],P[1],P[8],P[25],P[42],W[2],W[3],W[4],W[5]
143: ent K[1],K[2],K[3],G[1],G[2],D,E,F,G,M,Q,C,L
*29564
```

Calculation of Percent Moisture by Volume

```
144: O[1]*D→O[1];O[8]*E→O[8];O[25]*F→O[25];O[42]*G→O[42]
145: P[1]*D→P[1];P[8]*E→P[8];P[25]*F→P[25];P[42]*G→P[42]
*23434
```

Calculation of Percent Air

```
146: 1-O[1]-W[2]→U[1]
147: 1-P[1]-W[2]→V[1]
148: 1-O[8]-W[3]→U[8]
149: 1-P[8]-W[3]→V[8]
150: 1-O[25]-W[4]→U[25]
151: 1-P[25]-W[4]→V[25]
152: 1-O[42]-W[5]→U[42]
153: 1-P[42]-W[5]→V[42]
*17723
```

Specification of Thermal Conductivities

```
154: 1→I;2→X;cll 'CONDUC A'(U[I],O[I],W[X])
155: (O[1]*K[1]+r1*W[2]*K[2]+r2*U[1]*K[0])/(O[1]+r1*W[2]+r2*U[1])→C[1]
156: 1→I;2→X;cll 'CONDUC B'(V[I],P[I],W[X])
157: (P[1]*K[1]+r3*W[2]*K[3]+r2*V[1]*K[0])/(P[1]+r3*W[2]+r2*V[1])→D[1]
158: 8→I;3→X;cll 'CONDUC A'(U[I],O[I],W[X])
159: (O[8]*K[1]+r1*W[3]*K[2]+r2*U[8]*K[0])/(O[8]+r1*W[3]+r2*U[8])→C[8]
160: 8→I;3→X;cll 'CONDUC B'(V[I],P[I],W[X])
161: (P[8]*K[1]+r3*W[3]*K[3]+r2*V[8]*K[0])/(P[8]+r3*W[3]+r2*V[8])→D[8]
162: 25→I;4→X;cll 'CONDUC A'(U[I],O[I],W[X])
163: (O[25]*K[1]+r1*W[4]*K[2]+r2*U[25]*K[0])/(O[25]+r1*W[4]+r2*U[25])→C[25]
164: 25→I;4→X;cll 'CONDUC B'(V[I],P[I],W[X])
165: (P[25]*K[1]+r3*W[4]*K[3]+r2*V[25]*K[0])/(P[25]+r3*W[4]+r2*V[25])→D[25]
166: 42→I;5→X;cll 'CONDUC A'(U[I],O[I]W[X])
167: (O[42]*K[1]+r1*W[5]*K[2]+r2*U[42]*K[0])/(O[42]+r1*W[5]+r2*U[42])→C[42]
168: 42→I;5→X;cll 'CONDUC B'(V[I],P[I],W[X])
169: (P[42]*K[1]+r3*W[5]*K[3]+r2*V[42]*K[0])/(P[42]+r3*W[5]+r2*V[42])→D[42]
*7913
```

Specification of Heat Capacity

```
170. W[2]*G[2]+O[1]*G[1]→E[1]
171: W[2]*G[2]+P[1]*G[1]→F[1]
172: W[3]*G[2]+O[8]*G[1]→E[8]
173: W[3]*G[2]+P[8]*G[1]→F[8]
174: W[4]*G[2]+O[25]*G[1]→E[25]
175: W[4]*G[2]+P[25]*G[1]→F[25]
176: W[5]*G[2]+O[42]*G[1]→E[42]
177: W[5]*G[2]+P[42]*G[1]→F[42]
*16713
```

Interpolation of Thermal Conductivities and Heat Capacity

```
178: for I=2 to 24;C[8]-(C[25]-C[8])/17*(8-I)→C[I]
179: D[8]-(D[25]-D[8])/17*(8-I)→D[I]
180: E[8]-(E[25]-E[8])/17*(8-I)→E[I]
181: F[8]-(F[25]-F[8])/17*(8-I)→F[I];next I
182: for I=26 to 50;C[25]+(C[42]-C[25])/17*(I-25)→C[I]
183: D[25]+(D[42]-D[25])/17*(I-25)→D[I]
184: E[25]+(E[42]-E[25])/17*(I-25)→E[I]
185: F[25]+(F[42]-F[25])/17*(I-25)→F[I];next I
186: C[1]→C[0];D[1]→D[0];E[1]→E[0];F[1]→F[0]
*4021
```

Printout of Thermal Conductivity (cal/^{o}C cm)

```
187: fmt 1,7/,"CONDUCTIVITY";wrt 706.1
188: fmt 1,3/,4x,3"DEPTH   SITE A   SITE B   ";wrt 706.1
189: int(N/3)+1→r2
190: r2*3→r3
191: N-r3+1→r4
192: for I=0 to r2-1;I→r5→r6
193: if r4>=1;r6+1→r6
194: r6+r2→r7→r8
195: if r4>=2;r8+1→r8
196: r8+r2→r9
197: fmt 1,5x,f3.0,3x,f7.5,2x,f7.5,4x,f3.0,3x,f7.5,2x,f7.5,z
198: wrt 706.1,r5,C[r5],D[r5],r7,C[r7],D[r7]
199: fmt 2,4x,f3.0,3x,f7.5,2x,f7.5
200: wrt 706.2,r9,C[r9],D[r9];next I
*31908
```

Printout of Volumetric Heat Capacity (cal/cm^{3} sec ^{o}C)

```
201: fmt 1,9/,"HEAT CAPACITY";wrt 706.1
202: fmt 1,3/,4x,3"DEPTH   SITE A   SITE B   ";wrt 706.1
203: int(N/3)+1→r2
204: r2*3→r3
205: N-r3+1→r4
206: for I=0 to r2-1;I→r5→r6
207: if r4>=1;r6+1→r6
208: r6+r2→r7→r8
209: if r4>=1;r6+1→r6
210: r8+r2→r9
211: fmt 1,5x,f3.0,4x,f6.3,3x,f6.3,4x,f3.0,4x,f6.3,3x,f6.3,z
212: wrt 706.1,r5,E[r5],F[r5],r7,E[r7],F[r7]
213: fmt 2,4x,f3.0,4x,f6.3,3x,f6.3
214: wrt 706.2,r9,E[r9],F[r9];next I
*16222
```

Calculation of Thermal Inertia

```
215: for K=0 to 50
216: (C[K]*E[K])^.5→I[K]
217: (D[K]*F[K])^.5→J[K]
*24481
```

Calculation of Thermal Diffusivity

```
218: C[K]/E[K]→Q[K]
219: D[K]/F[K]→T[K]
220: next K
*29332
```

Printout of Thermal Inertia

```
221: fmt 1,9/,"THERMAL INERTIA";wrt 706.1
222: fmt 1,3/,4x,3"DEPTH    SITE A    SITE B    ";wrt 706.1
223: int(N/3)+1→r2
224: r2*3→r3
225: N-r3+1→r4
226: for I=0 to r2-1;I→r5→r6
227: if r4>=1;r6+1→r6
228: r6+r2→r7→r8
229: if r4>=2;r8+1→r8
230: r8+r2→r9
231: fmt 1,5x,f3.0,3x,f7.5,2x,f7.5,4x,f3.0,3x,f7.5,2x,f7.5,z
232: wrt 706.1,r5,I[r5],J[r5],r7,I[r7],J[r7]
233: fmt 2,4x,f3.0,3x,f7.5,2x,f7.5
234: wrt 706.2,r9,I[r9],J[r9];next I
*13488
```

Printout of Thermal Diffusivity

```
235: fmt 1,9/,"THERMAL DIFFUSSIVITY";wrt 706.1
236: fmt 1,3/,4x,3"DEPTH    SITE A    SITE B    ";wrt 706.1
237: int(N/3)+1→r2
238: r2*3→r3
239: N-r3+1→r4
240: for I=0 to r2-1;I→r5→r6
241: if r4>=1;r6+1→r6
242: r6+r2→r7→r8
243: if r4>=2;r8+1→r8
244: r8+r2→r9
245: fmt 1,5x,f3.0,3x,f7.5,2x,f7.5,4x,f3.0,3x,f7.5,2x,f7.5,z
246: wrt 706.1,r5,Q[r5],T[r5],r7,Q[r7],T[r7]
247: fmt 2,4x,f3.0,3x,f7.5,2x,f7.5
248: wrt 706.2,r9,Q[r9],T[r9];next I
*25225
```

Time Interval Between Calculations

```
249: T/(2*X[1]*X[1])→r1;gto 264
*3516
```

Call for Soil Heat Flux Subroutine

```
250: cll 'QHEAT'
*11251
```

Calculation of Nodal Temperatures and Lower Boundary

```
251: for I=1 to N-1;(E[I]/r1-C[I-1]-2*C[I]-C[I+1])*A[I]+r6
252: ((C[I-1]+C[I])*A[I-1]+(C[I]+C[I+1])*A[I+1]+r6)*r1/E[I]+R[I]
253: (F[I]/r1-D[I-1]-2*D[I]-D[I+1])*B[I]+r7
254: ((D[I-1]+D[I])*B[I-1]+(D[I]+D[I+1])*B[I+1]+r7)*r1/F[I]+S[I];next I
255: 4*X[1]*r11+(E[1]/r1-2*C[1]-2*C[2])*A[0]+(2*C[1]+2*C[2])*A[1]+R[0]
256: r1/C[1]*R[0]+R[0]
257: 4*X[1]*r12+(F[1]/r1-2*D[1]-2*D[2])*B[0]+(2*D[1]+2*D[2])*B[1]+S[0]
258: r1/F[1]*S[0]+S[0]
259: A[N]+R[N]
260: B[N]+S[N]
*32346
```

Reassignment of Nodal Temperatures for Succeeding Interation

```
261: for I=0 to N;R[I]+A[I];S[I]+B[I];next I
262: A[0]-B[0]+S[51]
*29299
```

Test for Printout Time

```
263: if N[4]<P;gto 306
*256
```

Printout of Pertinent Data

```
264: r10+1+r10
265: int(r10/2)+r11;r11*2+r12
266: fmt 1,4/,"TEMPERATURE PROFILE AT ",fz2.0,fz2.0," HOURS"
267: wrt 706.1,N[1],N[1]
268: fmt 2,/,/,"SURFACE TEMPERATURE DIFFERENCE =",f6.3
269: wrt 706.2,S[51]
270: fmt 4,/,"SOIL HEAT FLUX   SITE A = ",f12.9,"   SITE B = ",f12.9
271: wrt 706.4,A,B
272: fmt 1,2/,4x,3"DEPTH   TEMP A   TEMP B   "
273: wrt 706.1
274: int(N/3)+1+r2
275: r2*3+r3
276: N-r3+1+r4
277: for I=0 to r2-1;I+r5+r6
278: if r4>=1;r6+1+r6
279: r6+r2+r7+r8
280: if r4>=2;r8+1+r8
281: r8+r2+r9
282: fmt 1,5x,f3.0,4x,f6.3,3x,f6.3,4x,f3.0,4x,f6.3,3x,f6.3,z
283: wrt 706.1,r5,A[r5],B[r5],r7,A[r7],B[r7]
284: fmt 2,4x,f3.0,4x,f6.3,3x,f6.3
285: wrt 706.2,r9,A[r9],B[r9];next I
*6549
```

Procedural Step (Reset)

```
286: 0+N[4]
*3874
```

Call for Plot Routine

```
287: if r12#r10;gto 306
288: cll 'Plot3'
*19455
```

Plot of Theoretical and Experimental Soil Temperatures

```
289: for I=0 to 50;cll 'plotA'(A[I],L[I]);next I
290: if N[1]=0;24→N[1]
291: for J=1 to 5;cll 'realA'(Z[J,N[1]/2,1],N[J]);next J
292: for I=0 to 50;cll 'plotB'(B[I],L[I]);next I
293: for J=1 to 5;cll 'realB'(Z[J,N[1]/2,2],N[J]);next J
294: fmt 1,/,9x,5"DEPTH  TEMP    ";wrt 706.1
295: fmt 4,/,"SITE A",z;wrt 706.4
296: fmt 2,3x,f3.0,3x,f5.2,4x,f3.0,3x,f5.2,4x,f3.0,3x,f5.2,z
297: fmt 3,4x,f3.0,3x,f5.2,4x,f3.0,3x,f5.2
298: wrt 706
```

Plot of Theoretical and Experimental Soil Temperatures

```
289: for I=0 to 50;cll 'plotA'(A[I],L[I]);next I
290: if N[1]=0;24→N[1]
291: for J=1 to 5;cll 'realA'(Z[J,N[1]/2,1],N[J]);next J
292: for I=0 to 50;cll 'plotB'(B[I],L[I]);next I
293: for J=1 to 5;cll 'realB'(Z[J,N[1]/2,2],N[J]);next J
*6936
```

Printout of Experimental Soil Temperatures for Profile A

```
294: fmt 1,/,9x,5"DEPTH  TEMP    ";wrt 706.1
295: fmt 4,/,"SITE A",z;wrt 706.4
296: fmt 2,3x,f3.0,3x,f5.2,4x,f3.0,3x,f5.2,4x,f3.0,3x,f5.2,z
297: fmt 3,4x,f3.0,3x,f5.2,4x,f3.0,3x,f5.2
298: wrt 706.2,N[1],Z[1,N[1]/2,1],N[2],Z[2,N[1]/2,1],N[3],Z[3,N[1]/2,1]
299: wrt 706.3,N[4],Z[4,N[1]/2,1],N[5],Z[5,N[1]/2,1]
*2683
```

Printout of Experimental Soil Temperatures for Profile B

```
300: fmt 5,/,"SITE B",z;wrt 706.5
301: fmt 2,3x,f3.0,3x,f5.2,4x,f3.0,3x,f5.2,4x,f3.0,3x,f5.2,z
302: fmt 3,4x,f3.0,3x,f5.2,4x,f3.0,3x,f5.2
303: wrt 706.2,N[1],Z[1,N[1]/2,2],N[2],Z[2,N[1]/2,2],N[3],Z[3,N[1]/2,2]
304: wrt 706.3,N[4],Z[4,N[1]/2,2],N[5],Z[5,N[1]/2,2]
*24421
```

Test if Calculation Has Run Desired Time

```
305: if N[1]=24;0→N[1]
306: if N[1]<N[2];gto 313
307: if N[1]<N[2];gto 310
308: if Y[0]<Y[1];gto 310
309: gto 324
*711
```

Test if Temperature Difference is to be Calculated

```
310: M[3]+1→M[3]
311: if M[3]/(r13*20)>=1;gto 313
312: gto 317
313: r13+1→r13
*30522
```

Calculation of Surface and 5 cm Temperature Difference

```
314: A[0]-B[0]*U[M[3]/20]
315: A[5]-B[5]*V[M[3]/20]
*30792
```

Calculation of New Time

```
316: M[3]/60→O[M[3]/20]
317: M[4]+T→M[4]
318: M[1]+T/60→M[1]
319: if M[1]<60;gto 323
320: M[1]-60→M[1]
321: H[1]+1→H[1];if H[1]<24;gto 323
322: H[1]-24→H[1];Y[0]+1→Y[0]
323: gto 141
324: stp
*28526
```

Plotting of Surface and 5 cm Temperature Differences

```
325: cll 'Diff plot'
326: for I=1 to 72;cll 'plotS'(O[I],U[I]);next I
327: for I=1 to 72;cll 'plotC'(O[I],V[I]);next I
328: end
*29769
```